PHONON HALL EFFECT IN TWO-DIMENSIONAL LATTICES

ZHANG LIFA

NATIONAL UNIVERSITY OF SINGAPORE

2011

PHONON HALL EFFECT

IN

TWO-DIMENSIONAL LATTICES

ZHANG LIFA

M.Sc., Nanjing Normal University

A THESIS SUBMITTED

FOR THE DEGREE OF DOCTOR OF PHILOSOPHY

DEPARTMENT OF PHYSICS

NATIONAL UNIVERSITY OF SINGAPORE

2011

Acknowledgements

The four years in NUS is a very happy and valuable period of time for me, during which I learned from, discussed and collaborated with, and got along well with many kindly people, to whom I would like to express my sincere gratitude and regards.

First and foremost I am indebted to my supervisors, Professor Li Baowen and Professor Wang Jian-Sheng, for many fruitful guidance and countless discussions. As my mentor, Prof. Li not only constantly gave me perspicacious and constructive suggestion, practical and instructive guidance but also generously shared with me his interest and enthusiasm to inspire me for research, as well as the principle for behaving and working. As my co-supervisor, Prof. Wang not only continuously offered me professional and comprehensive instruction, enthusiastic and generous support, detailed and valuable discussion but also hard worked with broad and deep knowledge to elegantly demonstrate the way to do research.

I would also like to thank my collaborators, Prof. Pawel Keblinski, Prof. Wu Changqin, and Dr. Yan Yonghong, Mr. Ren Jie for their helpful discussion and happy collaborations. Additionally, I am appreciative of the colleagues, such as Prof. Yang Huijie, Prof. Zhang Gang, Prof. Huang Weiqing, Prof. Wang Jian, Dr. Lü Jingtao, Dr. Lan Jinghua, Dr. Li Nianbei, Dr. Zeng Nan, Dr. Yang Nuo, Dr. Jiang Jinwu, Dr. Yin Chuanyang, Dr. Tang Yunfei, Dr. Lu Xin, Dr. Xie Rongguo, Dr. Xu Xiangfan, Dr. Wu Xiang, Mr. Yao Donglai, Mr. Chen Jie, Ms. Ni Xiaoxi, Mr. Bui Congtin, Ms. Zhu Guimei,

Ms Zhang Kaiwen, Ms. Shi Lihong, Mr. Liu Sha, Mr. Zhang Xun, Mr. Feng Ling, Mr. Bijay K. Agarwalla, Mr. Li Huanan, for their valuable suggestions and comments.

I thank Prof. Gong Jiangbin and Prof. Wang Xuesheng for their excellent teaching of my graduate modules as well as much useful discussion. I thank Mr. Lim Joo Guan, our hardware administrator, for his kindness and help on various issues. I like to express my gratitude to Mr. Yung Shing Gene, our system administrator, for his kind assistance of the software. I would like to thank department of Physics and all the secretaries for numerous assistance on various issues. Especially, I am obliged to Prof. Feng Yuanping, Ms. Teo Hwee Sim, Ms. Teo Hwee Cheng, and Ms. Zhou Weiqian.

I would like to express my gratitude to to all other friends in Singapore. A partial list includes, Zhou Jie, Yang Pengyu, Shi Haibin, Yu Yinquan, Wang Li, Zhou Longjiang, Zhen Chao, Li Gang, Jiang Kaifeng, Zhou Xiaolei for their friendship.

I am very grateful to my parents in heaven for their past deep love. I also thank my brother for his great encouragement. Last but not least, I am greatly appreciative of my dear wife Congmei's thorough understanding, never-ending patience and constant support. Although my son Zeyu is a little naughty, I thank him for making me very happy most of the time.

Contents

Abstract

Based on Raman spin-phonon interaction, we theoretically and numerically studied the phonon Hall effect (PHE) in the ballistic multiple-junction finite two-dimensional (2D) lattices by nonequilibrium Green's function (NEGF) method and and in the infinite 2D ballistic crystal lattices by Green-Kubo formula.

We first proposed a theory of the PHE in finite four-terminal paramagnetic dielectrics using the NEGF approach. We derived Green's functions for the four-terminal junctions with a spin-phonon interaction, by using which a formula of the relative Hall temperature difference was derived to denote the PHE in four-terminal junctions. Based on such proposed theory, our numerical calculation reproduced the essential experimental features of PHE, such as the magnitude and linear dependence on magnetic fields. The dependence on strong field and large-range temperatures was also studied, together with the size effect of the PHE. Applying this proposed theory to the ballistic thermal rectification, two necessary conditions for thermal rectification were found: one is phonon incoherence, another is asymmetry. Furthermore, we also found a universal phenomenon for the thermal transport, that is, the thermal rectification can change sign in a certain parameter range.

In the second part of the thesis, we investigated the PHE in infinite periodic systems by using Green-Kubo formula. We proposed topological theory of the PHE from two different theoretical derivations. The formula of phonon Hall conductivity in terms of Berry curvatures was derived. We found that

there is no quantum phonon Hall effect because the phonon Hall conductivity is not directly proportional to the Chern number. However, it was found that the quantization effect, in the sense of discontinuous jumps in Chern numbers, manifests itself in the phonon Hall conductivity as singularity of the first derivative with respect to the magnetic field. The mechanism for the change of topology of band structures comes from the energy bands touching and splitting. For honeycomb lattices, there is one critical point. And for the kagome lattices there are three critical points correspond to the touching and splitting at three different symmetric center points in the wave-vector space.

From both the theories of PHE in four-terminal junctions and in infinite crystal systems, we found a nonmonotonic and even oscillatory behavior of PHE as a function of the magnetic field and temperatures. Both these two theories predicted a symmetry criterion for the PHE, that is, there is no PHE if the lattice satisfies a certain symmetry, which makes the dynamic matrix unchanged and the magnetic field reversed.

In conclusion, we confirmed the ballistic PHE from the proposed PHE theories in both finite and infinite systems, that is, nonlinearity is not necessary for the PHE. Together with the numerical finding of the various properties, this theoretical work on PHE can give sufficient guidance for the theoretical and experimental study on the thermal Hall effect in phonon or magnon systems for different materials. The topological nature and the associated phase transition of the PHE we found in this thesis provides a deep understanding of PHE and is also useful for uncovering intriguing Berry phase effects and topological properties in phonon transport and various phase transitions.

List of Figures

Chapter 1

Introduction

To transport energy in solids traditionally there are two ways: one is conducting by electron, another is carrying by phonons. For electrons, very matured theories have been developed and many wide applications have already entered every aspect of our daily life. However, for phonons, in the last century there were few applications because of the difficulty to control phonons, which are collective vibrations, not real particles. In spite of such difficulty, it is very desirable to efficiently control phonons because the phonon-carrying heat permeates everywhere in our lives, such as water heating, air conditioning, and heat dissipating from the computer. Not until the beginning of this century did the controlling of phonons and processing information by phonons become a reality, which has emerged as a new discipline – phononics. Various thermal devices such as thermal rectifiers or diode [1], thermal transistor [2], thermal logical gates [3], thermal memory [4] and some molecular level thermal machines [5, 6] have been proposed, which make the new discipline very exciting and hot nowadays [7]. To manipulate phonons, one can tune the mechanical parameters, change geometry of the structures, introduce disorder scattering,

or apply external electrical field. Moreover, the magnetic field is another degree of freedom which could be potentially used to control thermal transport in the magnetic materials.

The thermal transport in magnetic systems has become an active field recently, where some experimental and theoretical works on the spin chains showed anomalous transport due to integrability [8–11], such as the anisotropic Heisenberg S=1/2 model, the t-V model, and the XY spin chain. In the magneto-thermal transport systems, there are three kinds of particles or qusiparticles contributing to the heat conduction: electrons, magnons and phonons. For the insulating magnetic compounds, the contributions of electrons can be ignored, thus only the magnons and phonons carry the heat. Most of the work done on the magneto-thermal transport is on the spin chains, where only the magnons are considered. However for the magnetic insulating crystals, phonons will contribute a lot to the thermal transport. Therefore it is highly desirable to study the phonon transport in the magnetic materials with magnetic fields.

Very recently, a novel phenomenon – the phonon Hall effect (PHE)– has been experimentally discovered by Strohm, Rikken, and Wyder, where the authors found a temperature difference in the direction perpendicular to both the applied magnetic field and the heat current flowing through an ionic paramagnetic dielectric sample [12] (see Fig. 1.1). Due to the Lorentz force, the electronic Hall effect is easily understood. However, the PHE is indeed a big surprise, because the phonons, charge-free quisparticles, cannot couple the magnetic field directly through the Lorentz force. Similar to the quantum

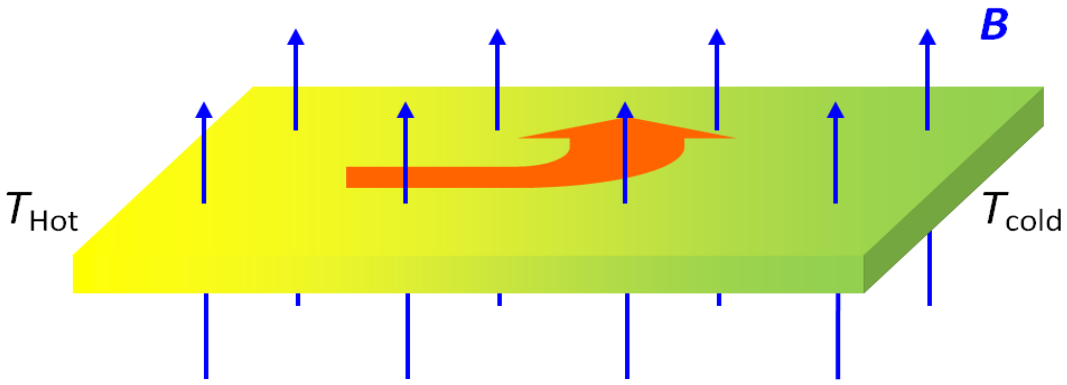

Figure 1.1: Schematic of the phonon Hall effect

effect of spin-orbit interaction, the spin or the local magnetization can interact with the lattice vibration, which can be called spin-phonon interaction. Based on such spin-phonon interaction, only two theoretical works have studied the phonon Hall effect using perturbation approximation [13, 14], and the underlying mechanism on the PHE is still unclear so far.

1.1 Phononics

Phononics, the science and technology in controlling heat flow and manipulating phonons, becomes a new physical dimension of information processing in addition to electronics and photonics after about one decade rapid development.

In 2002, Marcello Terraneo and co-workers proposed a simple model of a thermal rectifier based on resonance [15]. The authors found that heat can easily flow in one direction but not the other. By coupling two nonlinear one-dimensional lattices, Li *et al.* demonstrated a thermal diode model that worked in a wide range of system parameters, in which the rectification effect

was increased up to three orders of magnitude [1]. Inspired by this theoretical progress in thermal diode, in 2006 Chih-Wei Chang and co-workers built the first microscopic solid-state thermal rectifier, where they found the conductance was $3 \sim 7\%$ greater in one direction than the one in the other [16]. Another experimental observation of thermal rectification of 11% in a semiconductor quantum dot was reported by Scheibner and his co-workers [17]. The thermal diode was a major step towards phononics, which stimulated many works on the thermal rectification in spin-boson model, billiard systems, harmonic or nonlinear lattices, nano structures, quantum systems including spin chains, quantum circuits and quantum dots [18–35].

In 2006, Li *et al.* first demonstrated thermal transistor [2], which consisted of two segments (the source and the drain) with different resonant frequencies as well as a third segment (the gate) through which the input signal is transferred. The thermal transistor made it possible to build thermal logic gates, which was realized one year later by Wang and Li [3]. Shortly after the thermal resistor, via numerical simulation the same group demonstrated a thermal memory in which thermal information can be retained for a long time without being lost and also can be read out without being destroyed [4]. Therefore all the elements including thermal diode, thermal transistors, thermal logic gates, and thermal memory were theoretically and numerically proposed; perhaps even thermal computers would be realized in the near future.

Such rapid progress in phononic devices encourages lots of works on the thermal transport targeting for investigating the thermal properties such as thermal conductance and conductivity of different materials which include

carbon nanotubes [36–42], carbon nanotube networks [43, 44], graphene sheet and nanoribbons [45–47], silicon nanowires [48–50] and some interface structures [51–53]. To manipulate the thermal transport, there have been developed many ways, such as surface roughness [49, 54], doping or disorder effect [55,56,59] for introducing scattering to decrease the thermal conductivity, applying an external magnetic field in quantum magnetic systems [22,29,57–59] to change thermal conductivity or rectification. Applying a magnetic field to the paramagnetic insulating dielectrics, one could also observe the Hall effect of phonons. To understand such effect, in the following section, we will briefly introduce various Hall effects of electrons.

1.2 Hall Effects

In 1879, when Hall applied a magnetic field on a conductor sample where an electron current flowed through it, he found an electrical potential difference in the transverse direction perpendicular to both the current and the magnetic [60]. This effect was named Hall effect, which could be understood by the Lorentz force. One century later, quantum Hall effect, a striking manifestation of quantum nature, was found in 1980 by Klitzing *et al.*, where the Hall resistance depends only on integer numbers and fundamental constants when a high magnetic field is applied on the two-dimensional electron gas at sufficiently low temperatures [61]. Because of the significance of the work, Klitzing got the Nobel Prize in Physics in 1985. After the integer quantum Hall effect, in 1982, Tsui, Stromer and Gossard found the fractional quantum Hall effect [62], followed by the theory proposed by Laughling in 1983 [63].

For their discovery of fractionally charged electrons, Laughling, Stromer and Tsui shared the Nobel Prize in Physics in 1998. The outstanding work of the integer and fractional quantum Hall effects attracts many theoretical studies on the condensed matter physics and experimental works on the measuring of Hall resistance with unprecedented accuracy; until recent years, the quantum Hall effect is still a very active discipline [64–69].

All of the classical Hall effects, integer and fractional quantum Hall effects depend on the charge of electrons. Besides the charge of electrons, spin is another degree of freedom of electrons; and without charge current we can obtain a pure spin current. A natural question rises - whether can we find the spin Hall effect. In 1999, Hirsch theoretically proposed the principle of the extrinsic spin Hall effect [70], followed by the intrinsic spin Hall effect [71, 72]. Subsequently, the quantum spin Hall effect was independently proposed in graphene [73] and in strained semiconductors [74]. Followed by the quantum spin Hall effect, another topic of topological insulator becomes a very hot field in recent years [75, 76].

The discipline of Hall effects, which started more than one century ago, is still an active field. In both the electronic Hall effects and spin Hall effects, we need the charge carrier - electrons to transport. For the charge-free particles, such as phonons, photons and magnons, a question whether they have Hall effects rises naturally. There are few works about them because they cannot couple to the magnetic field via the Lorentz force. However, the spin-phonon interaction can make the phonon couple to the external magnetic field, which can be a possible coupling to induce the Hall effect of phonons.

1.3 Spin-Phonon Interaction

In quantum physics, when a particle moves, the spin of the particle couples to its motion by the spin-orbit interaction. The best known example of the spin-orbit interaction is the shift of an electron's atomic energy levels. Due to electromagnetic interaction between the electron's spin and the nucleus's magnetic field, the spin-orbit interaction can be detected by a splitting of spectral lines. Analogous to this coupling, when phonons transport in the insulators, the vibration of the ions interacts with the spin of the ions or the local magnetization of the ions, which we can call a spin-phonon interaction. Based on the symmetry consideration, a phenomenological description of the spin-phonon interaction was proposed [77–84], which described the coupling between the pseudo-spin representing the Kramers doublet and the lattice vibrations. For rare-earth ionic crystal lattice, one can assume all degeneracies of the ions except the Kramers one are lifted by the intra-atomic coupling and crystal fields [83, 84], such that the energy difference between the lowest excited states and the ground states is greater than the Debye energy. Thus at lower temperatures, we only consider the lowest Kramers doublet, which can be characterized by a pseudospin-1/2 operator $\vec{s}_n$. In the absence of external magnetic field, the Hamiltonian satisfies the time-reversal symmetry, and also the spatial symmetry of the crystal, then one could get a Raman spin-phonon interaction in the form as

$$H_I = g \sum_n \vec{s}_n \cdot (\vec{U}_n \times \vec{P}_n). \tag{1.1}$$

Here, g denotes a positive coupling constant. $\vec{U}_n$ and $\vec{P}_n$ are the vectors of displacement and momentum of the n-th lattice site. This interaction is not

particularly small, which dominates the spin lattice relaxation in many ionic insulators [77–79, 84]. In the presence of a magnetic field $\vec{B}$, the Kramers doublet carrying opposite magnetic moments split and give rise to a magnetization $\vec{M}$. For isotropic SPI, the isospin $\vec{s}_n$ is parallel to $\vec{M}_n$, and the ensemble average of the isospin is proportional to the magnetization, that is $\langle \vec{s}_n \rangle = c\vec{M}$. Therefore, under the mean-field approximation, the SPI can be represented as

$$H_I = \sum_n \vec{h} \cdot (\vec{U}_n \times \vec{P}_n), \tag{1.2}$$

where, $\vec{h} = gc\vec{M}$.

From the microscopic discussion of the phonons in a strong static magnetic field [85], we can also obtain a similar form of the spin-phonon interaction. Most of the studies on the spin-phonon coupling were focused on its effect of magnetic properties and longitudinal thermal transport properties. However, there were very few works studying the effect of the spin-phonon coupling on the transverse heat transport because most of the researchers think that the magnetic field cannot force the phonons to turn around to the transverse direction, and if it can, the effect is almost immeasurable.

1.4 Phonon Hall Effect

Surprisingly, contrary to general belief, Strohm, Rikken, and Wyder observed the PHE – a magnetotransverse effect, that is, a temperature difference found in the direction perpendicular to both the applied magnetic field and the heat current flowing [12]. The authors set up an experiment on samples of paramagnetic terbium gallium garnet $Tb_3Ga_5O_{12}$ (TGG) to detect the corresponding

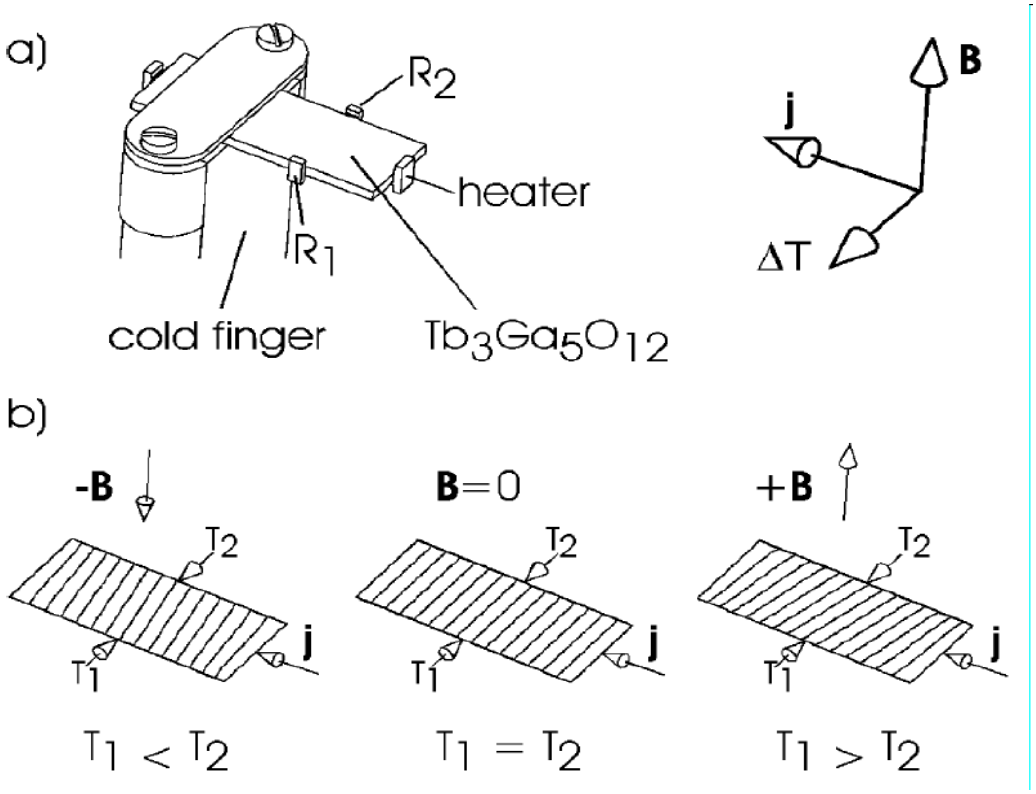

Figure 1.2: (a) Setup and geometry of the magnetotransverse phonon transport. (b) Phenomenology: Isotherms without and with a magnetic field. Copied from reference [12].

transverse temperature difference (ΔT_y) as an odd function of the magnetic field (B), which can be seen in Fig. 1.2. The authors observed a transverse temperature difference of up to 200 μK at an average temperature 5.45 K and a temperature longitudinal temperature difference (ΔT_x) of 1 K; and that PHE is linear in the magnetic field between 0 and 4 T.

The PHE was confirmed later by Inyushkin and Taldenkov [86], they found the coefficient of the phonon Hall effect ($(\nabla_y T/\nabla_x T)/B$) is equal to $(3.5 \pm 2) \times 10^{-5}$ T^{-1} in a magnetic field of 3 T at a temperature of 5.13 K. In order to understand the physics underlying the experiments, theoretical mod-

els for PHE have been proposed in Refs. [13, 14]. In Ref. [13], Sheng *et al.* first treated the phonons ballistically, and by using the nondegenerate perturbation theory to deal the spin-phonon interaction, the author then obtained an analytical expression for the thermal Hall conductivity after many approximations. However, according to Strohm et al [12], the mean free path (1 μm) is far less than the system size (15.7 mm); therefore, it is not appropriate to treat the diffusive PHE with a ballistic theory. In the work Ref. [14], Kagan *et al.* first considered the two-phonon scattering; however in the final form of the phonon Hall conductivity obtained by Born approximation in the mean field approach and a series of approximations, the anhormonicity did not appear.

The theoretical studies on the phonon Hall effect proposed by both Sheng et al. and Kagan et al. gave the readers an ambiguous picture because they treated the theories within ballistic phonon transport combining the perturbation of the spin-phonon interaction to explain the diffusive phonon Hall effect, which was incorrect. During the derivations, these authors used some approximations to obtain the phonon Hall conductivity, which was not rigorous and unhelpful to understand the mechanism of the PHE. Therefore such theories are not applicable to explain the phonon Hall effect; an exact theory for the phonon Hall effect is highly desirable.

1.5 Berry Phase Effect

In 1984, Michael Berry reported [87] about adiabatic evolution of an eigenstate when the external parameters change slowly and make up a loop in the parameter space, which has generated broad interests throughout the different

fields of physics including quantum chemistry [88]. In the absence of degeneracy, when it finishes the loop the eigenstate will go back to itself but with a different phase from the original one; the difference equal to dynamical phase factor (the time integral of the energy divided by $\hbar$) plus an extra which is later commonly called the Berry phase.

The Berry phase is an important concept because of three key properties as follows [88]. First it is gauge invariant, which can only be changed by an integer multiple of 2π but cannot be removed. Second, the Berry phase is geometrical, which can be written as an integral of the Berry curvature over a surface suspending the loop. Third, the Berry phase has close analogies to gauge field theories and differential geometry [89]. In primitive terms, the Berry phase is like the Aharonov-Bohm phase, while the Berry curvature is like the magnetic field. The integral of the Berry curvature over closed surfaces is topological and quantized as integers, known as Chern numbers, which is analogous to the Dirac monopoles of magnetic charges that must be quantized.

In the following we briefly introduce basic concepts of the Berry phase following Berry's original paper [87]. Let a Hamiltonian H varies in time through a set of parameters, denoted by $\vec{R} = (R_1, R_2, \dots)$. For a closed path in the parameter space, denoted as $\mathcal{C}$, $\vec{R}(t)$ the system evolves with $H = H(\vec{R}(t))$ and such that $\vec{R}(T) = \vec{R}(0)$. Assuming an adiabatic evolution of the system as $\vec{R}(t)$ moves slowly along the path $\mathcal{C}$, we have

$$H(\vec{R})|n(\vec{R})\rangle = \varepsilon_n(\vec{R})|n(\vec{R})\rangle \ . \tag{1.3}$$

However, the above equation implies that there is no relations between the phases factor of the orthonormal eigenstates $|n(\vec{R})\rangle$. One can make a phase

choice, also known as a gauge, provided that the phase of the basis function is smooth and single-valued along the path $\mathcal{C}$ in the parameter space. A system prepared in one state $|n(\vec{R}(0))\rangle$ will evolve with $H(\vec{R}(t))$ so be in the state $|n(\vec{R}(t))\rangle$ in time t according the quantum adiabatic theorem [90, 91], thus one can write the state at time t as

$$|\psi_n(t)\rangle = e^{i\gamma_n(t)} e^{-\frac{i}{\hbar}\int_0^t dt' \varepsilon_n(\vec{R}(t'))} |n(\vec{R}(t))\rangle \ , \tag{1.4}$$

where the second exponential is known as the dynamical phase factor. Inserting Eq. (1.4) into the time-dependent Schrödinger equation $i\hbar\frac{\partial}{\partial t}|\psi_n(t)\rangle = H(\vec{R}(t))|\psi_n(t)\rangle$ and multiplying it from the left by $\langle n(\vec{R}(t)|$, one finds that γ_n can be expressed as an integral in the parameter space

$$\gamma_n = \oint_{\mathcal{C}} d\vec{R} \cdot \vec{\mathcal{A}}_n(\vec{R}) \ , \tag{1.5}$$

where $\vec{\mathcal{A}}_n(\vec{R})$ is Berry connection or the Berry vector potential written as

$$\vec{\mathcal{A}}_n(\vec{R}) = i\langle n(\vec{R})|\frac{\partial}{\partial \vec{R}}|n(\vec{R})\rangle \ . \tag{1.6}$$

The Berry vector potential $\vec{\mathcal{A}}_n(\vec{R})$ is gauge-dependent. If we make a gauge transformation $|n(\vec{R})\rangle \rightarrow e^{i\zeta(\vec{R})}|n(\vec{R})\rangle$ with $\zeta(\vec{R})$ being an arbitrary smooth function, $\vec{\mathcal{A}}_n(\vec{R})$ transforms according to $\vec{\mathcal{A}}_n(\vec{R}) \rightarrow \vec{\mathcal{A}}_n(\vec{R}) - \frac{\partial}{\partial \vec{R}}\zeta(\vec{R})$. However because of the system evolves along a closed path $\mathcal{C}$ with $\vec{R}(T) = \vec{R}(0)$, the phase choice we made earlier on the basis function $|n(\vec{R})\rangle$ requires $e^{i\zeta(\vec{R})}$ in the gauge transformation to be single-valued, which implies $\zeta(\vec{R}(0)) - \zeta(\vec{R}(T)) = 2\pi \times$ integer. This shows that γ_n can be only changed by an integer multiple of 2π and it cannot be removed. Therefore the Berry phase γ_n is a gauge-invariant physical quantity.

In analogy to electrodynamics, a gauge field tensor is derived from the Berry vector potential:

$$\begin{aligned} B^n_{\mu\nu}(\vec{R}) &= \frac{\partial}{\partial R^\mu}\mathcal{A}^n_\nu(\vec{R}) - \frac{\partial}{\partial R^\nu}\mathcal{A}^n_\mu(\vec{R}) \\ &= i\Big[\langle\frac{\partial n(\vec{R})}{\partial R^\mu}|\frac{\partial n(\vec{R})}{\partial R^\nu}\rangle - (\nu \leftrightarrow \mu)\Big] . \end{aligned} \tag{1.7}$$

This field is called the Berry curvature, which can be also written as a summation over the eigenstates:

$$B^n_{\mu\nu}(\vec{R}) = i\sum_{n'\neq n}\frac{\langle n|\frac{\partial H(\vec{R})}{\partial R^\mu}|n'\rangle\langle n'|\frac{\partial H(\vec{R})}{\partial R^\nu}|n\rangle - (\nu \leftrightarrow \mu)}{(\varepsilon_n - \varepsilon_{n'})^2} . \tag{1.8}$$

Berry phase effects are fundamentally important in understanding electrical transport property in quantum Hall effect [92, 93], anomalous Hall effect [69, 94], and anomalous thermoelectric transport [95]. It is successful in characterizing the underlying mechanism of quantum spin Hall effect [96, 97]. Such an elegant connection between mathematics and physics provides a broad and deep understanding of basic material properties. There also have been some works using Berry phase description to study the underlying properties of the phonon transport, such as topological phonon modes in dynamic instability of microtubules [98], Berry-phase-induced heat pumping [99], and the Berry-phase contribution of molecular vibrational instability [100]. However, because of the very different nature of electrons and phonons, the underlying Berry phase effect and topological picture related to the PHE is not straightforward and obvious, and therefore, is still lacking.

1.6 Objectives

Current theories based on the perturbation approximation are not successful to explain the phonon Hall effect due to their controversial ambiguous derivations. It is unclear whether the phonon Hall effect can present in a ballistic phonon system. Based on the current theories, we still do not know the essential mechanism of the phonon Hall effect, and the various properties about the phonon Hall effect are lacking. The main aim of this thesis is to propose exact theories of the phonon Hall effect to uncover the underlying mechanism to investigate the existence and properties of phonon Hall effect in two-dimensional lattices. The objectives of this research are to

1. propose a theory of the phonon Hall effect in finite phonon systems by using nonequlibrium Green's function method applicable to a four-terminal junction crystal lattice;

2. examine conditions for existence of the phonon Hall effect by considering the symmetry of the dynamic matrix;

3. develop exact theories of the phonon Hall effect in infinite periodic systems by using the Green-Kubo formula;

4. study topological nature of the phonon Hall effect by looking at the Berry phase effect of the phonon bands, thus we can examine whether a quantized phonon Hall effect exists;

5. discuss various properties on the phonon Hall effect, such as dependence on the large range of magnetic fields and temperatures and associated

other effects.

The results of the present research may have significance on the understanding of the mechanism of the phonon Hall effect and could be generally applicable to different systems. This study may provide insights into the topological nature of not only the phonon Hall effect but also other boson Hall effects. The results of various properties could provide guidelines for the experiments on the phonon Hall effect. The focus of this thesis is to propose exact theories on the phonon Hall effect based on the Raman spin-phonon interaction. A first principle investigation on the spin-phonon coupling is excluded from this study. It should also be noted that the proposed exact theories in this study are restricted on the ballistic phonon system without nonlinear interaction. In this thesis, we will introduce the methods of nonequilibrium Green's function and Green-Kubo formula in Chapter 2; followed by the study on the phonon Hall effect in four-terminal junctions in Chapter 3. In Chapter 4, the theory of the phonon Hall effect in infinite periodic systems is proposed. At last, a conclusion of this study is given in Chapter 5.

Chapter 2

Methods

In this thesis, to study the PHE in finite junctions and in infinite crystal lattices, we will apply two approaches which have been the most commonly used methods in the thermal transport study. One is the nonequilibrium Green's function (NEGF) method which investigates the nonequilibrium steady state by connecting a system to heat baths at different fixed temperatures. The other one is the Green-Kubo Formula which studies the thermal conductivity relating with the equilibrium current correlation function. In the following two sections we give a brief introduction of these methods.

2.1 The NEGF Method

The NEGF method, which was first invented for electron transport, is an elegant and powerful method to calculate steady state properties of a finite system connected to reservoirs. The NEGF method has its root in quantum field theory [101]. The NEGF method treats nonequilibrium and interacting systems in a rigorous way; some of early formulations have been derived by

Schwinger [102], Kadanoff and Baym [103], and Keldysh [104]. Keldysh developed a diagram approach by using Feynman diagrams; Kadanoff and Baym created an equations of motion approach. Both approaches are well suitable for studying a dynamic system in nonequilibrium state. Using the Keldysh formalism of NEGF, one can obtain formal expressions of the current and other quantities such as electron density. The Keldysh diagrammatic expansion method has also been generalized to cases of correlated initial states [105]. Many studies on the electrical transport through junctions have been done by using NEGF [106, 107]; and some necessary backgrounds on the such method can be found in the books by Datta [147] and Haug and Jauho [109]. However, the application of NEGF method to thermal transport is relatively new. In recent ten years, the NEGF apprach has been used on thermal transport not only in ballistic transport [110–112,135] but also nonlinear transport [114–118]. Very recently, Wang *et al.* [119] has given a detailed review on the quantum thermal transport in nanostructures on the application of NEGF method to the thermal transport.

In the following, we will give an illustration on the NEGF application to the ballistic transport. For the thermal transport with nonlinear interaction, the procedure is similar, except for the self energy which could be treated by perturbation using Feynman diagrams.

2.1.1 Motivation for NEGF

In general, we can use a model of junction connected to two leads to study the thermal transport. We use a transformation for the coordinates, $u_j = \sqrt{m_j}\, x_j$,

where x_j is the relative displacement of j-th degree of freedom; and in this way, the kinetic energy is always in the form of $\frac{1}{2}\dot{u}^T\dot{u}$ (where T stands for matrix transpose). We use a superscript α to denote the region. Then u_j^α belongs to the region α; $\alpha = L, C, R$, for the left, center, and right regions, respectively. The Hamiltonian of the system is given by

$$H = \sum_{\alpha=L,C,R} H_\alpha + (u^L)^T V^{LC} u^C + (u^C)^T V^{CR} u^R + V_n, \tag{2.1}$$

where $H_\alpha = \frac{1}{2}(\dot{u}^\alpha)^T \dot{u}^\alpha + \frac{1}{2}(u^\alpha)^T K^\alpha u^\alpha$ represents the Hamiltonian of the region α; u^α is a column vector consisting of all the displacement variables in region α, and $\dot{u}^\alpha$ is the corresponding conjugate momentum. K^α is the spring constant matrix and $V^{LC} = (V^{CL})^T$ is the coupling matrix of the left lead to the central region; similarly for V^{CR}. There is no interaction between the two leads. The nonlinear part of the interaction V_n can be arbitrary; in this thesis we set $V_n = 0$ for ballistic transport.

As well known, the most important quantity to calculate in thermal transport is the heat flux. The heat flux is defined as the energy transferred from the heat source to the junction in a unit time, which is equal to the energy transferred from the junction to the heat sink in a unit time, with the assumption that no energy is accumulated in the junction. According to this definition, the heat flux out of the left lead is

$$I_L = -\langle \dot{H}_L(t) \rangle = i\langle [H_L(t), H] \rangle = i\langle [H_L(t), V^{LC}(t)] \rangle. \tag{2.2}$$

In the steady state, energy conservation means that $I_L + I_R = 0$. For simplicity, we set $\hbar = 1$ in this section. Using the Heisenberg equation of motion, we

obtain,

$$\begin{aligned} I_L &= \langle (\dot{u}^L)^T(t) V^{LC} u^C(t) \rangle \\ &= \sum_{j,k} \langle \dot{u}_j^L(t) V_{jk}^{LC} u_k^C(t) \rangle \\ &= \lim_{t' \to t} \sum_{j,k} V_{jk}^{LC} \langle \dot{u}_j^L(t') u_k^C(t) \rangle. \end{aligned} \tag{2.3}$$

Thus the heat flux depends on the expectation value of $\dot{u}_j^L(t')u_k^C(t)$. Such expectation value can be expressed in terms of the Green's function $G_{CL}^<(t,t') = -i\langle u^L(t')u^C(t)^T\rangle^T$. Since operators u and $\dot{u}$ are related in Fourier space as $\dot{u}[\omega] = -i\,\omega u[\omega]$, we can eliminate the derivative and get,

$$I_L = -\frac{1}{2\pi} \int_{-\infty}^{\infty} \mathrm{Tr}\left(V^{LC} G_{CL}^<[\omega]\right) \omega \, d\omega. \tag{2.4}$$

Therefore, If we obtain the Green's functions, we can calculate the heat flux. In the following section, we will introduce the several versions of the Green's functions and their relations.

2.1.2 Definitions of the Green's Functions and Their Relations

We start with the definition of six Green's functions [119–121]:

$$G^r(t,t') = -i\theta(t-t')\langle [u(t), u(t')^T] \rangle, \tag{2.5}$$

$$G^a(t,t') = i\theta(t'-t)\langle [u(t), u(t')^T] \rangle, \tag{2.6}$$

$$G^>(t,t') = -i\langle u(t)u(t')^T \rangle, \tag{2.7}$$

$$G^<(t,t') = -i\langle u(t')u(t)^T \rangle^T, \tag{2.8}$$

$$G^t(t,t') = \theta(t-t')G^>(t,t') + \theta(t'-t)G^<(t,t'), \tag{2.9}$$

$$G^{\bar{t}}(t,t') = \theta(t'-t)G^>(t,t') + \theta(t-t')G^<(t,t'). \tag{2.10}$$

They are known as retarded, advanced, greater, lesser, time-ordered, and anti-time ordered Green's functions, respectively. $u(t)$ is a column vector of the particle displacement in Heisenberg picture. The step function $\theta(t) = 1$ if $t \geq 0$ and 0 if $t < 0$. The notation $\langle [A, B^T] \rangle$ represents a matrix and should be interpreted as $\langle AB^T \rangle - \langle BA^T \rangle^T$.

In equilibrium or nonequilibrium steady states, the Green's functions depend only on the difference in time, $t-t'$. The Fourier transform of $G^r(t-t') = G^r(t,t')$ is defined as $G^r[\omega] = \int_{-\infty}^{+\infty} G^r(t) e^{i\omega t} dt$. The following linear relations hold in both frequency and time domains from the basic definitions [119]:

$$G^r - G^a = G^> - G^<, \tag{2.11}$$

$$G^t + G^{\bar{t}} = G^> + G^<, \tag{2.12}$$

$$G^t - G^{\bar{t}} = G^r + G^a. \tag{2.13}$$

Out of the six Green's functions, only three of them are linearly independent. However, in systems with time translational invariance, the functions G^r and G^a are hermitian conjugate of one other:

$$G^a[\omega] = (G^r[\omega])^\dagger. \tag{2.14}$$

So in general nonequilibrium steady-state situations, only two of them are independent. We usually choose G^r and $G^<$, but other choices are possible. There are other relations in the frequency domain as well [119]:

$$G^<[\omega]^\dagger = -G^<[\omega], \tag{2.15}$$

$$G^r[-\omega] = G^r[\omega]^*, \tag{2.16}$$

$$G^<[-\omega] = G^>[\omega]^T = -G^<[\omega]^* + G^r[\omega]^T - G^r[\omega]^*. \tag{2.17}$$

The last two equations show that we only need to compute the positive frequency part of the functions.

Equations (2.11) to (2.17) are generally valid for nonequilibrium steady states. In thermal equilibrium, there is an additional equation relating G^r and $G^<$:

$$G^<[\omega] = f(\omega)\Big(G^r[\omega] - G^a[\omega]\Big), \tag{2.18}$$

where $f(\omega)$ is the Bose-Einstein distribution function at temperature T. In equilibrium, we also have $G^>[\omega] = e^{\beta\omega}G^<[\omega]$. Thus in equilibrium, there is only one independent Green's function; we take it to be G^r.

2.1.3 Contour-Ordered Green's Function

To compute the Green's functions of the nonequilibrium systems, we need to use the concept of adiabatic switch-on. We imagine that at $t = -\infty$ the system has three decoupled regions, each at separate temperatures, T_L, T_C, and T_R. The couplings between the regions are turned off. The equilibrium Green's functions g^α at temperature T_α are known. The couplings V^{LC} and V^{CR} are then turned on slowly, and a steady state of the linear system is established at some time t_0. For this linear problem, the result does not depend on T_C; the initial condition of the finite center part is forgotten. If the system has nonlinear interaction V_n, we need another adiabatic switch-on for V_n. In this thesis, we will not consider the nonlinear interaction. By the adiabatic switch-on we can project the density matrix to the initial decoupled system,

for example, the time-order Green-function can be written as

$$\begin{aligned} G^t_{jk}(t,t') &= -i\langle T u_j(t) u_k(t')\rangle, \\ &\Downarrow \quad \text{if } t > t' \text{ then} \\ &= -i\mathrm{Tr}\left(\rho_H(t_0) U(t_0,t) u^t_j U(t,t_0) U(t_0,t') u^{t'}_k U(t',t_0)\right) \\ &\Downarrow \quad \rho_H(t_0) = \rho_S(t_0) = U(t_0,-\infty)\rho_S(-\infty)U(-\infty,t_0) \\ &= -i\mathrm{Tr}\big(\rho_S(-\infty)U(-\infty,t_0)U(t_0,t)U(t,\infty)U(\infty,t) \\ &\quad u^t_j U(t,t_0)U(t_0,t')u^{t'}_k U(t',t_0)U(t_0,-\infty)\big) \end{aligned} \tag{2.19}$$

Here $U(t,t')$ is the evolution operator with interface coupling V^{LC} and V^{CR}; ρ_H and ρ_S are the density matrix in Heisenberg and Schrödinger representations, respectively. Therefore the Green's function relates to the evolution along the path from $-\infty$ to $+\infty$ and back from $+\infty$ to $-\infty$, we can define the contour-ordered Green's function as

$$\begin{aligned} G(\tau,\tau') &= -i\mathrm{Tr}\left(\rho_S(-\infty) T_\tau e^{-i\int_c H(\tau'')d\tau''} u^\tau u^{\tau' T}\right) \\ &= -i\langle T_\tau u(\tau) u(\tau')^T\rangle, \end{aligned} \tag{2.20}$$

where the variable τ is on a Keldysh contour from $-\infty$ to $+\infty$ and back from $+\infty$ to $-\infty$. The contour-ordered Green's function includes four different Green's functions given earlier [119]:

$$G^{\sigma\sigma'}(t,t') = \lim_{\epsilon\to 0^+} G(t+i\epsilon\sigma, t'+i\epsilon\sigma'), \quad \sigma = \pm(1). \tag{2.21}$$

We have introduced a branch index σ, such that $\tau = t + i\epsilon\sigma$. $\sigma = +1$ means τ is at the $-\infty$ to $+\infty$ branch, while $\sigma = -1$ means τ is at the returning branch. With this notation, we can identify that $G^{++} = G^t$, $G^{--} = G^{\bar{t}}$, $G^{+-} = G^<$,

and $G^{-+} = G^{>}$, or in a matrix form

$$G(\tau, \tau') \rightarrow \begin{pmatrix} G^{t} & G^{<} \\ G^{>} & G^{\bar{t}} \end{pmatrix}. \tag{2.22}$$

In dealing with the contour-ordered Green's functions, we often encounter convolution of the form

$$B(\tau, \tau') = \int d\tau_1 \int d\tau_2 \cdots A_1(\tau, \tau_1) A_2(\tau_1, \tau_2) \cdots A_n(\tau_{n-1}, \tau'). \tag{2.23}$$

This form of expression can be easily translated into the retarded and lesser Green's functions in frequency domain by the Langreth theorem as [109, 119, 122, 123]

$$B^{r,a}[\omega] = A_1^{r,a}[\omega] A_2^{r,a}[\omega] \cdots A_n^{r,a}[\omega], \quad n = 2, 3, \cdots \tag{2.24}$$

$$\begin{aligned} B^{<,>}[\omega] = {} & A_1^{r}[\omega] \cdots A_{n-1}^{r}[\omega] A_n^{<,>}[\omega] + \\ & A_1^{r}[\omega] \cdots A_{n-2}^{r}[\omega] A_{n-1}^{<,>}[\omega] A_n^{a}[\omega] + \\ & \cdots + A_1^{<,>}[\omega] A_2^{a}[\omega] \cdots A_{n-1}^{a}[\omega] A_n^{a}[\omega]. \end{aligned} \tag{2.25}$$

2.1.4 Equation of Motion

An efficient method to obtain the Green's functions of interacting systems is through the equation of motion of the Green's functions. The equation of motion for the nonequilibrium Green's function is equivalent to the Keldysh formalism [119, 124].

If we regard the system as a whole, the contour ordered Green's function satisfies

$$-\frac{\partial^2 G(\tau, \tau')}{\partial \tau^2} - K G(\tau, \tau') = I \delta(\tau, \tau'). \tag{2.26}$$

This is obtained from taking derivatives twice to the definition of the contour-ordered Green's function [119]. If we partition the matrix G to the submatrices $G^{\alpha,\alpha'}$, $\alpha, \alpha' = L, C, R$, and similarly for K, we can obtain the equations related on $G^{\alpha,\alpha'}$. We can easily get the free Green's function for the system decoupled as

$$-\frac{\partial^2 g^\alpha(\tau,\tau')}{\partial\tau^2} - K^\alpha g^\alpha(\tau,\tau') = I\delta(\tau,\tau'). \tag{2.27}$$

The corresponding ordinary Green's functions in frequency domain can be written as

$$g^r_\alpha[\omega] = \left[(\omega+i\eta)^2 - K^\alpha\right]^{-1}, \tag{2.28}$$

where η is an infinitesimal positive quantity to single out the correct path around the poles when performing an inverse Fourier transform, such that $g^r(t) = 0$ for $t < 0$. Other Green's functions can be obtained through the general relations among the Green's functions, e.g., $g^<[\omega] = f(\omega)\big(g^r[\omega] - g^a[\omega]\big)$.

We also can obtain the contour-ordered nonequilibrium Green's functions as

$$G^{LC}(\tau,\tau') = \int d\tau'' g^L(\tau,\tau'')V^{LC}G_0^{CC}(\tau'',\tau'), \tag{2.29}$$

$$\begin{aligned} G^{CC}(\tau,\tau') &= g^C(\tau,\tau') + \\ &\int d\tau_1 \int d\tau_2\, g^C(\tau,\tau_1)\Sigma(\tau_1,\tau_2)G^{CC}(\tau_2,\tau'). \end{aligned} \tag{2.30}$$

The self-energy $\Sigma(\tau_1,\tau_2)$ is given by

$$\Sigma(\tau_1,\tau_2) = V^{CL}g^L(\tau_1,\tau_2)V^{LC} + V^{CR}g^R(\tau_1,\tau_2)V^{RC}. \tag{2.31}$$

In ordinary Green's functions and in frequency domain (ω argument suppressed), the above Dyson equation has solutions [109]:

$$G^r_{CC} = \big((\omega+i\eta)^2 I - K^C - \Sigma^r\big)^{-1}, \tag{2.32}$$

$$G^<_{CC} = G^r_C \Sigma^< G^a_C. \tag{2.33}$$

2.1.5 Heat Flux and Conductance

By applying the Langreth theorem Eq. (2.25) to Eq. (2.29), we have $G^<_{CL}[\omega] = G^r_{CC}[\omega]V^{CL}g^<_L[\omega] + G^<_{CC}[\omega]V^{CL}g^a_L[\omega]$. Then the heat flux can be written as

$$I_L = -\frac{1}{2\pi}\int_{-\infty}^{+\infty} d\omega\, \omega\, \mathrm{Tr}\Big(G^r[\omega]\Sigma^<_L[\omega] + G^<[\omega]\Sigma^a_L[\omega]\Big), \tag{2.34}$$

For notational simplicity, we have dropped the subscript C on the Green's functions denoting the central region. We can obtain a symmetrized expression with respect to left and right lead and make it explicitly real,

$$I = \frac{1}{4}(I_L + I^*_L - I_R - I^*_R) \tag{2.35}$$

In the end, we can get the Landauer-like formula

$$I = \int_0^\infty \frac{d\omega}{2\pi}\, \hbar\omega\, T[\omega]\big(f_L - f_R\big), \tag{2.36}$$

where $f_{L,R} = \big\{\exp[\hbar\omega/(k_B T_{L,R})] - 1\big\}^{-1}$ is the Bose-Einstein (or Planck) distribution for phonons, and $T[\omega]$ is known as the transmission coefficient, written in the so-called Caroli formula as

$$T[\omega] = \mathrm{Tr}(G^r \Gamma_L G^a \Gamma_R). \tag{2.37}$$

Here, $G^r = G^r_{CC} = \big[(\omega+i\eta)^2 I - K^C - \Sigma^r_L - \Sigma^r_R\big]^{-1}$, the self-energy of the leads is $\Sigma^r_\alpha = V^{C\alpha} g^r_\alpha V^{\alpha C}$, and $\Gamma_\alpha = i(\Sigma^r_\alpha - \Sigma^a_\alpha) = -2\,\mathrm{Im}\,(V^{C\alpha} g^r_\alpha V^{\alpha C})$.

We define the thermal conductance as

$$\sigma = \lim_{\Delta T \to 0} \frac{I}{\Delta T}, \tag{2.38}$$

where ΔT is the difference of the temperatures between the leads, such that $T_L = T + \Delta T/2$ and $T_R = T - \Delta T/2$. For the ballistic transport, the conductance can be written as

$$\sigma = \frac{1}{2\pi} \int_0^\infty d\omega \, \omega \, T[\omega] \frac{\partial f(\omega)}{\partial T}. \tag{2.39}$$

2.2 Green-Kubo Formula

The Green-Kubo formula, which provides a relation between the thermal conductivity κ or the electrical conductivity σ and equilibrium time correlation functions of the corresponding current, is widely used to study the electrical and thermal transport. For the thermal conductivity in a classical infinite $1D$ system, the Green-Kubo formula reads:

$$\kappa = \frac{1}{k_B T^2} \lim_{t \to \infty} \lim_{L \to \infty} \frac{1}{L} \int_0^t dt \langle J(0) J(t) \rangle, \tag{2.40}$$

where J is the total heat current, $\langle \cdot \rangle$ denote the average over the equilibrium ensemble at a temperature T.

Based on certain assumptions, such as normal diffusion, Green and Kubo first derived the Green-Kubo formula [125–128], followed by a number of various derivations [129–135], all of which require certain assumptions thus none of these derivations are rigorous. However, they are quite convincing because the assumptions made are satisfied in a large number of practical application. Thus it is justified for the wide use of the Green-Kubo formula in calculating thermal conductivity and transport properties of different systems [135].

Very recently, Liu *et. al* [136] derives a universal equality relating heat current autocorrelation function to the variance of the energy distribution, based on which the authors recover the existing theories for normal heat conduction using the Green-Kubo formula. And on the other hand, with the assumption of normal conduction one can easily obtain the Green-Kubo formula. According to Ref. [136], an schematic derivation of the Green-Kubo formula is given in the following, by which the physical picture can be easily understood. For a 1D continuous and infinite system in thermal equilibrium, we have the the energy continuity equation as

$$\frac{\partial \epsilon(x,t)}{\partial t} + \frac{\partial j(x,t)}{\partial x} = 0. \tag{2.41}$$

Where $\epsilon(x,t)$ and $j(x,t)$ denote the energy density fluctuation and heat flux density at position x at time t, respectively. Multiplying Eq. (2.41) by $\epsilon(x',t')$ and $j(x',t')$ respectively, and taking the average, we obtain [136]:

$$\frac{\partial^2 C_{\epsilon\epsilon}(x,t)}{\partial t^2} + \frac{\partial^2 C_{jj}(x,t)}{\partial x^2} = 0, \tag{2.42}$$

where $C_{\epsilon\epsilon}(x,t) = \langle \epsilon(0,0)\epsilon(x,t)\rangle$ and $C_{jj}(x,t) = \langle j(0,0)j(x,t)\rangle$.

According Ref. [136, 137], the probability density function for the energy diffusion can be written as

$$\rho(x,t) = \frac{1}{k_B T^2 c}\langle \epsilon(x,t)\epsilon(0,0)\rangle = \frac{1}{k_B T^2 c} C_{\epsilon\epsilon}(x,t), \tag{2.43}$$

which is obtained from equilibrium statistical mechanics. Here, c specific heat capacity. Based on Eq. (2.43), the variance of the distribution is written as $\langle x^2(t)\rangle = \frac{1}{k_B T^2 c}\int_{-\infty}^{\infty} x^2 C_{\epsilon\epsilon}(x,t)dx$. Using the relation of Eq. (2.42), we obtain [136]

$$\frac{d^2\langle x^2(t)\rangle}{dt^2} = \frac{2}{k_B T^2 c}\int_{-\infty}^{\infty} C_{jj}(x,t)dx, \tag{2.44}$$

We know that $\int_{-\infty}^{\infty} C_{jj}(x,t)dx = \lim_{L\to\infty} \frac{1}{L}\langle J(0)J(t)\rangle$, where J is the total heat current. For a normal diffusion, $\langle x^2(t)\rangle = 2Dt\,(t>0)$, where D is the diffusion coefficient. The energy current satisfies Fourier's law which we write in the form $J(x,t) = -D\partial u(x,t)/\partial x$ where $D = \kappa/c$. Based on such assumption, in the end we can obtain the Green-Kubo formula as

$$\kappa = \frac{1}{k_B T^2} \lim_{L\to\infty} \frac{1}{L} \int_0^{\infty} dt \langle J(0)J(t)\rangle. \tag{2.45}$$

For finite systems, people also use the Green-Kubo formula to study the thermal conductivity by coupling the system to infinite reservoirs [138–140]. It has been shown that Green-Kubo like expressions for the linear-response heat current in finite open systems can be derived rigorously by using the steady state fluctuation theorem [141–145]. which has been done for lattice models coupled to stochastic Markovian baths [135].

For the ballistic transport, the thermal conductivity diverges; thus the Green-Kubo formula is not applicable to study the thermal transport. In such case, one is interested in the conductance instead of the conductivity. For the phonon Hall conductivity, the spin-phonon interaction plays an key role for the transverse thermal transport, the conductivity κ_{xy} may not be divergent, thus the Green-Kubo formula could be applicable. The Green-Kubo formula shown above is the classic version, for quantum transport, we should replace the current correlation with canonical correlation of the two currents, then the formula reads as

$$\kappa = \frac{1}{k_B T^2} \lim_{L\to\infty} \frac{1}{L} \int_0^{\infty} dt \langle J(0); J(t)\rangle, \tag{2.46}$$

where the canonical correlation is defined as

$$\langle a; b\rangle = \frac{1}{\beta}\int_0^\beta d\xi \mathrm{Tr}[e^{-\beta H}e^{\xi H}ae^{-\xi H}b]/\mathrm{Tr}[e^{-\beta H}]. \tag{2.47}$$

By variable substitution $\lambda = \xi\hbar$, and using the relation $a(t) = e^{iHt/\hbar}a(0)e^{-iHt/\hbar}$, in the end the Green-Kubo formula for the quantum thermal transport can be written as

$$\kappa = \frac{1}{\hbar TL}\int_0^{\hbar/(k_BT)} d\lambda \int_0^\infty dt \left\langle J(-i\lambda)J(t)\right\rangle. \tag{2.48}$$

Chapter 3

Phonon Hall Effect in Four-Terminal Junctions

In this chapter, we study the PHE in a finite four-terminal system by taking into account the actual experimental measuring process. By connecting the two-dimensional (2D) sample (certain thin film paramagnetic dielectrics) to two heat baths in two different temperatures, a steady heat flux will flow along the sample in longitudinal direction. Applying a magnetic field perpendicular to the heat flux (the plane of the sample), we connect two probe-leads (two thermometers) to the middle of sample in the transverse direction, as shown in Fig. 3.1. After the thermal transport reaches a steady state when the heat enter the probe leads is zero, we would obtain two different temperatures at the upper and lower probe-leads if the PHE can exist in the system. We will use the NEGF approach to study the PHE in such four-terminal nanoscale system to calculate the temperature difference in the transverse direction.

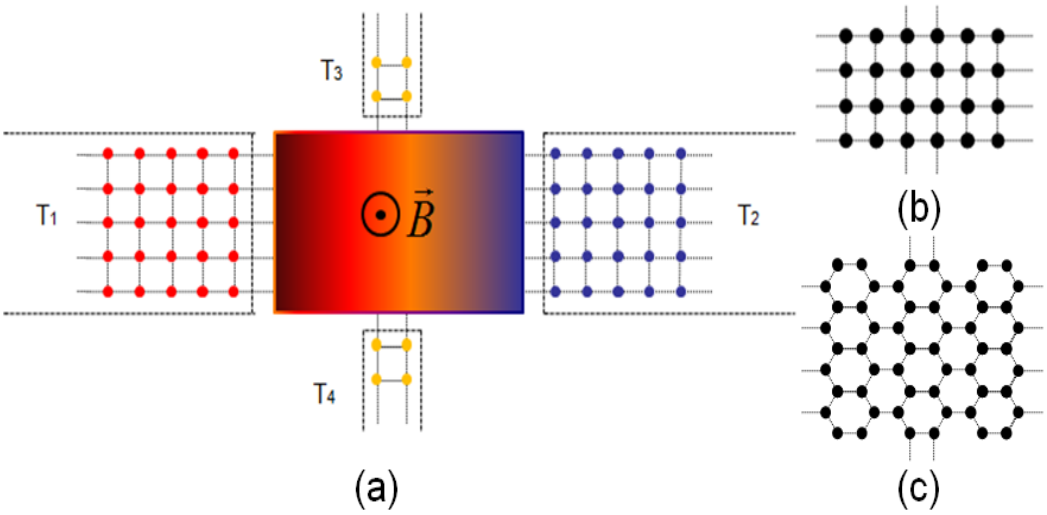

Figure 3.1: The four-terminal PHE setup used for calculating the thermal conductance and the temperature difference $T_3 - T_4$. (a) The left and right leads have temperatures T_1 and T_2, the upper and lower probe-leads have temperatures T_3 and T_4. The center part can be different lattices, such as square lattices (b) or honeycomb lattices (c).

3.1 Model

To develop a nonperturbative theory for PHE in nanoscale four terminal junctions, we consider a model shown Fig. 3.1. The left and right heat baths are at temperature T_1 and T_2. If we apply a magnetic field normal to the plane of the setup, we would obtain two different temperatures at the upper and lower probe-leads, that is, $T_3 - T_4 \neq 0$, if the PHE can occur in the system. The center part can be different lattices, such as square, triangle or honeycomb lattices. We denote the lattice as $N_R \times N_C$, where N_R, N_C correspond to the number of rows and columns, respectively. For Fig. 3.1(b), $N_R = 4$, $N_C = 6$; for Fig. 3.1(c), $N_R = 9$, $N_C = 6$. Our model systems can produce features similar to experiments, such as the magnitude of Hall temperature difference and the linear dependence on magnetic fields, even though our systems are of

nanometer scale while the experimental systems are of millimeter scale and are in the diffusive regime.

3.2 Theory for the PHE Using NEGF

3.2.1 Hamiltonian

We consider the Hamiltonian of SPI as discussed in the chapter of introduction, which is written as

$$H_I = \sum_n \vec{h} \cdot (\vec{U}_n \times \vec{P}_n), \tag{3.1}$$

where, $\vec{h} = gc\vec{M}$, has the units of frequency. According to [13], h is estimated to be $0.1\,\mathrm{cm}^{-1} \approx 3 \times 10^9\,\mathrm{Hz}$ at $B = 1\,\mathrm{T}$ and $T = 5.45\,\mathrm{K}$, which is within the possible range of the coupling strength in ionic insulators [79, 80]. In our calculation, we will use this relation to map h to magnetic field B.

The total Hamiltonian is assumed to be

$$H = \sum_{\alpha=C,L,R,U,N} H_\alpha + \sum_{\beta=L,R,U,N} (U^\beta)^T V^{\beta C} U^C + (U^C)^T A P^C, \tag{3.2}$$

where $H_\alpha = \frac{1}{2}\left((P^\alpha)^T P^\alpha + (U^\alpha)^T K^\alpha U^\alpha\right)$; and A is an antisymmetric, block diagonal matrix with the diagonal elements $\begin{pmatrix} 0 & h \\ -h & 0 \end{pmatrix}$. Here, the notations C, L, R, U, and N are associated with the center region, left, right, upper, and nether leads, respectively. U^α (P^α) are column vectors consisting of all the displacement (momentum) variables in region α. K^α is the spring constant matrix and $V^{\beta C} = (V^{C\beta})^T$ is the coupling matrix between the β lead and the

central region. The dynamic matrix of the full linear system without SPI is

$$K = \begin{pmatrix} K^L & 0 & V^{LC} & 0 & 0 \\ 0 & K^U & V^{UC} & 0 & 0 \\ V^{CL} & V^{CU} & K^C & V^{CN} & V^{CR} \\ 0 & 0 & V^{NC} & K^N & 0 \\ 0 & 0 & V^{RC} & 0 & K^R \end{pmatrix}. \tag{3.3}$$

There will be no interaction between the leads. We consider the leads as semi-infinite quasi-one dimensional square lattices as discussed in Sec.2.1 of Chapter 2.

3.2.2 Green's Functions

Based on the Hamiltonian Eq. (3.2), we obtain the equation for U^C and P^C as

$$\frac{\partial U^C(\tau)}{\partial \tau} = P^C(\tau) - AU^C(\tau); \tag{3.4}$$

$$\frac{\partial P^C(\tau)}{\partial \tau} = -K^C U^C(\tau) - \sum_{\beta=L,R,U,N} V^{C\beta} U^\beta - AP^C(\tau). \tag{3.5}$$

We define the contour-ordered Green's function as

$$G^{\alpha\beta}(\tau,\tau') \equiv -\frac{i}{\hbar}\left\langle T_c\, U^\alpha(\tau)(U^\beta(\tau'))^T \right\rangle, \tag{3.6}$$

where α and β refer to the region that the coordinates belong to and T_c is the contour-ordering operator. Then the first derivative of the contour ordered Green's function with respect to τ can be derived as

$$\frac{\partial}{\partial \tau} G^{CC}(\tau,\tau') = -\frac{i}{\hbar}\left\langle T_c\, P^C(\tau)(U^C(\tau'))^T \right\rangle - AG^{CC}(\tau,\tau'). \tag{3.7}$$

We define $Y(\tau,\tau') \equiv -\frac{i}{\hbar}\left\langle T_c\, P^C(\tau)(U^C(\tau'))^T\right\rangle$, then we obtain

$$\frac{\partial}{\partial\tau}Y(\tau,\tau') = -\delta(\tau,\tau') - K^C G^{CC}(\tau,\tau') - \int \Sigma(\tau,\tau'')G^{CC}(\tau'',\tau')d\tau'' - AY(\tau,\tau'), \tag{3.8}$$

where $\Sigma(\tau,\tau') = \sum_{\alpha=L,R,U,N}\Sigma_\alpha(\tau,\tau')$, and $\Sigma_\alpha(\tau,\tau')$ is the self energy of each lead. Combining Eqs. (3.7, 3.8), $Y(\tau,\tau')$ can be eliminated, and the equation of motion of the Green's function can be written as

$$(\frac{\partial^2}{\partial\tau^2} + K^C + A^2 + 2A\frac{\partial}{\partial\tau})G^{CC}(\tau,\tau') = -\delta(\tau,\tau') - \int \Sigma(\tau,\tau'')G^{CC}(\tau'',\tau')d\tau''. \tag{3.9}$$

By doing Fourier transformation, the retarded Green's function for the central region in frequency domain is

$$G^r[\omega] = \Big[(\omega+i\eta)^2 - K^C - \Sigma^r[\omega] - A^2 + 2i\omega A\Big]^{-1}. \tag{3.10}$$

Here, $\Sigma^r[\omega] = \sum_{\alpha=L,R,U,N}\Sigma^r_\alpha[\omega]$; and $\Sigma^r_\alpha[\omega] = V_{C\alpha}g^r_\alpha[\omega]V_{\alpha C}$ is the self-energy due to interaction with the heat bath; and $g^r_\alpha[\omega] = [(\omega+i\eta)^2 - K^\alpha]^{-1}$ is the Green's function of the lead. We omit the notation CC here and in the following for simplicity. The lesser Green's function of the central region is obtained through

$$G^<[\omega] = G^r[\omega]\Sigma^<[\omega]G^a[\omega]$$

in the usual way. Here A term contributes to the less Green's function $G^<$ through both G^r and G^a.

3.2.3 Heat Current

The energy flux to the central region from the lead α is,

$$I_\alpha = -\left\langle \dot{H}_\alpha\right\rangle = \frac{i}{\hbar}\left\langle[H_\alpha, H]\right\rangle, \quad \alpha = L,R,U,N. \tag{3.11}$$

By inserting the Hamiltonian H, H_α and using the commutation relation between U and P, we obtain

$$\begin{aligned} I_\alpha &= \left\langle (U^C)^T V^{C\alpha} P^\alpha \right\rangle \\ &= \sum_{l,j} \left\langle U_l^C V_{lj}^{C\alpha} P_j^\alpha \right\rangle \\ &= \sum_{l,j} V_{jl}^{\alpha C} \left\langle P_j^\alpha U_l^C \right\rangle . \end{aligned} \tag{3.12}$$

Here, U^C and P^α ($\alpha \neq C$) commute at the same time, and $V_{lj}^{C\alpha} = V_{jl}^{\alpha C}$. By definition of

$$G_{lj}^{C\alpha <}(t,t') \equiv -\frac{i}{\hbar} \left\langle U_j^\alpha(t') U_l^C(t) \right\rangle , \tag{3.13}$$

and

$$\frac{\partial}{\partial \tau'} G_{lj}^{C\alpha <}(t,t') \equiv -\frac{i}{\hbar} \left\langle P_j^\alpha(t') U_l^C(t) \right\rangle , \tag{3.14}$$

we can rewrite the heat flux as

$$\begin{aligned} I_\alpha &= \sum_{l,j} V_{jl}^{\alpha C} i\hbar \frac{\partial}{\partial t'} G_{lj}^{C\alpha <}(t,t')|_{t=t'} \\ &= i\hbar \mathrm{Tr}\big[V^{\alpha C} \frac{\partial}{\partial t'} G^{C\alpha <}(t,t')|_{t=t'} \big]. \end{aligned} \tag{3.15}$$

Using the Fourier transformation

$$G^{C\alpha <}(t,t') = \int_{-\infty}^{\infty} \frac{d\omega}{2\pi} G^{C\alpha <}[\omega] e^{-i(t-t')\omega}, \tag{3.16}$$

we obtain

$$I_\alpha = -\int_{-\infty}^{\infty} \frac{d\omega}{2\pi} \hbar\omega \mathrm{Tr}(V^{\alpha C} G^{C\alpha <}[\omega]). \tag{3.17}$$

For our multi-lead system, we also can derive the contour Green's function of

$$G^{C\alpha}(\tau,\tau') = \int G^{CC}(\tau,\tau'') V^{C\alpha} g^\alpha(\tau'',\tau) d\tau'', \tag{3.18}$$

and applying Langreth theorem, we get

$$G^{C\alpha <}(t,t') = \int \left[G^r(t,t'')V^{C\alpha}g^<_\alpha(t'',t) + G^<(t,t'')V^{C\alpha}g^a_\alpha(t'',t)\right]dt'', \quad (3.19)$$

in frequency domain which can be written as

$$G^{C\alpha <}[\omega] = G^r[\omega]V^{C\alpha}g^<_\alpha[\omega] + G^<[\omega]V^{C\alpha}g^a_\alpha[\omega], \quad (3.20)$$

then the heat flux reads as

$$I_\alpha = -\int_{-\infty}^{\infty}\frac{d\omega}{2\pi}\,\hbar\omega \mathrm{Tr}\big(G^r\Sigma^<_\alpha + G^<\Sigma^a_\alpha\big). \quad (3.21)$$

Using the relation of

$$\begin{aligned}\Sigma^<_\alpha &= f_\alpha(\Sigma^r_\alpha - \Sigma^a_\alpha)\\ &= -if_\alpha\Gamma_\alpha,\end{aligned} \quad (3.22)$$

with $f = \left(e^{\hbar\omega/k_BT}-1\right)^{-1}$ and $\Gamma_\alpha = i\big(\Sigma^r_\alpha[\omega] - \Sigma^a_\alpha[\omega]\big)$, we obtain

$$I_\alpha = -\int_{-\infty}^{\infty}\frac{d\omega}{4\pi}\,\hbar\omega \mathrm{Tr}\big(-if_\alpha(G^r - G^a)\Gamma_\alpha + G^r(\sum_\beta f_\beta\Gamma_\beta)G^a\Gamma_\alpha\big). \quad (3.23)$$

Where we replace the heat flux with a half of the sum of itself and its complex conjugate because the heat flux must be real. Using Eq. (3.10) and the antisymmetric property of A, $A^\dagger = -A$, we obtain

$$G^{r-1} - G^{a-1} = i\sum_\beta \Gamma_\beta, \quad (3.24)$$

then we get

$$G^a - G^r = iG^r\sum_\beta \Gamma_\beta G^a. \quad (3.25)$$

Therefore, the heat flux can be further written as

$$I_\alpha = \int_{-\infty}^{\infty}\frac{d\omega}{4\pi}\,\hbar\omega \sum_{\beta=L,R,U,N} T_{\beta\alpha}[\omega](f_\alpha - f_\beta), \quad (3.26)$$

where $T_{\beta\alpha}$ is the transmission coefficient from αth lead to βth lead, written as

$$T_{\beta\alpha}[\omega] = \mathrm{Tr}\big(G^r[\omega]\Gamma_\beta[\omega]G^a[\omega]\Gamma_\alpha[\omega]\big). \tag{3.27}$$

Because of $G^r[-\omega] = G^r[\omega]^*$, $G^a[-\omega] = G^a[\omega]^*$, and $\Gamma[-\omega] = -\Gamma[\omega]^*$, we can get

$$T_{\beta\alpha}[-\omega] = T_{\beta\alpha}[\omega]^* = T_{\beta\alpha}[\omega]. \tag{3.28}$$

We know the $T_{\beta\alpha}$ should be real form the above derivation. Using the sum of $T_{\beta\alpha}$ and its complex conjugate to derive the heat flux, therefore we finally get the heat flux as

$$I_\alpha = \int_0^\infty \frac{d\omega}{2\pi}\,\hbar\omega \sum_{\beta=L,R,U,N} T_{\beta\alpha}[\omega](f_\alpha - f_\beta). \tag{3.29}$$

If the temperature differences among the leads are very small, we can treat the system in linear response regime, $T_\alpha = T + \Delta_\alpha$. The linearized heat flux from each heat bath can be written as

$$I_\alpha = \sum_{\beta=1}^{4} \sigma_{\beta\alpha}(\Delta_\alpha - \Delta_\beta). \tag{3.30}$$

The conductance from heat bath α to β is defined as

$$\sigma_{\beta\alpha} = \int_0^\infty \frac{d\omega}{2\pi}\,\hbar\omega T_{\beta\alpha}[\omega]\frac{\partial f}{\partial T}. \tag{3.31}$$

Equations (3.30) and (3.31) are the Landauer-Büttiker theory [147,148] applied to the multiple-lead thermal transport.

3.2.4 Relative Hall Temperature Difference

In the following we simplify the notation of L, R, U, and N as 1, 2, 3, and 4, respectively. To measure the phonon Hall effect, we adjust temperatures

of the upper and nether probes T_3 and T_4 such that the heat currents from these two leads vanish, namely, $I_3 = I_4 = 0$. Because $\sum_\alpha I_\alpha = 0$, we obtain $I_1 + I_2 = 0$. Using the Eq. (3.30), we then obtain the following equations:

$$\begin{aligned} I_1 &= \sigma_{21}(\Delta_1 - \Delta_2) + \sigma_{31}(\Delta_1 - \Delta_3) + \sigma_{41}(\Delta_1 - \Delta_4) = I; && (3.32)\\ I_2 &= \sigma_{12}(\Delta_2 - \Delta_1) + \sigma_{32}(\Delta_2 - \Delta_3) + \sigma_{42}(\Delta_2 - \Delta_4) = -I; && (3.33)\\ I_3 &= \sigma_{13}(\Delta_3 - \Delta_1) + \sigma_{23}(\Delta_3 - \Delta_2) + \sigma_{43}(\Delta_3 - \Delta_4) = 0; && (3.34)\\ I_4 &= \sigma_{14}(\Delta_4 - \Delta_1) + \sigma_{24}(\Delta_4 - \Delta_2) + \sigma_{34}(\Delta_4 - \Delta_3) = 0. && (3.35) \end{aligned}$$

We define the relative Hall temperature difference as

$$R = \frac{T_3 - T_4}{T_1 - T_2} = \frac{\Delta_3 - \Delta_4}{\Delta_1 - \Delta_2}. \tag{3.36}$$

We can get the relative Hall temperature difference as

$$R = \frac{\sigma_{13}\sigma_{24} - \sigma_{14}\sigma_{23}}{(\sigma_{13} + \sigma_{23} + \sigma_{43})(\sigma_{14} + \sigma_{24} + \sigma_{34}) - \sigma_{43}\sigma_{34}}. \tag{3.37}$$

3.2.5 Symmetry of $T_{\alpha\beta}, \sigma_{\alpha\beta}$ and R

From the above derivation, we know that

$$T_{\beta\alpha}[\omega, A] = T_{\beta\alpha}[-\omega, A]. \tag{3.38}$$

From Eq. (3.10), we obtain

$$G^r[-\omega, A] = G^a[\omega, -A]; \tag{3.39}$$

and we also have

$$\begin{aligned} \Gamma[-\omega] &= i(\Sigma^r[-\omega] - \Sigma^a[-\omega]) \\ &= i(\Sigma^a[\omega] - \Sigma^r[\omega]) \\ &= -\Gamma[\omega], \end{aligned} \tag{3.40}$$

which is independent of A, thus we get

$$\begin{aligned} T_{\beta\alpha}[\omega, A] &= \mathrm{Tr}\big(G^r[-\omega, A]\Gamma_\beta[-\omega]G^a[-\omega, A]\Gamma_\alpha[-\omega]\big) \\ &= \mathrm{Tr}\big(G^a[\omega, -A]\Gamma_\beta[\omega]G^r[\omega, -A]\Gamma_\alpha[\omega]\big) \\ &= \mathrm{Tr}\big(G^r[\omega, -A]\Gamma_\alpha[\omega]G^a[\omega, -A]\Gamma_\beta[\omega]\big) \\ &= T_{\alpha\beta}[\omega, -A]. \end{aligned} \tag{3.41}$$

Then symmetry of the transmission is

$$T_{\beta\alpha}[\omega, h] = T_{\alpha\beta}[\omega, -h], \tag{3.42}$$

Using Eq.(3.31), we easily obtain the symmetry of the conductance as

$$\sigma_{\beta\alpha}(h) = \sigma_{\alpha\beta}(-h). \tag{3.43}$$

To investigate the phonon Hall effect, we should avoid the transverse temperature difference from the structural asymmetry. Therefore, we choose our system parameters which have mirror reflection symmetries along both x and y directions. Then we obtain the following relations,

$$\sigma_{13}(h) = \sigma_{14}(-h), \tag{3.44}$$

$$\sigma_{23}(h) = \sigma_{24}(-h). \tag{3.45}$$

Combining the Eq. (3.43), we can easily find that the numerator of R in Eq. (3.37) is odd function of h, and the dominator of R is even function of h, thus the symmetry of R is

$$R(-h) = -R(h). \tag{3.46}$$

Therefore the PHE is an odd function of the magnetic field if the PHE can exist in the system, which is consistent with all the experiments and theoretical studies.

3.2.6 Necessary Condition for PHE

If $R = 0$, then we could say that there is no PHE in the system. To yield $R = 0$, we could choose

$$\sigma_{\alpha\beta}(-h) = \sigma_{\alpha\beta}(h). \tag{3.47}$$

Within such choice, we could get

$$\sigma_{13}(h) = \sigma_{13}(-h) = \sigma_{14}(h), \tag{3.48}$$

$$\sigma_{24}(h) = \sigma_{24}(-h) = \sigma_{23}(h); \tag{3.49}$$

Then we easily obtain the result $R = 0$. Due to Eq. (3.31), for no PHE, we only need to find the condition to satisfy

$$T_{\alpha\beta}(-h) = T_{\alpha\beta}(h). \tag{3.50}$$

Based on such consideration, we find that if there is a symmetry operation S such that

$$S\,K\,S^{-1} = K, \quad S\,A\,S^{-1} = -A, \tag{3.51}$$

where the matrix S is a big matrix which is block diagonal with the symmetry operation element, such as the mirror reflection for our model. Such symmetry operation also holds for all the matrices K^{α} and $V^{\alpha\beta}$ then $T_{\alpha\beta}(-h) = T_{\alpha\beta}(h)$, and no PHE exists in the system. We prove this in the following. Under the symmetry operation, we get

$$\begin{aligned} S\,g^r[\omega]\,S^{-1} &= S\,[(\omega + i\eta)^2 - K^{\alpha}]^{-1}\,S^{-1} \\ &= \{S\,[(\omega + i\eta)^2 - K^{\alpha}]\,S^{-1}\}^{-1} \\ &= g^r[\omega]; \end{aligned} \tag{3.52}$$

and we also can get

$$S\,\Sigma^r[\omega]\,S^{-1} = \Sigma^r[\omega]; \quad S\,\Gamma^r[\omega]\,S^{-1} = \Gamma^r[\omega]. \tag{3.53}$$

Based on Eq. (3.10) and the relation Eq. (3.51), we get

$$\begin{aligned} SG^r(A)S^{-1} &= S\Big[(\omega+i\eta)^2 - K^C - \Sigma^r[\omega] - A^2 + 2i\omega A\Big]^{-1} S^{-1} \\ &= \Big\{S\big[(\omega+i\eta)^2 - K^C - \Sigma^r[\omega] - A^2 + 2i\omega A\big]S^{-1}\Big\}^{-1} \\ &= G^r(-A). \end{aligned} \tag{3.54}$$

That means $SG^r(h)S^{-1} = G^r(-h)$ because A is proportional to h. Similarly we can derive $SG^a(h)S^{-1} = G^a(-h)$. In the end, by inserting some $S^{-1}S$ to Eq. (3.27), we obtain $T_{\beta\alpha}[h] = T_{\beta\alpha}[-h]$. Therefore, if the dynamic matrix of the system could satisfy the symmetry of Eq. (3.51), there is no PHE. In other words, the necessary condition for PHE is that there is no symmetric operation can make the system satisfy the relation of Eq. (3.51).

3.3 Numerical Results and Discussion

In the following calculation, we assume a lattice constant $a = 2.465\,\text{Å}$, and the force constants $K_L = 0.02394\,\text{eV/(amu·Å}^2)$, $K_T = K_L/4$. The ratio of the longitudinal and transverse sound speed is assumed to be $\delta = v_L/v_T \approx \sqrt{K_L/K_T} = 2$. As mentioned above, h is estimated to be about $3 \times 10^9\,\text{Hz} \approx 2.0 \times 10^{-6}\,\text{eV}/\hbar$ at $B = 1\,\text{T}$. We set all the couplings between the leads and central region the same; and all the leads and central region have the same spring constants for simplicity.

We discuss numerical results in the following. Fig. 3.2 shows the temperature difference vs magnetic field at temperature $T = 5.45\,\text{K}$ for the honeycomb

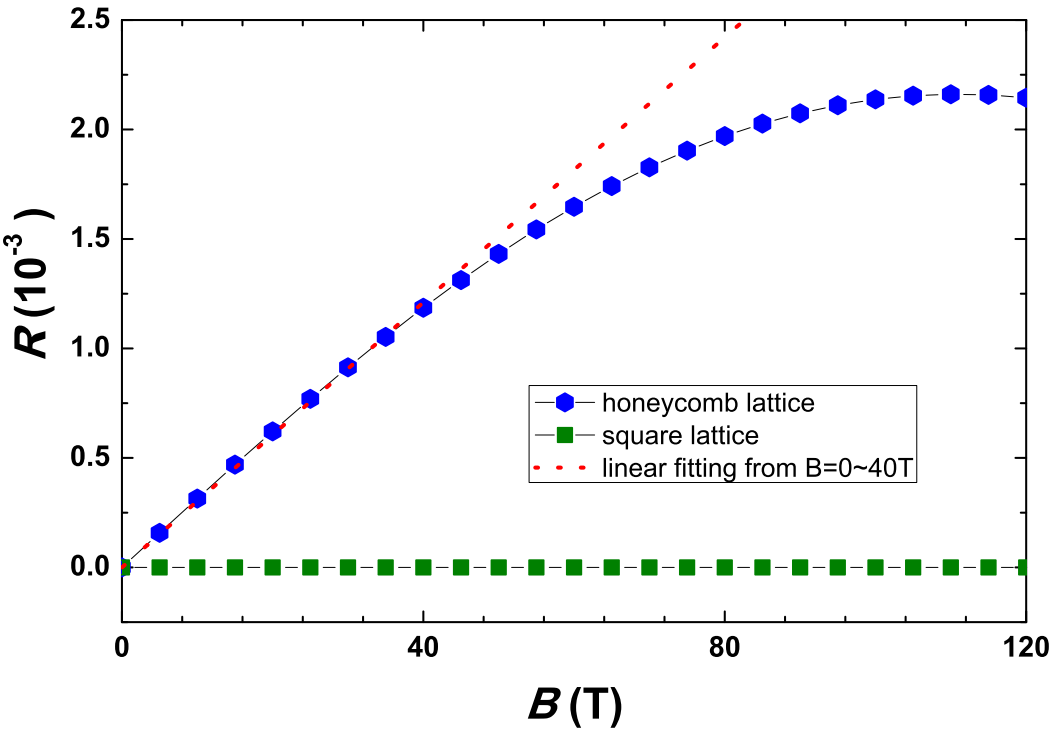

Figure 3.2: The relative Hall temperature difference R versus magnetic field B at temperature $T = 5.45\,\mathrm{K}$. The hexagon and square line correspond central regions for the honeycomb and square lattices with a nearest-neighbor coupling. The red dotted line is a best fit line from 0 to 40 T. The size of the center region for honeycomb lattices is 9×6, the same with the inset (c) in Fig. 3.1

and square lattices with nearest-neighbor couplings. For the honeycomb case, the Hall temperature is odd and linear in the magnetic field between 0 and 40 T, in that range the slope of the curve is 3×10^{-5} K/T, comparable to the experimental data in Ref. [12]. When the magnetic field is extremely large, it will decrease. From our calculation, we find that the triangular lattice has a similar behavior. However, for a square lattice with the nearest-neighbor coupling, there is no PHE at all. The spring constant matrix between every nearest coupling sites is diagonal for the square lattice. This matrix and also the full matrix K are invariant with respect to a reflection in x or y direction, thus satisfying Eq. (3.51). If we consider next-neighbor couplings of the lattice, the dynamic matrix K will not have the mirror reflection symmetry, and the PHE appears.

We show the conductances among different leads in Fig. 3.3. Because of the symmetry of the system, we have additional relations, $\sigma_{13} = \sigma_{32} = \sigma_{24} = \sigma_{41}$, and $\sigma_{14} = \sigma_{42} = \sigma_{23} = \sigma_{31}$. We find that the conductances between two longitudinal leads or two transverse probe-leads are even functions of the magnetic field, which can be seen in Fig. 3.3(a), σ_{34} has the same property. However, for honeycomb lattice the conductance between one longitudinal lead and one transverse probe-lead is not an even function of magnetic field [Fig. 3.3(b)], which gives contribution to the Hall temperature difference. Therefore, for honeycomb lattice, the temperature difference is not zero. But for square lattices, σ_{13} is an even function of magnetic field, the same is true for other components. no PHE exists in such systems.

We show the numerical results of the relative Hall temperature difference

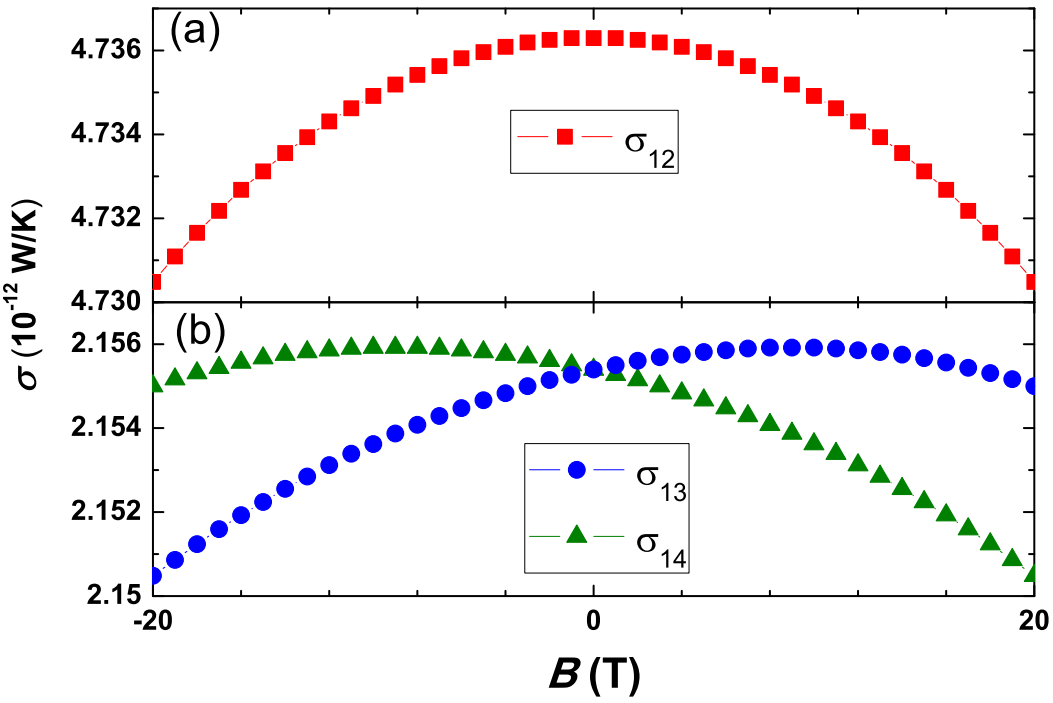

Figure 3.3: Thermal conductance versus the magnetic field at temperature $T = 5.45$K for the honeycomb lattice. (a) shows the conductance between two longitudinal leads σ_{12}. (b) shows the conductance between one longitudinal lead and one transverse probe-lead. The circle and triangular lines correspond to σ_{13} and σ_{14}, respectively. The size of center region is 9×6.

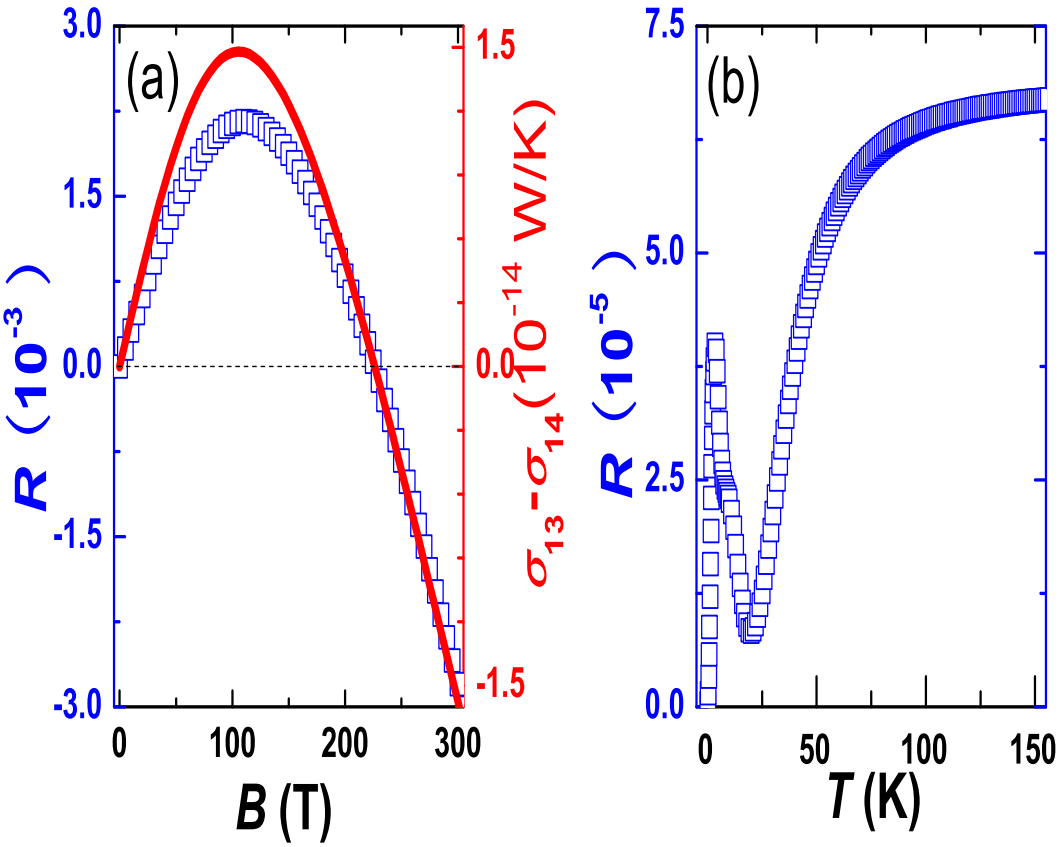

Figure 3.4: The relative Hall temperature difference R versus the large magnetic field B (a) and high equilibrium temperature T for honeycomb lattice (b). (a) square shows R changing with the magnetic field (left scale), the red solid line shows the conductance difference $\sigma_{13} - \sigma_{14}$ versus magnetic field (right scale). (b), R vs. equilibrium temperature at $B = 1\,\mathrm{T}$.

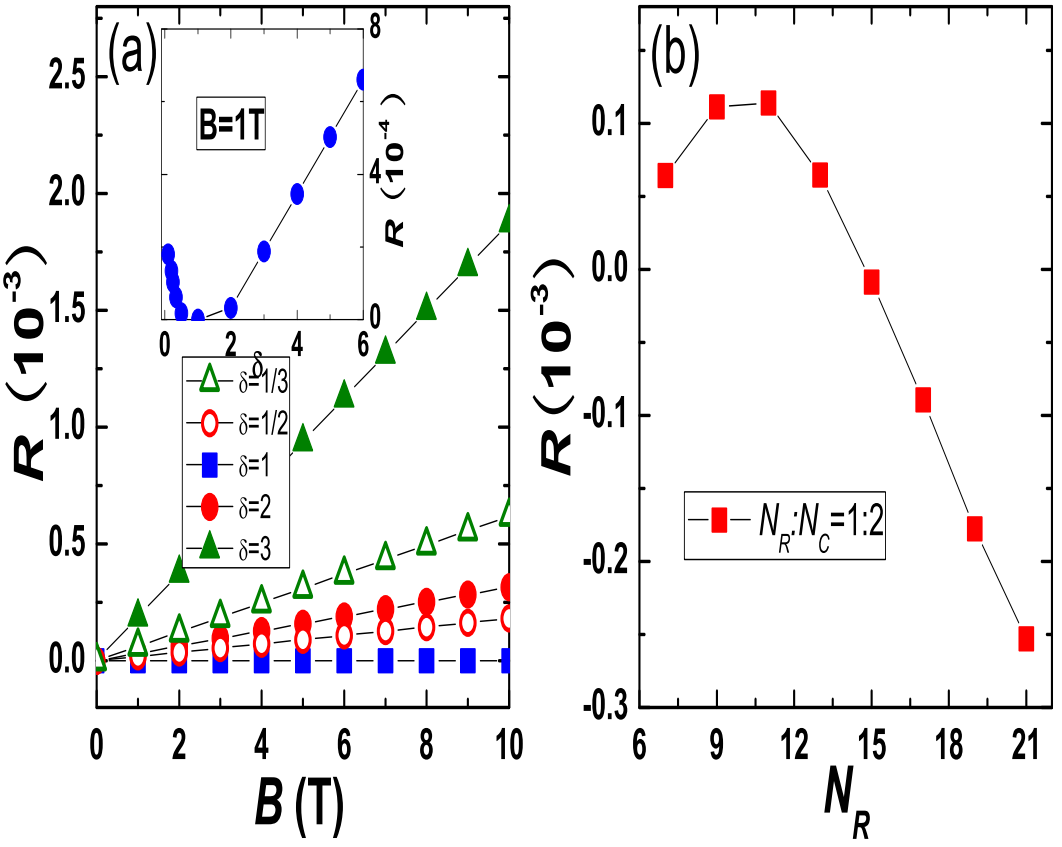

Figure 3.5: (a) The relative Hall temperature difference versus magnetic field for different ratio of the longitudinal and transverse sound speed $\delta = v_L/v_T$. The inset shows R versus δ at $B = 1$T. The data are for 9×6 honeycomb lattices at $T = 5.45$K. (b) The relative Hall temperature difference versus the number of rows of atoms for fixed aspect ratio $N_R : N_C = 1 : 2$ at B=1 T and $T = 5.45$ K.

R at $T = 5.45$K for honeycomb lattices in Fig. 3.4(a). The temperature difference R will not be linear when the magnetic field is larger than 40 T; after about 110 T, it will decrease; and about $B_c \approx 230$ T, R changes sign to negative. It is the same critical point for the difference of conductances $\sigma_{13} - \sigma_{14}$, which is consistent with Eq. (3.37). In Fig. 3.4(b), we show R versus temperature at $B = 1$ T. When the temperature increases, R will increase almost linearly. After some value, it decreases, and then increases again. In the end, it tends to a constant. This behavior is due to the competition of the numerator and denominator in Eq. (3.37). When the temperature is very high, all conductances tend to constants due to the ballistic thermal transport.

In Ref. [13], it was shown that R decreases with increasing ratio of the longitudinal and transverse sound speed $\delta = v_L/v_T$ and changes sign when δ becomes large than 5. However, we find that when the ratio ($\delta > 1$) becomes large, R increases, see Fig. 3.5(a). At exactly $\delta = 1$, when the longitudinal speed equals to the transverse speed, there is no PHE, which testifies our condition, Eq. (3.51), for the absence of PHE. All the spring constant matrices between the nearest-neighbors become diagonal at $\delta = 1$; the condition Eq. (3.51) holds for a mirror reflection operation. If $\delta < 1$, R increases again with the decreasing of δ. Although the ratio R does not change sign with δ, due to the ballistic nature of a small system, the ratio R is sensitive to the geometric details, which is shown in Fig. 3.5(b), the magnitude and the sign of R change as the size increases.

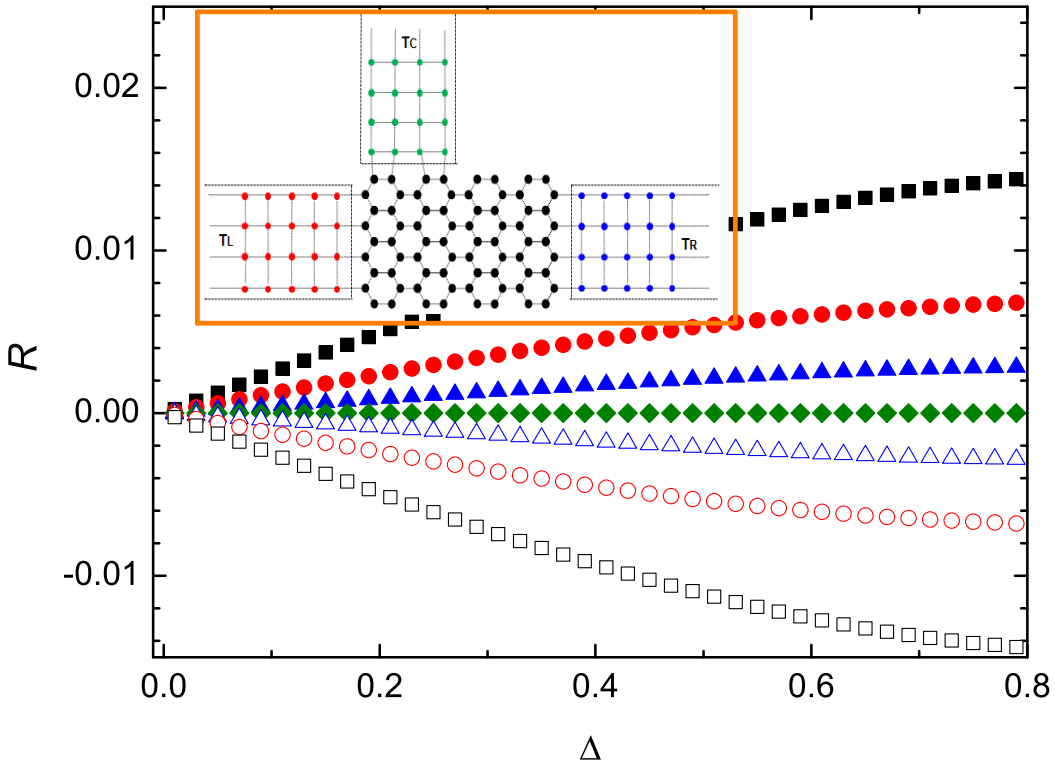

Figure 3.6: Rectification as a function of relative temperature difference of the hot and cold heat baths. The parameter of the setup is $N_R = 9$, $N_C = 16$, $N_{CL} = 2$. The temperature of the heat bath are $T_+ = T_0(1+\Delta)$ and $T_- = T_0(1-\Delta)$, where $T_0 = 0.2$ is the mean temperature. The solid square, solid circle, solid triangle, diamond, hollow triangle, hollow circle, hollow square correspond to $N_{CD} = -7$, -5, -3, 0, 3, 5 and 7, respectively. The inset: The three-terminal junction setup to study the ballistic thermal transport. The left and right leads have temperatures T_L and T_R, the control terminal lead is adjusted to be T_C.

3.4 An Application

The ballistic thermal transport in two-terminal junctions can be described by the Landauer formula. Since the temperatures enter only through the Bose distribution, it is obvious that if we reverse the heat bath temperatures, the heat flux only changes sign, and no rectification is expected. How about the ballistic thermal transport in multiple-terminal junctions? We know that the third terminal can introduce incoherence or phase breaking to the transport. So it is our interest to investigate whether a multiple-terminal junction is a proper option for ballistic thermal rectification, that is, whether the incoherence through the third terminal can induce rectification effect. In the following we apply our formulas of multiple-terminal thermal transport from NEGF to study the thermal rectification.

We consider the ballistic thermal transport in a three-terminal nanojunction as shown in inset of Fig. 3.6, where a two-dimensional atomic lattice sample, which is a honeycomb lattice, is connected with three ideal semi-infinite leads. The atoms are coupled through nearest neighbors by elastic springs (with longitudinal and transverse force constants). We denote the center lattice as $N_R \times N_C$, where N_R, N_C correspond to the number of rows and columns, respectively. The external magnetic field can be perpendicularly applied to this part. We use N_{CL} to denote the number of columns of the control lead and N_{CD} to denote the number of columns deviating from the middle of the center part; if $N_{CD} = 0$, the whole setup is symmetric. In the inset of Fig. 3.6, $N_R = 9$, $N_C = 8$, $N_{CL} = 4$, $N_{CD} = -2$.

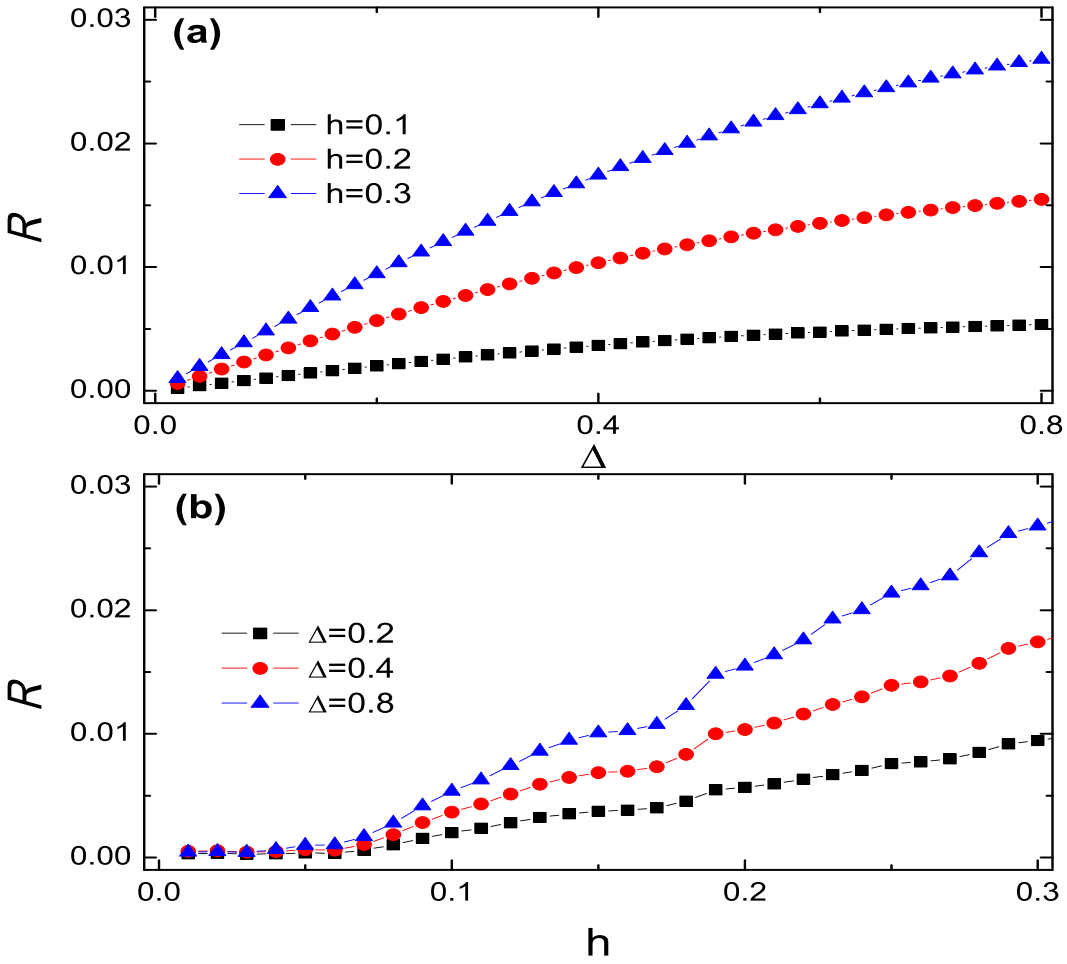

Figure 3.7: (a) Thermal rectification as function of relative temperature difference Δ for different external magnetic fields. (b) Thermal rectification as a function of magnetic field h. For both (a) and (b): $N_R = 9$, $N_C = 16$, $N_{CL} = 2$, $N_{CD} = 0$. $T_+ = T_0(1 + \Delta)$, $T_- = T_0(1 - \Delta)$. T_0=0.2.

3.4.1 Ballistic Thermal Rectification

We set $\hbar = 1$ and $k_B = 1$ in the following calculation for ballistic rectification. Using the formulas above, in the forward process, $T_L = T_+$, $T_R = T_-$, we can calculate J_+ and J_C, and also can get the heat fluxes J_- and $J_C^{'}$ in the backward process $T_L = T_-$, $T_R = T_+$. From the equations of $J_C = 0$ and $J_C^{'} = 0$ we can obtain the temperatures of the control bath T_C and $T_C^{'}$; inserting them to the formulae of J_+ and J_-, the rectification

$$R = (J_+ - J_-)/\max\{J_+, J_-\}, \tag{3.55}$$

can be calculated.

Firstly, we consider the ballistic thermal transport in an asymmetric structure without an external magnetic field. We set the longitudinal spring constant $k_L = 1.0$, and the transverse one $k_T = 0.25$. If the control lead is connected to the middle of upper edge of the center, that is, $N_{CD} = 0$, the forward process and backward one are exactly the same; no rectification will be expected, as shown in Fig. 3.6 (the diamond symbols). If the control lead moves away from the center, the rectification effect appears. When the lead is moved the same distance to the left or right, the rectification coefficient has the same magnitude but opposite sign, which is because that the two cases only exchange the value of J_+ and J_-. If the distance between the control lead and the middle of the center part is longer, the rectification effect is larger. In Fig. 3.6, we can see that the case of $N_{CD} = \pm 7$, when the control lead is next to left or right lead, has biggest rectification. The rectification increases with the temperature difference at far-from-linear-response regime.

From the previous studies on thermal rectification, we know that in order to get rectification, we need the structural asymmetry. However, in the nanoscale rectifier, it is not easy to control the structural asymmetry or to distinguish the rectification direction by the structural asymmetry. Is there any other means to introduce asymmetry to induce rectification? From the above study of phonon Hall effect it is known that the magnetic field can influence the thermal transport by the spin-phonon interaction. Thus the magnetic field can break the symmetry of the phonon transport. We apply an external magnetic field perpendicular to the center part of a symmetric structure to study the ballistic thermal transport, the results are shown in Fig. 3.7. The thermal rectification effect as a function of the temperature difference is shown in Fig. 3.7(a). R increases with the temperature difference, and can be about 3% if $\Delta = 0.8$ and $h = 0.3$ at $T_0 = 0.2$. Figure 3.7(b) shows that the rectification can monotonically increase with the external magnetic field in the range of $h = 0 \sim 0.3$.

3.4.2 Reversal of Thermal Rectification

Figure 3.8(a) shows the rectification dependence on temperature, and reproduce the reversal of rectification found in Ref. [31]. At a low temperature, the contribution to thermal transport only comes from the low frequency phonons; if the temperature increases, more high frequency phonons will contribute to the heat transport. From Fig. 3.8(b), the relations between transmissions τ_{LC} and τ_{RC} in low frequency domain and high frequency domain are opposite, so that the rectification reverses with the temperature increasing. When the temperature increases further, the system will go to the classic limit, the rectifica-

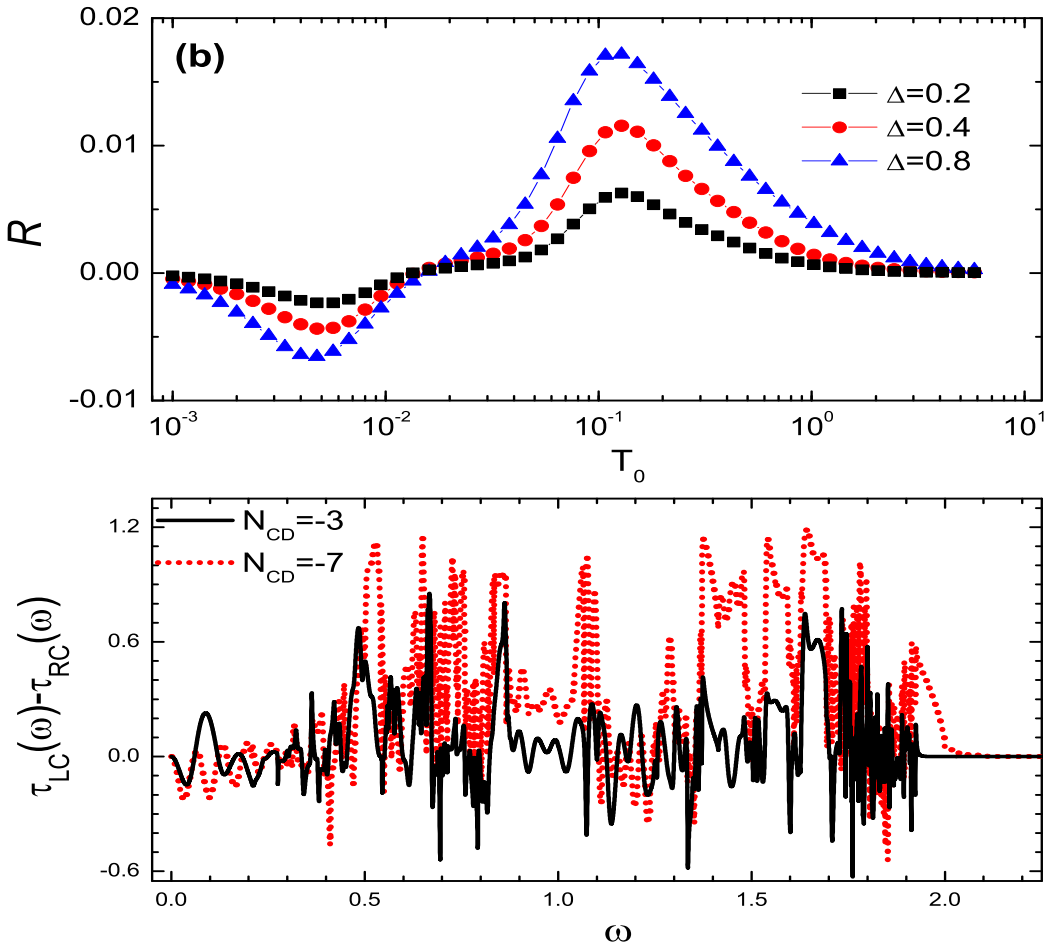

Figure 3.8: (a) Thermal rectification as function of mean temperature for different relative temperature difference. $N_{CD} = -7$, $T_+ = T_0(1+\Delta)$ and $T_- = T_0(1-\Delta)$. (b) The difference of transmission coefficients: $\tau_{LC} - \tau_{RC}$, as a function of frequency. The solid, dot curves correspond to $N_{CD} = -3$ and $N_{CD} = -7$, respectively. For both (a) and (b), $N_R = 9$, $N_C = 16$, $N_{CL} = 2$.

tion disappears. The reversal of rectification is also found in our another study on the thermal rectification in quantum spin-chain systems by using quantum master equations [31]. It shows that rectification can change sign when the magnetic field, temperature, the anisotropy, and the system size change. Although the reversal of rectification is complicated parameter-dependent, we believe that it shall be a universal phenomenon for the thermal transport in low dimensional systems.

3.5 Summary

In summary, a theory for PHE in nanoscale lattices by NEGF approach is developed. Using the proposed formula of the relative Hall temperature difference, we can efficiently study the PHE in four-terminal junctions. Our results are consistent with the essential experimental features of PHE, such as the magnitude and linear magnetic-field dependence of the observed transverse temperature difference. With increasing of the magnetic field, the PHE will change from the linear dependence to sublinear one, then decrease and change the sign from positive to negative after certain magnetic field. We find a symmetry criterion for the PHE, that is, there is no PHE if the lattice satisfies a certain symmetry, which makes the dynamic matrix unchanged and the magnetic field reversed. The symmetry broken of the dynamic matrix K plays a pivotal role for the existence of PHE. The Hall temperature difference changes with equilibrium temperature and tends to be a constant at last. And the Hall temperature difference does not change sign with the ratio of the longitudinal and transverse sound speed in the range of $\delta \in (0.1, 10)$; but it changes sign

as the system size increases. Therefore, the PHE can indeed be present in the ballistic system provided the symmetry criterion is not satisfied.

By applying our theory to the ballistic thermal rectification in three terminal junctions, we find two necessary conditions for thermal rectification. One is the phonon incoherence, which can be induced by nonlinearity or scattering boundaries or scattering leads. The other one is asymmetry, which can be introduced by structural asymmetry or an applied external magnetic field through the spin-phonon interaction. Furthermore, we find that the thermal rectification can change sign in certain parameter range, which is a universal phenomenon for the thermal transport.

Chapter 4

Phonon Hall Effect in Two-Dimensional Periodic Lattices

In the previous chapter, we find that the ballistic four-terminal junctions are capable of producing the PHE provided that certain symmetry is broken. However, in such four-terminal structure, the relative Hall temperature difference is dependent on the system size, which could not be used as a good physical quantity to embody the PHE property of a certain material. The thermal conductivity is a good candidate to represent the capability of the thermal transport. With an applied magnetic field, in two-dimensional systems the thermal conductivity is a tensor (2×2 matrix); and the off-diagonal elements, which we call the phonon Hall conductivity here, can reflect the PHE of the special material.

In this chapter, we study the PHE in two-dimensional infinite periodic lattice. We will propose exact theories for the PHE to calculate the phonon Hall conductivity. When phonons transport is investigated in the moment

space, a nontrivial Berry phase may come out to play an important role for the PHE. Therefore it is also our key task to investigate the Berry phase effect for the phonons transport with an applied magnetic field, and to study the topological nature of the PHE.

4.1 Hamiltonian

In the presence of a magnetic field, the kinetic energy of each site in ionic crystal lattices is expressed as [85]:

$$T_\alpha = \frac{1}{2} m_\alpha |\dot{\mathbf{r}}_\alpha|^2 = \frac{1}{2m_\alpha} |\mathbf{p}_\alpha \sqrt{m_\alpha} - q_\alpha \mathbf{A}_\alpha|^2, \tag{4.1}$$

where, $\mathbf{r}_\alpha = \mathbf{R}_\alpha + \mathbf{u}_\alpha/\sqrt{m_\alpha}$, $\mathbf{R}_\alpha$ is the equilibrium coordinate of the ion at site α, and $\mathbf{u}_\alpha$ denotes the displacement multiplied by the square root of the ion mass m_α. $\mathbf{p}_\alpha$ is the corresponding momentum divided by the square root of mass m_α. q_α is the ionic charge at site α. $\mathbf{A}_\alpha$ denotes the electromagnetic vector potential, which, by using the Lorenz gauge condition, can be related to the ionic displacement as [85]

$$\mathbf{A}_\alpha = \frac{1}{2} \mathbf{B} \times \mathbf{u}_\alpha / \sqrt{m_\alpha}. \tag{4.2}$$

Thus, Eq. (4.1) is recasted as:

$$T_\alpha = \frac{1}{2} |\mathbf{p}_\alpha - \frac{q_\alpha}{2m_\alpha} \mathbf{B} \times \mathbf{u}_\alpha|^2. \tag{4.3}$$

If a magnetic field with magnitude B is applied along z direction and we only consider the two-dimensional (x and y direction) motion of the system, then the kinetic energy of ion α can be expressed (it is straightforward to generalize to high dimensions) as:

$$T_\alpha = \frac{1}{2} (p_\alpha - \Lambda_\alpha u_\alpha)^T (p_\alpha - \Lambda_\alpha u_\alpha), \tag{4.4}$$

where $p_\alpha = (p_{\alpha x}, p_{\alpha y})^T$, $u_\alpha = (u_{\alpha x}, u_{\alpha y})^T$, and $\Lambda_\alpha = \begin{pmatrix} 0 & h_\alpha \\ -h_\alpha & 0 \end{pmatrix}$, where $h_\alpha = -q_\alpha B/(2m_\alpha)$. Note that there are both positive and negative ions in one unit cell. For a general ionic paramagnetic dielectric, mostly, the mass of the positive ion is larger than that of the negative one. For instance, in the experimental sample $Tb_3Ga_5O_{12}$, the ratio $m(+q)/m(-q)$ is about 4.3 in one unit cell. Therefore the negative ions will dominate the contribution to h_α, which makes h_α have the same sign as that of the applied magnetic field B. Under the mean-field approximation, we can set $h_\alpha = h$, which is site-independent and is proportional to the magnitude of the applied magnetic field.

Combining the kinetic energy with the harmonic inter-potential energy, we can write the whole Hamiltonian as

$$H = \frac{1}{2}(p - \tilde{A}u)^T(p - \tilde{A}u) + \frac{1}{2}u^T K u, \tag{4.5}$$

where $\tilde{A}$ is an antisymmetric real matrix with block-diagonal elements Λ_α. u and p are column vectors denoting displacements and momenta respectively, for all the degrees of freedom. K indicates the force constant matrix. Finally, after the rearrangement, we have

$$H = \frac{1}{2}p^T p + \frac{1}{2}u^T(K - \tilde{A}^2)u + u^T\tilde{A}\,p, \tag{4.6}$$

which is positive definite.

The Hamiltonian Eq. (4.6) is essentially the same as Eq. (3.2) in Chapter 3 and that used in Refs. [13, 14], resulting from the phenomenological Raman interaction. The only difference is the term proportional to $\tilde{A}^2$ which makes

the above Hamiltonian positive definite. As discussed in Chapter 3, in the mean-field approximation, the Raman type SPI reduces to

$$H_I = \mathbf{h} \cdot (\mathbf{u} \times \mathbf{p}), \tag{4.7}$$

where $\mathbf{h} = gc\mathbf{M}$, and $\mathbf{M}$ is proportional to the magnetic field $\mathbf{B}$. If the magnetic field is applied along the z direction, then the SPI can be written as

$$H_I = u^T \tilde{A}\, p. \tag{4.8}$$

By treating the phonon system under harmonic approximation, the total Hamiltonian for the whole lattice can be written as (Refs. [13, 14, 149])

$$H = \frac{1}{2} p^T p + \frac{1}{2} u^T K u + u^T \tilde{A}\, p. \tag{4.9}$$

Note that this Hamiltonian Eq. (4.9) is not positive definite. In Ref. [149], the authors added an arbitrary onsite potential in order to make the Hamiltonian positive definite. However, in the calculation of phonon Hall effect for the four-terminal junctions, such non-positive-definite Hamiltonian does not cause any problem because the thermal junctions will stabilize the system [150].

From the first physical picture of spin-phonon interaction in ionic crystal lattice with an applied magnetic field (Eqs. (4.1∼4.6)), the additional term proportional to $\tilde{A}^2$ emerges naturally to make the Hamiltonian positive definite. Therefore, in this chapter we choose the positive definite Hamiltonian Eq. (4.6).

4.2 Eigenvalue Problem

The Hamiltonian Eq. (4.6) is quadratic in u and p, and we can write the equation of motion as

$$\dot{p} = -(K - \tilde{A}^2)u - \tilde{A}p, \tag{4.10}$$

$$\dot{u} = p - \tilde{A}u. \tag{4.11}$$

The equation of motion for the coordinate is,

$$\ddot{u} + 2\tilde{A}\dot{u} + \tilde{A}^2 u + (K - \tilde{A}^2)u = 0. \tag{4.12}$$

Since the lattice is periodic, we can apply the Bloch's theorem $u_l = \epsilon e^{i(\mathbf{R}_l \cdot \mathbf{k} - \omega t)}$. The polarization vector ϵ satisfies

$$\big[(-i\omega + A)^2 + D\big]\epsilon = 0, \tag{4.13}$$

where

$$D(\mathbf{k}) = -A^2 + \sum_{l'} K_{l,l'} e^{i(\mathbf{R}_{l'} - \mathbf{R}_l)\cdot \mathbf{k}} \tag{4.14}$$

denotes the dynamic matrix with a shift A^2, and A is block diagonal with elements Λ. $D, K_{l,l'}$, and A are all $nd \times nd$ matrices, where n is the number of particles in one unit cell and d is the dimension of the motion.

From Eq. (4.13), we can require the following relations:

$$\epsilon^*_{-k} = \epsilon_k;\ \omega_{-k} = -\omega_k. \tag{4.15}$$

Here, we use the short-hand notation $k = (\mathbf{k}, \sigma)$ to specify both the wavevector and the phonon branch. $-k$ means $(-\mathbf{k}, -\sigma)$, the negative branch index $\sigma < 0$ will be explained later.

Equation (4.13) is not a standard eigenvalue problem. However, we can describe the system by the polarization vector $x = (\mu, \epsilon)^T$, where μ and ϵ are associated with the momenta and coordinates, respectively. And from Eq. (4.11), the momentum and displacement polarization vectors are related through

$$\mu_k = -i\omega_k \epsilon_k + A\epsilon_k. \tag{4.16}$$

Using Bloch's theorem, Eqs. (4.10) and (4.11) can be recasted as:

$$i\frac{\partial}{\partial t}x = H_{\text{eff}}x, \qquad H_{\text{eff}} = i\begin{pmatrix} -A & -D \\ I_{nd} & -A \end{pmatrix}. \tag{4.17}$$

Here the I_{nd} is the $nd \times nd$ identity matrix.

We need to find both the right and left eigenvectors. Because of the special form of H_{eff}, then the eigenvalue problem of the equation of motion (4.17) reads:

$$H_{\text{eff}}\, x_k = \omega_k\, x_k, \quad \tilde{x}_k^T\, H_{\text{eff}} = \omega_k\, \tilde{x}_k^T. \tag{4.18}$$

where the right eigenvector $x_k = (\mu_k, \epsilon_k)^T$, the left eigenvector

$$\tilde{x}_k^T = (\epsilon_k^\dagger, -\mu_k^\dagger)/(-2i\omega_{,k}) \tag{4.19}$$

in such choice the second quantization of the Hamiltonian Eq. (4.6) holds. Because the effective Hamiltonian H_{eff} is not hermitian, the orthonormal condition then holds between the left and right eigenvectors, as

$$\tilde{x}_{\sigma,\mathbf{k}}^T\, x_{\sigma',\mathbf{k}} = \delta_{\sigma\sigma'}. \tag{4.20}$$

We also have the completeness relation as

$$\sum_\sigma x_{\sigma,\mathbf{k}} \otimes \tilde{x}_{\sigma,\mathbf{k}}^T = I_{2nd}. \tag{4.21}$$

The normalization of the eigenmodes is equivalent to [149]

$$\epsilon_k^\dagger \, \epsilon_k + \frac{i}{\omega_k} \epsilon_k^\dagger \, A \, \epsilon_k = 1. \tag{4.22}$$

4.3 PHE Approach One

By taking into account only positive eigen-modes ($\omega > 0$), displacement and momentum operators are taken in the second quantization form [149, 152]:

$$u_l = \sum_k \epsilon_k e^{i(\mathbf{R}_l \cdot \mathbf{k} - \omega_k t)} \sqrt{\frac{\hbar}{2\omega_k N}} \, a_k + \text{h.c.}, \tag{4.23}$$

$$p_l = \sum_k \mu_k e^{i(\mathbf{R}_l \cdot \mathbf{k} - \omega_k t)} \sqrt{\frac{\hbar}{2\omega_k N}} \, a_k + \text{h.c.}, \tag{4.24}$$

where $\sigma > 0$, a_k is the annihilation operator, and h.c. stands for hermitian conjugate. We can verify that the canonical commutation relations are satisfied: $[u_l, p_{l'}^T] = i\hbar\delta_{l,l'} I_{nd}$, and $H = \sum_k \hbar\omega_k (a_k^\dagger a_k + 1/2)$.

4.3.1 Heat Current Density Operator

The energy current density is given as [151]:

$$\mathbf{J} = \frac{1}{2V} \sum_{l,l'} (\mathbf{R}_l - \mathbf{R}_{l'}) u_l^T K_{l,l'} \dot{u}_{l'}, \tag{4.25}$$

where V is the total volume of N unit cells. Inserting the Eq. (4.23) and its first derivative the current density vector can be expressed in two parts as

$$\mathbf{J} = \mathbf{J}_1(a^\dagger a) + \mathbf{J}_2(a^\dagger a^\dagger, aa), \tag{4.26}$$

Due to the definition of the dynamic matrix Eq. (4.14), we have the following property:

$$D_{ab}(-\mathbf{k}) = D_{ab}^*(\mathbf{k}) = D_{ba}(\mathbf{k}); \tag{4.27}$$

and

$$\frac{\partial D(\mathbf{k})}{\partial \mathbf{k}} = \sum_{l'} i(\mathbf{R}_{l'} - \mathbf{R}_l) K_{l,l'} e^{i(\mathbf{R}_{l'} - \mathbf{R}_l)\cdot \mathbf{k}}; \tag{4.28}$$

Combining the relation of

$$\sum_{l} e^{i\mathbf{R}_l \cdot (\mathbf{k}' - \mathbf{k})} = N\delta_{\mathbf{k}'\mathbf{k}}, \tag{4.29}$$

then we can obtain

$$\begin{aligned}
\mathbf{J}_1 &= \tfrac{\hbar}{4V} \sum_{k,k'} \left(\sqrt{\tfrac{\omega_k}{\omega_{k'}}} a_k^\dagger a_{k'} + \sqrt{\tfrac{\omega_{k'}}{\omega_k}} a_{k'} a_k^\dagger \right) \epsilon_k^\dagger \tfrac{\partial D(\mathbf{k})}{\partial \mathbf{k}} \epsilon_{k'} \delta_{\mathbf{k},\mathbf{k}'} e^{i(\omega_k - \omega_{k'})t}; \\
\mathbf{J}_2 &= \tfrac{\hbar}{4V} \sum_{k,k'} \sqrt{\tfrac{\omega_{k'}}{\omega_k}} \left(\epsilon_k^\dagger \tfrac{\partial D(\mathbf{k})}{\partial \mathbf{k}} \epsilon_{k'}^* a_k^\dagger a_{k'}^\dagger e^{i(\omega_k + \omega_{k'})t} + \epsilon_k^T \tfrac{\partial D^*(\mathbf{k})}{\partial \mathbf{k}} \epsilon_{k'} a_k a_{k'} e^{-i(\omega_k + \omega_{k'})t} \right) \delta_{\mathbf{k},-\mathbf{k}'}.
\end{aligned} \tag{4.30}$$

Due to the commutation relation of $[a_{\mathbf{k},\sigma'}, a_{\mathbf{k},\sigma}^\dagger] = \delta_{\sigma',\sigma}$, we can rewrite $\mathbf{J}_1$ as

$$\mathbf{J}_1 = \frac{\hbar}{4V} \left[\sum_{k,k'} \left(\sqrt{\frac{\omega_k}{\omega_{k'}}} + \sqrt{\frac{\omega_{k'}}{\omega_k}} \right) \epsilon_k^\dagger \frac{\partial D(\mathbf{k})}{\partial \mathbf{k}} \epsilon_{k'}\, a_k^\dagger a_{k'} \delta_{\mathbf{k},\mathbf{k}'} e^{i(\omega_k - \omega_{k'})t} + \sum_{\mathbf{k},\sigma} 2\epsilon_k^\dagger \frac{\partial D(\mathbf{k})}{\partial \mathbf{k}} \epsilon_k \right] \tag{4.31}$$

And from the Eq. (4.18), we get

$$\frac{\partial H_{\text{eff}}}{\partial \mathbf{k}}\, x_k + H_{\text{eff}}\, \frac{x_k}{\partial \mathbf{k}} = \frac{\omega_k}{\partial \mathbf{k}}\, x_k + \omega_k\, \frac{x_k}{\partial \mathbf{k}}. \tag{4.32}$$

Using $\tilde{x}_k^T$ to multiply both sides from left, and due to Eq. (4.20), we obtain

$$\tilde{x}_k^T \frac{\partial H_{\text{eff}}}{\partial \mathbf{k}}\, x_k = \frac{\omega_k}{\partial \mathbf{k}}, \tag{4.33}$$

which means

$$\epsilon_k^\dagger \frac{\partial D(\mathbf{k})}{\partial \mathbf{k}}\, \epsilon_k = -2i\omega_k \frac{\omega_k}{\partial \mathbf{k}}, \tag{4.34}$$

which is an odd function of $\mathbf{k}$, then we obtain

$$\sum_{\mathbf{k}} \epsilon_k^\dagger \frac{\partial D}{\partial \mathbf{k}} \epsilon_k = -2i \sum_{\mathbf{k}} \omega_k \tilde{x}_k^T \frac{\partial H_{\text{eff}}}{\partial \mathbf{k}} x_k = -2i \sum_{\mathbf{k}} \omega_k \frac{\partial \omega_k}{\partial \mathbf{k}} = 0, \tag{4.35}$$

thus second term of $\mathbf{J}_1$ is zero.

Therefore, the heat flux operator can be written as

$$\begin{aligned}
&\mathbf{J} = \mathbf{J}_1(a^\dagger a) + \mathbf{J}_2(a^\dagger a^\dagger, aa),\\
&\mathbf{J}_1 = \tfrac{\hbar}{4V}\textstyle\sum_{k,k'}\left(\sqrt{\frac{\omega_k}{\omega_{k'}}}+\sqrt{\frac{\omega_{k'}}{\omega_k}}\right)\epsilon_k^\dagger\frac{\partial D(\mathbf{k})}{\partial \mathbf{k}}\epsilon_{k'}\, a_k^\dagger a_{k'}\delta_{\mathbf{k},\mathbf{k}'}e^{i(\omega_k-\omega_{k'})t};\\
&\mathbf{J}_2 = \tfrac{\hbar}{4V}\sum_{k,k'}\sqrt{\tfrac{\omega_{k'}}{\omega_k}}\,(\epsilon_k^\dagger\tfrac{\partial D(\mathbf{k})}{\partial \mathbf{k}}\epsilon_{k'}^* a_k^\dagger a_{k'}^\dagger e^{i(\omega_k+\omega_{k'})t} + \epsilon_k^T\tfrac{\partial D^*(\mathbf{k})}{\partial \mathbf{k}}\epsilon_{k'}a_k a_{k'}e^{-i(\omega_k+\omega_{k'})t})\delta_{\mathbf{k},-\mathbf{k}'}.
\end{aligned} \tag{4.36}$$

We note that the $a^\dagger a^\dagger$ and aa terms also contribute to the off-diagonal elements of the thermal conductivity tensor, although they have no contribution to the average energy current.

4.3.2 Phonon Hall Conductivity

Based on the expression of heat current, the phonon Hall conductivity can be obtained through the Green-Kubo formula [121]:

$$\kappa_{xy} = \frac{V}{\hbar T}\int_0^{\hbar/(k_BT)} d\lambda \int_0^\infty dt \left\langle J^x(-i\lambda)J^y(t)\right\rangle_{\text{eq}}, \tag{4.37}$$

where the average is taken over the equilibrium ensemble with Hamiltonian H. Substituting the expression $\mathbf{J}$ into Eq. (4.37), the phonon Hall conductivity is obtained as

$$\begin{aligned}
&\kappa_{xy} = \kappa_{xy}^{(1)} + \kappa_{xy}^{(2)};\\
&\kappa_{xy}^{(1)} = \tfrac{V}{\hbar T}\textstyle\int_0^{\hbar/(k_BT)} d\lambda \int_0^\infty dt \left\langle J_1^x(-i\lambda)J_1^y(t)\right\rangle_{\text{eq}};\\
&\kappa_{xy}^{(2)} = \tfrac{V}{\hbar T}\textstyle\int_0^{\hbar/(k_BT)} d\lambda \int_0^\infty dt \left\langle J_2^x(-i\lambda)J_2^y(t)\right\rangle_{\text{eq}}.
\end{aligned} \tag{4.38}$$

Note that the averages of the cross terms $\left\langle J_1^x(-i\lambda)J_2^y(t)\right\rangle_{\text{eq}}$ and $\left\langle J_2^x(-i\lambda)J_1^y(t)\right\rangle_{\text{eq}}$ are zero.

First we calculate the term $\kappa_{ab}^{(1)}$. Combining the result

$$\langle a_i^\dagger a_j a_k^\dagger a_l\rangle_{\text{eq}} = f_i f_k\delta_{ij}\delta_{kl} + f_i(f_j+1)\delta_{il}\delta_{jk}, \tag{4.39}$$

where $f_i = (e^{\beta\hbar\omega_i} - 1)^{-1}$ is the Bose distribution function, with the result of Eq. (4.35), we obtain

$$\kappa_{xy}^{(1)} = \frac{\hbar}{16VT} \sum_{\mathbf{k},\sigma>0,\sigma'>0} [f(\omega_\sigma) - f(\omega'_\sigma)](\omega_\sigma + \omega'_\sigma)^2 \frac{i}{\omega_\sigma \omega_{\sigma'}} \frac{\epsilon_\sigma^\dagger \frac{\partial D}{\partial k_x} \epsilon_{\sigma'} \epsilon_{\sigma'}^\dagger \frac{\partial D}{\partial k_y} \epsilon_\sigma}{(\omega_\sigma - \omega_{\sigma'})^2}. \tag{4.40}$$

Because of Eq. (4.15) and Eq. (4.27), we can transform from the positive-frequency bands to the negative-frequency band. Before this transformation, we only consider the branches of $\sigma > 0$. Using $\omega(-\mathbf{k}, -\sigma) = -\omega(\mathbf{k}, \sigma)$, we transform the half of the summation in Eq. 4.40 from $\sigma > 0$, $\sigma' > 0$ to $\sigma < 0$, $\sigma' < 0$ and then sum them together; the summation will be done for all branches of $\sigma\sigma' > 0$, which can be written as

$$\kappa_{xy}^{(1)} = \frac{\hbar}{8VT} \sum_{\mathbf{k},\sigma\sigma'>0} [f(\omega_\sigma) - f(\omega_{\sigma'})](\omega_\sigma + \omega_{\sigma'})^2 \frac{i}{4\omega_\sigma \omega_{\sigma'}} \frac{\epsilon_\sigma^\dagger \frac{\partial D}{\partial k_x} \epsilon_{\sigma'} \epsilon_{\sigma'}^\dagger \frac{\partial D}{\partial k_y} \epsilon_\sigma}{(\omega_\sigma - \omega_{\sigma'})^2}. \tag{4.41}$$

Here, it should be noted that σ, σ' can be both positive or negative.

Second, we calculate $\kappa_{ab}^{(2)}$. Utilizing the results

$$\begin{aligned} \langle a_i^\dagger a_j^\dagger a_k a_l \rangle_{\text{eq}} &= f_i f_j (\delta_{ik}\delta_{jl} + \delta_{il}\delta_{jk}); \\ \langle a_i a_j a_k^\dagger a_l^\dagger \rangle_{\text{eq}} &= (1 + f_i)(1 + f_j)(\delta_{ik}\delta_{jl} + \delta_{il}\delta_{jk}), \end{aligned} \tag{4.42}$$

and the relation $f(-\omega) = -1 - f(\omega)$, after some algebraic derivation similar to the above, we obtain

$$\kappa_{xy}^{(2)} = \frac{\hbar}{8VT} \sum_{\mathbf{k},\sigma\sigma'<0} [f(\omega_\sigma) - f(\omega_{\sigma'})](\omega_\sigma + \omega_{\sigma'})^2 \frac{i}{4\omega_\sigma \omega_{\sigma'}} \frac{\epsilon_\sigma^\dagger \frac{\partial D}{\partial k_x} \epsilon_{\sigma'} \epsilon_{\sigma'}^\dagger \frac{\partial D}{\partial k_y} \epsilon_\sigma}{(\omega_\sigma - \omega_{\sigma'})^2}. \tag{4.43}$$

Therefore, the total phonon Hall conductivity can be written as

$$\kappa_{xy} = \frac{\hbar}{8VT} \sum_{\mathbf{k},\sigma\neq\sigma'} [f(\omega_\sigma) - f(\omega_{\sigma'})](\omega_\sigma + \omega_{\sigma'})^2 \frac{i}{4\omega_\sigma \omega_{\sigma'}} \frac{\epsilon_\sigma^\dagger \frac{\partial D}{\partial k_x} \epsilon_{\sigma'} \epsilon_{\sigma'}^\dagger \frac{\partial D}{\partial k_y} \epsilon_\sigma}{(\omega_\sigma - \omega_{\sigma'})^2}. \tag{4.44}$$

We can prove $\kappa_{xy} = -\kappa_{yx}$, such that

$$\kappa_{xy} = \frac{\hbar}{16VT} \sum_{\mathbf{k},\sigma\neq\sigma'} [f(\omega_\sigma) - f(\omega_{\sigma'})](\omega_\sigma + \omega_{\sigma'})^2 B^{\sigma\sigma'}_{k_x k_y}, \tag{4.45}$$

$$B^{\sigma\sigma'}_{k_x k_y} = \frac{i}{4\omega_\sigma\omega_{\sigma'}} \frac{\epsilon^\dagger_\sigma \frac{\partial D}{\partial k_x}\epsilon_{\sigma'}\epsilon^\dagger_{\sigma'}\frac{\partial D}{\partial k_y}\epsilon_\sigma - \epsilon^\dagger_\sigma \frac{\partial D}{\partial k_y}\epsilon_{\sigma'}\epsilon^\dagger_{\sigma'}\frac{\partial D}{\partial k_x}\epsilon_\sigma}{(\omega_\sigma - \omega_{\sigma'})^2}. \tag{4.46}$$

Because of $B^{\sigma\sigma'}_{k_x k_y} = -B^{\sigma'\sigma}_{k_x k_y}$, the phonon Hall conductivity can be written eventually as

$$\kappa_{xy} = \frac{\hbar}{8VT} \sum_{\mathbf{k},\sigma\neq\sigma'} f(\omega_\sigma)(\omega_\sigma + \omega_{\sigma'})^2 B^{\sigma\sigma'}_{k_x k_y}, \tag{4.47}$$

where V is the total volume of $N = N_L^2$ unit cells. In the above formula, the phonon branch σ includes both positive and negative values without restriction. We start with the positive frequency bands to derive the conductivity formula. Through some transformations, we finally obtain the simplified formula for phonon Hall conductivity which combines the contribution from all the frequency bands. The formula Eq. (4.47) is different from that given in Ref. [149]. In Ref. [149] the contribution for phonon Hall conductivity from J_2 was omitted, which is incorrect.

4.3.3 Onsager Relation

From the Eq. (4.13), we obtain

$$\epsilon^*_{-\mathbf{k},\sigma}(-A) = \epsilon_{\mathbf{k},\sigma}(A);\ \omega_{-\mathbf{k},\sigma}(-A) = \omega_{\mathbf{k},\sigma}(A). \tag{4.48}$$

We know that most lattices, such as square, triangle, honeycomb or kagome lattices, have inversion symmetry (2-fold symmetry). Then the dynamic matrix D is hermitian conjugate, and the determinant of $(-i\omega + A)^2 + D$ in Eq. (4.13) is a an even function of $\mathbf{k}$. Thus the eigen values satisfy $\omega_\sigma(\mathbf{k}) = \omega_\sigma(-\mathbf{k})$.

Combining Eq. (4.15, 4.48) we obtain

$$\omega_\sigma(\mathbf{k},-A)=\omega_\sigma(\mathbf{k},A),\ \omega_\sigma(-\mathbf{k},A)=\omega_\sigma(\mathbf{k},A),\ \omega_{-\sigma}(\mathbf{k},A)=-\omega_\sigma(\mathbf{k},A). \tag{4.49}$$

And because of $D(\mathbf{k})=D^*(-\mathbf{k})$, $\epsilon_\sigma^T\frac{\partial D^*}{\partial k_x}\epsilon_{\sigma'}^*=\epsilon_{\sigma'}^\dagger\frac{\partial D}{\partial k_x}\epsilon_\sigma$, we have

$$B_{k_xk_y}^{\sigma\sigma'}(\mathbf{k},-A)=B_{k_yk_x}^{\sigma\sigma'}(-\mathbf{k},A)=-B_{k_xk_y}^{\sigma\sigma'}(-\mathbf{k},A). \tag{4.50}$$

So we obtain

$$\kappa_{xy}(-A)=\kappa_{yx}(A)=-\kappa_{xy}(A). \tag{4.51}$$

The Onsager reciprocal relations are satisfied.

4.3.4 Symmetry Criterion

If the system possesses the symmetry which satisfies

$$SDS^{-1}=D,\ SAS^{-1}=-A, \tag{4.52}$$

where S represents any symmetric operation, and from Eq. (4.13), we obtain

$$S\epsilon(A)=\epsilon(-A). \tag{4.53}$$

Using the definition of the dynamic matrix $D=-A^2+\sum_{l'}K_{l,l'}e^{i(\mathbf{R}_{l'}-\mathbf{R}_l)\cdot\mathbf{k}}$ and $SDS^{-1}=D$, we can obtain

$$S\frac{\partial D}{\partial k_\alpha}S^{-1}=\frac{\partial D}{\partial k_\alpha},\qquad(\alpha=x,y). \tag{4.54}$$

Inserting $S^{-1}S=I$ into Eq. (4.46), we obtain

$$B_{k_xk_y}^{\sigma\sigma'}(-A)=B_{k_xk_y}^{\sigma\sigma'}(A). \tag{4.55}$$

Then it is easy to obtain $\kappa_{xy}(-A) = \kappa_{xy}(A)$, and because of the Onsager relation, one can easily obtain that

$$\kappa_{xy} = 0, \text{ if } SDS^{-1} = D,\ SAS^{-1} = -A. \tag{4.56}$$

This symmetry criterion is the same as the necessary condition for PHE which is discussed in Sec. 3.2.6 of Chapter 3 by using the NEGF approach.

4.3.5 The Berry Phase and Berry Curvature

Using the similar method proposed by Berry [87], we derive the Berry phase and Berry curvature in the following. Starting from

$$i\frac{\partial}{\partial t}x(t) = H_{\text{eff}}x(t) \tag{4.57}$$

and substituting

$$x(t) = e^{i\gamma_\sigma(t) - i\int_0^t dt'\omega_\sigma(\mathbf{k}(t'))}x_\sigma(\mathbf{k}(t)), \tag{4.58}$$

we can obtain the Berry phase across the Brillouin zone as

$$\gamma_\sigma = \oint \mathbf{A}^\sigma(\mathbf{k})d\mathbf{k}, \qquad \mathbf{A}^\sigma(\mathbf{k}) = i\tilde{x}_\sigma^T\frac{\partial}{\partial\mathbf{k}}x_\sigma. \tag{4.59}$$

Here $\mathbf{A}^\sigma(\mathbf{k})$ is the so-called Berry vector potential.

Therefore the Berry curvature is obtained through the Stokes theorem as:

$$B^\sigma_{k_xk_y} = \frac{\partial}{\partial k_x}\mathbf{A}^\sigma_{k_y} - \frac{\partial}{\partial k_y}\mathbf{A}^\sigma_{k_x} = i\sum_{\sigma'\neq\sigma}\frac{\tilde{x}_\sigma^T\frac{\partial H_{\text{eff}}}{\partial k_x}x_{\sigma'}\tilde{x}_{\sigma'}^T\frac{\partial H_{\text{eff}}}{\partial k_y}x_\sigma - (k_x \leftrightarrow k_y)}{(\omega_\sigma - \omega_{\sigma'})^2} \tag{4.60}$$

Inserting the vector x and the expression of matrix H_{eff}, we obtain

$$B^\sigma_{k_xk_y} = \sum_{\sigma'\neq\sigma}\frac{i}{4\omega_\sigma\omega_{\sigma'}}\frac{\epsilon_\sigma^\dagger\frac{\partial D}{\partial k_x}\epsilon_{\sigma'}\epsilon_{\sigma'}^\dagger\frac{\partial D}{\partial k_y}\epsilon_\sigma - (k_x \leftrightarrow k_y)}{(\omega_\sigma - \omega_{\sigma'})^2} = \sum_{\sigma'\neq\sigma}B^{\sigma\sigma'}_{k_xk_y} \tag{4.61}$$

Thus we find the physical picture of Eq. (4.46), that is, $B^{\sigma\sigma'}_{k_x k_y}$ indicates the contribution to the Berry curvature of the band σ from a different band σ'. Therefore, the phonon Hall conductivity formula Eq. (4.47) can be interpreted in terms of the Berry curvature. The topological Chern number is obtained by integrating the Berry curvature over the first Brillouin zone as

$$C^{\sigma} = \frac{1}{2\pi} \int_{\mathbf{BZ}} dk_x dk_y B^{\sigma}_{k_x k_y}. \tag{4.62}$$

For numerical calculation, we use

$$C^{\sigma} = \frac{2\pi}{L^2} \sum_{\mathbf{k}} B^{\sigma}_{k_x k_y}. \tag{4.63}$$

where $\frac{1}{L^2}\sum_{\mathbf{k}} = \int \frac{dk_x dk_y}{(2\pi)^2}$ and $V = L^2 a$, L^2 is the area of the sample.

In this section, firstly from the Green-Kubo formula and considering the contributions from all the phonon bands, we obtain the general formula for the phonon Hall conductivity Eq. (4.47). We start from the positive bands for the derivation. It should be noted that the correlation of aa and $a^{\dagger}a^{\dagger}$ contributes to the Hall conductivity. Considering the eigensystem of vectors of both momenta and displacements, the eigenvalues include both positive and negative frequencies. Using the relations between positive frequencies and negative ones, we can obtain the formula of phonon Hall conductivity in which the contribution from negative frequencies has the same weight as that from the positive ones. Then by looking at the phases of the polarization vectors of both the displacements and conjugate momenta as a function of the wave vector, a Berry curvature Eq. (4.61) can be defined uniquely for each band which can have a positive or negative frequency. Combining the above two steps, at last the phonon Hall conductivity can be written in terms of Berry

curvatures. Such derivation gives us the clear picture of the contribution to the phonon Hall current from all the phonon branches, and the relation between the phonon Hall conductivity with the geometrical phase of the polarization vectors, thus can help us to understand the topological picture of the PHE.

4.4 PHE Approach Two

We know that for the Hall effect of the electrons, in addition to the normal velocity from usual band dispersion contribution, the Berry curvature induces an anomalous velocity always transverse to the electric field, which gives rise to a Hall current, thus the Hall effect occurs. For the magnon Hall effect recently observed, the authors also found the anomalous velocity due to the Berry connection which is responsible for the thermal Hall conductivity. However, the above section of PHE approach one [152] cannot give us such a picture. Therefore in this section we will derive PHE approach two [153] in a more natural way where the Berry phase effect inducing the anomalous velocity contributes to the extra term of the heat current. Thus the Berry phase effect is straightforward to take the responsibility of the PHE.

4.4.1 The Second Quantization

In PHE Approach One, we first only take the positive phonon branch, that is $\sigma, \omega \geq 0$, as a convention. However, from the eigenvalue problem Eq. (4.18), we know that the complete set contains the branch of the negative frequency. And by some transformation from positive branches to negative ones, the formulas of both the Berry curvature and phonon Hall conductivity are written in the

form comprising the contribution of all the branches including both positive and negative frequency branches. Therefore it would be more convenient to take both positive and negative frequencies at the beginning. In order to simplify the notation, for all the branches, we define

$$a_{-k} = a_k^\dagger. \tag{4.64}$$

The time dependence of the operators is given by:

$$a_k(t) = a_k e^{-i\omega_k t}, \tag{4.65}$$

$$a_k^\dagger(t) = a_k^\dagger e^{i\omega_k t}. \tag{4.66}$$

The commutation relation is

$$[a_k, a_{k'}^\dagger] = \delta_{k,k'}\text{sign}(\sigma). \tag{4.67}$$

And we can get

$$\langle a_k^\dagger a_k\rangle = f(\omega_k)\text{sign}(\sigma); \tag{4.68}$$

$$\langle a_k a_k^\dagger\rangle = \big[1 + f(\omega_k)\big]\text{sign}(\sigma). \tag{4.69}$$

The displacement and momentum operators can be written in the following second quantization forms

$$u_l = \sum_k \epsilon_k e^{i\mathbf{R}_l\cdot\mathbf{k}} \sqrt{\frac{\hbar}{2N|\omega_k|}}\, a_k; \tag{4.70}$$

$$p_l = \sum_k \mu_k e^{i\mathbf{R}_l\cdot\mathbf{k}} \sqrt{\frac{\hbar}{2N|\omega_k|}}\, a_k. \tag{4.71}$$

Here, $|\omega_k| = \omega_k\text{sign}(\sigma)$. We can verify that the canonical commutation relations are satisfied: $[u_l, p_{l'}^T] = i\hbar\delta_{ll'}I_{nd}$ by using the completeness Eq. (4.21) and

the commutation relation Eq. (4.67). The Hamiltonian Eq. (4.6) then can be written as

$$H = \frac{1}{2}\sum_{l,l'} \tilde{\chi}_l^T \begin{pmatrix} A\delta_{l,l'} & K_{l,l'} - A^2\delta_{l,l'} \\ -I_{nd}\delta_{l,l'} & A\delta_{l,l'} \end{pmatrix} \chi_{l'} \tag{4.72}$$

where

$$\chi_l = \begin{pmatrix} p_l \\ u_l \end{pmatrix} = \sqrt{\frac{\hbar}{N}} \sum_k x_k e^{i\mathbf{R}_l\cdot\mathbf{k}} c_k \, a_k; \tag{4.73}$$

$$\tilde{\chi}_l = \begin{pmatrix} u_l \\ -p_l \end{pmatrix} = \sqrt{\frac{\hbar}{N}} \sum_k \tilde{x}_k e^{-i\mathbf{R}_l\cdot\mathbf{k}} \tilde{c}_k \, a_k^\dagger. \tag{4.74}$$

Here $c_k = \sqrt{\frac{1}{2|\omega_k|}}$ and $\tilde{c}_k = (-2i\omega_k)\sqrt{\frac{1}{2|\omega_k|}}$. It is easy to verify that $[\chi_l, \tilde{\chi}_{l'}^T] = -i\hbar\delta_{ll'} I_{2nd}$.

Because of $e^{i(\mathbf{R}_{l'}\cdot\mathbf{k}'-\mathbf{R}_l\cdot\mathbf{k})} = e^{i(\mathbf{R}_l\cdot(\mathbf{k}'-\mathbf{k})+(\mathbf{R}_{l'}-\mathbf{R}_l)\cdot\mathbf{k}')}$ and the definition of the dynamic matrix D, then the Hamiltonian can be written as

$$\begin{aligned} H &= \frac{\hbar}{2N}\sum_{k,k',l} e^{i\mathbf{R}_l\cdot(\mathbf{k}'-\mathbf{k})} \tilde{c}_k \, c_{k'} \tilde{x}_k^T \begin{pmatrix} A & D(\mathbf{k}') \\ -I_{nd} & A \end{pmatrix} x_{k'} a_k^\dagger a_{k'} \\ &= \frac{\hbar}{2N}\sum_{k,k',l} e^{i\mathbf{R}_l\cdot(\mathbf{k}'-\mathbf{k})} \tilde{c}_k \, c_{k'} \tilde{x}_k^T i H_{\text{eff}} x_{k'} a_k^\dagger a_{k'} \\ &= \frac{1}{2}\sum_k \hbar|\omega_k| a_k^\dagger a_k \end{aligned} \tag{4.75}$$

which contains both the positive and negative branches. Here we use the identity $\sum_l e^{i\mathbf{R}_l\cdot(\mathbf{k}'-\mathbf{k})} = N\delta_{\mathbf{k}'\mathbf{k}}$ and the eigenvalue problem Eq. (4.18). Using the relations Eqs. (4.64) and (4.67), it is easy to prove that Eq. (4.75) is equivalent to the form $H = \sum_k \hbar\omega_k(a_k^\dagger a_k + 1/2)$ which only includes the nonnegative branches.

4.4.2 Heat Current Density Operator

Because of the equation of motion Eq. (4.11), we can rewrite the heat current of Eq. (4.25) as

$$\mathbf{J} = \frac{1}{4V}\sum_{l,l'} \tilde{\chi}_l^T \mathbf{M}_{l\,l'} \chi_{l'}, \tag{4.76}$$

where

$$\mathbf{M}_{l\,l'} = \begin{pmatrix} (\mathbf{R}_l - \mathbf{R}_{l'})K_{ll'} & -(\mathbf{R}_l - \mathbf{R}_{l'})(K_{ll'}A + AK_{ll'}) \\ 0 & (\mathbf{R}_l - \mathbf{R}_{l'})K_{ll'} \end{pmatrix}. \tag{4.77}$$

Inserting the Eqs. (4.73,4.74), we obtain

$$\mathbf{J} = \frac{\hbar}{4VN}\sum_{k,k',l,l'} \tilde{c}_k c_{k'} e^{i(\mathbf{R}_{l'}\cdot\mathbf{k}' - \mathbf{R}_l\cdot\mathbf{k})} \tilde{x}_k^T \mathbf{M}_{l\,l'} x_{k'} a_k^\dagger a_{k'}. \tag{4.78}$$

Because of

$$\sum_l e^{i\mathbf{R}_l\cdot(\mathbf{k}'-\mathbf{k})} \sum_{l'} e^{i(\mathbf{R}_{l'}-\mathbf{R}_l)\cdot\mathbf{k}'} (\mathbf{R}_l - \mathbf{R}_{l'})K_{ll'} = iN\delta_{\mathbf{k}'\mathbf{k}} \frac{\partial D}{\partial \mathbf{k}'}, \tag{4.79}$$

the heat current can be written as

$$\mathbf{J} = \frac{i\hbar}{4V}\sum_{\sigma,\sigma',\mathbf{k}} \tilde{c}_{\sigma,\mathbf{k}} c_{\sigma',\mathbf{k}} \tilde{x}_{\sigma,\mathbf{k}}^T \frac{\partial H_{\text{eff}}^2}{\partial \mathbf{k}} x_{\sigma',\mathbf{k}} a_{\sigma,\mathbf{k}}^\dagger a_{\sigma',\mathbf{k}}, \tag{4.80}$$

here we use

$$\frac{\partial H_{\text{eff}}^2}{\partial \mathbf{k}} = \begin{pmatrix} \frac{\partial D}{\partial \mathbf{k}} & -(A\frac{\partial D}{\partial \mathbf{k}} + \frac{\partial D}{\partial \mathbf{k}}A) \\ 0 & \frac{\partial D}{\partial \mathbf{k}} \end{pmatrix} \tag{4.81}$$

by doing the first derivative of the square of the effective Hamiltonian Eq. (4.17) with respect to the wave vector $\mathbf{k}$. From the eigenvalue problem Eq. (4.18), we have

$$H_{\text{eff}} X = X\Omega; \quad \tilde{X}^T H_{\text{eff}} = \Omega \tilde{X}^T. \tag{4.82}$$

Where the $2nd \times 2nd$ matrices $X = (x_1, x_2, ..., x_{2nd}) = \{x_\sigma\}$ (the system has $2nd$ phonon branches), $\tilde{X} = \{\tilde{x}_\sigma\}$, and $\Omega = \mathrm{diag}(\omega_1, \omega_2, ..., \omega_{2nd}) = \{\omega_\sigma\}$. Because of the completeness relation Eq. (4.21), $X\tilde{X}^T = I_{2nd}$, then we get

$$H_{\mathrm{eff}}^2 = X\Omega^2\tilde{X}^T. \tag{4.83}$$

By calculating the derivative of the above equation, and using the definition of Berry connection,

$$\mathcal{A} = \tilde{X}^T\frac{\partial X}{\partial \mathbf{k}}. \tag{4.84}$$

Taking the first derivative of Eq. (4.83) with respect to $\mathbf{k}$, we obtain

$$\frac{\partial H_{\mathrm{eff}}^2}{\partial \mathbf{k}} = X\left(\frac{\partial \Omega^2}{\partial \mathbf{k}} + [\mathcal{A}, \Omega^2]\right)\tilde{X}^T. \tag{4.85}$$

Because of the the orthogonality relation between left and right eigenvector Eq. (4.20), at last we obtain the heat current as

$$\mathbf{J} = \frac{i\hbar}{4V}\sum_{\sigma,\sigma',\mathbf{k}} \tilde{c}_{\sigma,\mathbf{k}}c_{\sigma',\mathbf{k}}a^\dagger_{\sigma,\mathbf{k}}\left(\frac{\partial \Omega^2}{\partial \mathbf{k}} + [\mathcal{A}, \Omega^2]\right)_{\sigma,\sigma'} a_{\sigma',\mathbf{k}}. \tag{4.86}$$

The first term $\frac{\partial \Omega^2}{\partial \mathbf{k}}$ in the bracket is a diagonal one corresponding to $\omega_\sigma\frac{\partial \omega_\sigma}{\partial \mathbf{k}}$ relating to the group velocity. The second term in the bracket $[\mathcal{A}, \Omega^2]$ gives the off-diagonal elements of the heat current density, which can be regarded as the contribution from anomalous velocities similar to the one in the intrinsic anomalous Hall effect. The Berry connection $\mathcal{A}$, or we can call it Berry vector potential matrix (the Berry vector potential defined in Ref. [152], $\mathbf{A}^\sigma(\mathbf{k})$, is equal to $i\mathcal{A}^{\sigma\sigma} = i\tilde{x}_\sigma^T\frac{\partial x_\sigma}{\partial \mathbf{k}}$), induces the anomalous velocities to the heat current, which will take the responsibility of the PHE. Therefore, the Berry vector potential comes naturally into the heat current and the PHE, such picture is clearer than that in PHE Approach One.

4.4.3 Phonon Hall Conductivity

Inserting the coefficients $\tilde{c}$ and c to Eq. (4.86), we get

$$\mathbf{J} = \frac{\hbar}{4V}\sum_{\sigma,\sigma',\mathbf{k}} \frac{\omega_{\sigma,\mathbf{k}}}{\sqrt{|\omega_{\sigma,\mathbf{k}}\omega_{\sigma',\mathbf{k}}|}} a^{\dagger}_{\sigma,\mathbf{k}} \left(\frac{\partial\Omega^2}{\partial\mathbf{k}} + [\mathcal{A},\Omega^2]\right)_{\sigma,\sigma'} a_{\sigma',\mathbf{k}}. \tag{4.87}$$

This expression is equivalent to that given in Refs. [152] and [154]. Based on such expression of heat current, the phonon Hall conductivity can be obtained through the Green-Kubo formula Eq. (4.37).

The time dependence of the creation and annihilation operators are given as Eqs. (4.65) and (4.66), which are also true if t is imaginary. Inserting the heat current operators, we can write the phonon Hall conductivity as

$$\begin{aligned}
\kappa_{xy} &= \frac{V}{\hbar T}\left(\frac{\hbar}{4V}\right)^2 \sum_{\sigma,\sigma',\mathbf{k};\bar{\sigma},\bar{\sigma'},\bar{\mathbf{k}}} \frac{\omega_{\sigma,\mathbf{k}}}{\sqrt{|\omega_{\sigma,\mathbf{k}}\omega_{\sigma',\mathbf{k}}|}} \frac{\omega_{\bar{\sigma},\bar{\mathbf{k}}}}{\sqrt{|\omega_{\bar{\sigma},\bar{\mathbf{k}}}\omega_{\bar{\sigma'},\bar{\mathbf{k}}}|}} \\
&\times \left(\frac{\partial\Omega^2}{\partial k_x} + [\mathcal{A}_{k_x},\Omega^2]\right)_{\sigma,\sigma'} \left(\frac{\partial\Omega^2}{\partial \bar{k_y}} + [\mathcal{A}_{\bar{k_y}},\Omega^2]\right)_{\bar{\sigma},\bar{\sigma'}} \langle a^{\dagger}_{\sigma,\mathbf{k}} a_{\sigma',\mathbf{k}} a^{\dagger}_{\bar{\sigma},\bar{\mathbf{k}}} a_{\bar{\sigma'},\bar{\mathbf{k}}}\rangle \\
&\times \int_0^{\hbar/k_BT} d\lambda \int_0^{\infty} dt e^{i(\omega_{\sigma,\mathbf{k}}-\omega_{\sigma',\mathbf{k}})(-i\lambda)} e^{i(\omega_{\bar{\sigma},\bar{\mathbf{k}}}-\omega_{\bar{\sigma'},\bar{\mathbf{k}}})t}.
\end{aligned} \tag{4.88}$$

From the Wick theorem, we have

$$\begin{aligned}
\langle a^{\dagger}_{\sigma,\mathbf{k}} a_{\sigma',\mathbf{k}} a^{\dagger}_{\bar{\sigma},\bar{\mathbf{k}}} a_{\bar{\sigma'},\bar{\mathbf{k}}}\rangle &= \langle a^{\dagger}_{\sigma,\mathbf{k}} a_{\sigma',\mathbf{k}}\rangle\langle a^{\dagger}_{\bar{\sigma},\bar{\mathbf{k}}} a_{\bar{\sigma'},\bar{\mathbf{k}}}\rangle \\
&+ \langle a^{\dagger}_{\sigma,\mathbf{k}} a^{\dagger}_{\bar{\sigma},\bar{\mathbf{k}}}\rangle\langle a_{\sigma',\mathbf{k}} a_{\bar{\sigma'},\bar{\mathbf{k}}}\rangle \\
&+ \langle a^{\dagger}_{\sigma,\mathbf{k}} a_{\bar{\sigma'},\bar{\mathbf{k}}}\rangle\langle a_{\sigma',\mathbf{k}} a^{\dagger}_{\bar{\sigma},\bar{\mathbf{k}}}\rangle.
\end{aligned} \tag{4.89}$$

Using the properties of the operators $a^\dagger$ and a as Eq. (4.68), we have

$$\begin{aligned}
&\langle a^\dagger_{\sigma,\mathbf{k}} a_{\sigma',\mathbf{k}}\rangle\langle a^\dagger_{\bar{\sigma},\bar{\mathbf{k}}} a_{\bar{\sigma}',\bar{\mathbf{k}}}\rangle \\
&= f(\omega_{\sigma,\mathbf{k}}) f(\omega_{\bar{\sigma},\bar{\mathbf{k}}})\delta_{\sigma\sigma'}\delta_{\bar{\sigma}\bar{\sigma}'}\mathrm{sign}(\sigma)\mathrm{sign}(\bar{\sigma}), \\
&\langle a^\dagger_{\sigma,\mathbf{k}} a^\dagger_{\bar{\sigma},\bar{\mathbf{k}}}\rangle\langle a_{\sigma',\mathbf{k}} a_{\bar{\sigma}',\bar{\mathbf{k}}}\rangle \\
&= f(\omega_{\sigma,\mathbf{k}})(f(\omega_{\sigma',\mathbf{k}})+1)\delta_{\bar{\mathbf{k}},-\mathbf{k}}\delta_{\sigma,-\bar{\sigma}}\delta_{\sigma',-\bar{\sigma}'}\mathrm{sign}(\sigma)\mathrm{sign}(\sigma') \\
&\langle a^\dagger_{\sigma,\mathbf{k}} a_{\bar{\sigma}',\bar{\mathbf{k}}}\rangle\langle a_{\sigma',\mathbf{k}} a^\dagger_{\bar{\sigma},\bar{\mathbf{k}}}\rangle \\
&= f(\omega_{\sigma,\mathbf{k}})(f(\omega_{\sigma',\mathbf{k}})+1)\delta_{\bar{\mathbf{k}},\mathbf{k}}\delta_{\sigma,\bar{\sigma}'}\delta_{\sigma',\bar{\sigma}}\mathrm{sign}(\sigma)\mathrm{sign}(\sigma').
\end{aligned} \tag{4.90}$$

Then the phonon Hall conductivity κ_{xy} can be written in three parts. The first part relating to the normal velocities has no contribution to the PHE, because of the odd function of $\frac{\partial\Omega^2}{\partial k_\alpha}$. And the other two parts have the equal contribution. After some algebraic calculations, we get the phonon Hall conductivity as

$$\begin{aligned}
\kappa_{xy} &= \frac{\hbar}{8VT}\sum_{\mathbf{k},\sigma,\sigma'\neq\sigma}[f(\omega_\sigma)-f(\omega_{\sigma'})](\omega_\sigma+\omega_{\sigma'})^2 \\
&\quad\times\frac{i}{4\omega_\sigma\omega_{\sigma'}}\frac{\epsilon^\dagger_\sigma\frac{\partial D}{\partial k_x}\epsilon_{\sigma'}\epsilon^\dagger_{\sigma'}\frac{\partial D}{\partial k_y}\epsilon_\sigma}{(\omega_\sigma-\omega_{\sigma'})^2}.
\end{aligned} \tag{4.91}$$

Here we simplify the notation of the subscripts of ω, ϵ which have the same wave vector $\mathbf{k}$. Using $\kappa_{xy} = -\kappa_{yx}$, thus we obtain the same formula as Eq. (4.47) in PHE Approach One, with

$$\begin{aligned}
B^{\sigma\sigma'}_{k_xk_y} &= \frac{i}{4\omega_\sigma\omega_{\sigma'}}\frac{\epsilon^\dagger_\sigma\frac{\partial D}{\partial k_x}\epsilon_{\sigma'}\epsilon^\dagger_{\sigma'}\frac{\partial D}{\partial k_y}\epsilon_\sigma-(k_x\leftrightarrow k_y)}{(\omega_\sigma-\omega_{\sigma'})^2} \\
&= i\frac{\tilde{x}^T_\sigma\frac{\partial H_{\mathrm{eff}}}{\partial k_x}x_{\sigma'}\tilde{x}^T_{\sigma'}\frac{\partial H_{\mathrm{eff}}}{\partial k_y}x_\sigma-(k_x\leftrightarrow k_y)}{(\omega_\sigma-\omega_{\sigma'})^2}.
\end{aligned} \tag{4.92}$$

Because of the relation $\tilde{x}^T_\sigma\frac{\partial H_{\mathrm{eff}}}{\partial k_x}x_{\sigma'} = (\omega_{\sigma'}-\omega_\sigma)\tilde{x}^T_\sigma\frac{\partial}{\partial k_x}x_{\sigma'}$ and the definition of

$\mathcal{A}$ in Eq. (4.84), we obtain

$$B^{\sigma\sigma'}_{k_xk_y} = -i\left(\mathcal{A}^{\sigma\sigma'}_{k_x}\mathcal{A}^{\sigma'\sigma}_{k_y} - (k_x \leftrightarrow k_y)\right). \tag{4.93}$$

And the Berry curvature is

$$\begin{aligned} B^{\sigma}_{k_xk_y} &= \sum_{\sigma'\neq\sigma} B^{\sigma\sigma'}_{k_xk_y} \\ &= -i\sum_{\sigma'}\left(\mathcal{A}^{\sigma\sigma'}_{k_x}\mathcal{A}^{\sigma'\sigma}_{k_y} - (k_x \leftrightarrow k_y)\right) \\ &= i\left(\frac{\partial}{\partial k_x}\mathcal{A}^{\sigma\sigma}_{k_y} - (k_x \leftrightarrow k_y)\right), \end{aligned} \tag{4.94}$$

by using the orthonormal condition Eq. (4.20) and the completeness relation Eq. (4.21).

Such Berry curvature is the same with that of PHE Approach One, that is, $B^{\sigma}_{k_xk_y} = \frac{\partial}{\partial k_x}\mathbf{A}^{\sigma}_{k_y} - \frac{\partial}{\partial k_y}\mathbf{A}^{\sigma}_{k_x}$. From the above derivation, we find that a Berry curvature can be defined uniquely for each band by looking at the phases of the polarized vectors of both the displacements and conjugate momenta as functions of the wave vector. If we only look at the polarized vector ϵ of the displacement, a Berry curvature cannot properly be defined. We need both ϵ and μ. The nontrivial Berry vector potential take the responsibility of the PHE.

4.5 Numerical Results and Discussion

From both the PHE Approach One and the PHE Approach Two, we obtain the phonon Hall conductivity as

$$\kappa_{xy} = \frac{\hbar}{8VT}\sum_{\mathbf{k},\sigma,\sigma'\neq\sigma} f(\omega_\sigma)(\omega_\sigma + \omega_{\sigma'})^2 B^{\sigma\sigma'}_{k_xk_y},$$

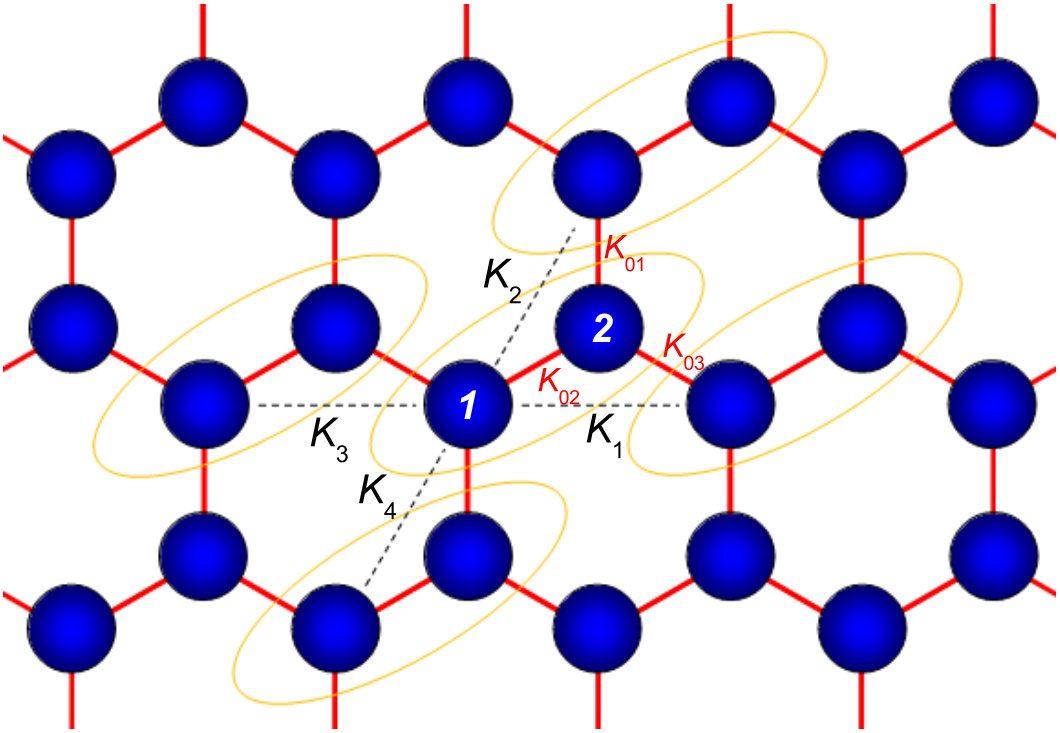

Figure 4.1: The schematic picture of honeycomb lattice. Each unit cell has two atoms such as the number shown 1,2. The coupling between the atoms are K_{01}, K_{02}, K_{03}. Each unit cell (shown in the ellipse) has four nearest neighbors; the coupling between the unit cell and the neighbors are K_1, K_2, K_3, and K_4.

here $B^{\sigma\sigma'}_{k_xk_y} = \frac{i}{4\omega_\sigma\omega_{\sigma'}} \frac{\epsilon^\dagger_\sigma \frac{\partial D}{\partial k_x}\epsilon_{\sigma'}\epsilon^\dagger_{\sigma'}\frac{\partial D}{\partial k_y}\epsilon_\sigma - (k_x \leftrightarrow k_y)}{(\omega_\sigma - \omega_{\sigma'})^2}$, and the Berry curvature and Chern number of a phonon band is

$$B^\sigma_{k_xk_y} = \sum_{\sigma'\neq\sigma} B^{\sigma\sigma'}_{k_xk_y}, \quad C^\sigma = \frac{1}{2\pi}\int_{\mathbf{BZ}} dk_x dk_y B^\sigma_{k_xk_y}.$$

Based on these formulas, in the following we can study the phonon Hall conductivity and the related topological nature of the PHE.

4.5.1 Honeycomb Lattices

Dynamic matrix

In order to calculate the phonon Hall conductivity, we first need to calculate the dynamic matrix $D(\mathbf{k})$. In the following, we give two examples, honeycomb and kagome lattices. We only discuss the two-dimensional motion and consider the nearest neighbor interaction. The spring constant matrix along x direction is

$$K_x = \begin{pmatrix} K_L & 0 \\ 0 & K_T \end{pmatrix}. \tag{4.95}$$

$K_L = 0.144\,\mathrm{eV/(u\AA^2)}$ is the longitudinal spring constant and the transverse one K_T is 4 times smaller. The unit cell lattice vectors are $(a, 0)$ and $(a/2, a\sqrt{3}/2)$ with $a = 1\,\mathrm{\AA}$.

Firstly we discuss the two-dimensional honeycomb lattice, where $n = 2, d = 2$, shown in Fig. 4.1. To obtain the explicit formula for the dynamic matrix, we first define a rotation operator in two dimensions as:

$$U(\theta) = \begin{pmatrix} \cos\theta & -\sin\theta \\ \sin\theta & \cos\theta \end{pmatrix}.$$

The three kinds of spring-constant matrices between two atoms are $K_{01} = U(\pi/2)K_xU(-\pi/2)$, $K_{02} = U(\pi/6)K_xU(-\pi/6)$, $K_{03} = U(-\pi/6)K_xU(\pi/6)$, shown in Fig. (4.1), which are 2×2 matrices. Then we can obtain the on-site spring-constant matrix and the four spring-constant matrices between the unit

cell and its four nearest neighbors as:

$$K_0 = \begin{pmatrix} K_{01}+K_{02}+K_{03} & -K_{02} \\ -K_{02} & K_{01}+K_{02}+K_{03} \end{pmatrix},$$
$$K_1 = \begin{pmatrix} 0 & 0 \\ -K_{03} & 0 \end{pmatrix}, \quad K_2 = \begin{pmatrix} 0 & 0 \\ -K_{01} & 0 \end{pmatrix},$$
$$K_3 = \begin{pmatrix} 0 & -K_{03} \\ 0 & 0 \end{pmatrix}, \quad K_4 = \begin{pmatrix} 0 & -K_{01} \\ 0 & 0 \end{pmatrix}, \tag{4.96}$$

which are 4×4 matrices. Finally we can obtain the 4×4 dynamic matrix $D(\mathbf{k})$ as

$$D(\mathbf{k}) = -A^2 + K_0 + K_1 e^{ik_x} + K_2 e^{i(k_x/2+\sqrt{3}k_y/2)} + K_3 e^{-ik_x} + K_4 e^{-i(k_x/2+\sqrt{3}k_y/2)}, \tag{4.97}$$

where, $A^2 = -h^2 \cdot I_4$, and I_4 denotes the 4×4 identity matrix.

Phonon Hall conductivity

After we get the expression for the dynamic matrix, we can calculate the eigenvalues and eigenvectors of the effective Hamiltonian. Inserting the eigenvalues, eigenvectors and the D matrix to the formula Eq. (4.47), we are able to compute the the phonon Hall conductivity.

Fig. 4.2 shows the phonon Hall conductivity with magnetic field for different temperatures. We find that in the weak magnetic field range, the phonon Hall conductivity κ_{xy} is proportional to the magnetic field, which is consistent with all the experimental and our results of PHE in four-terminal junctions.

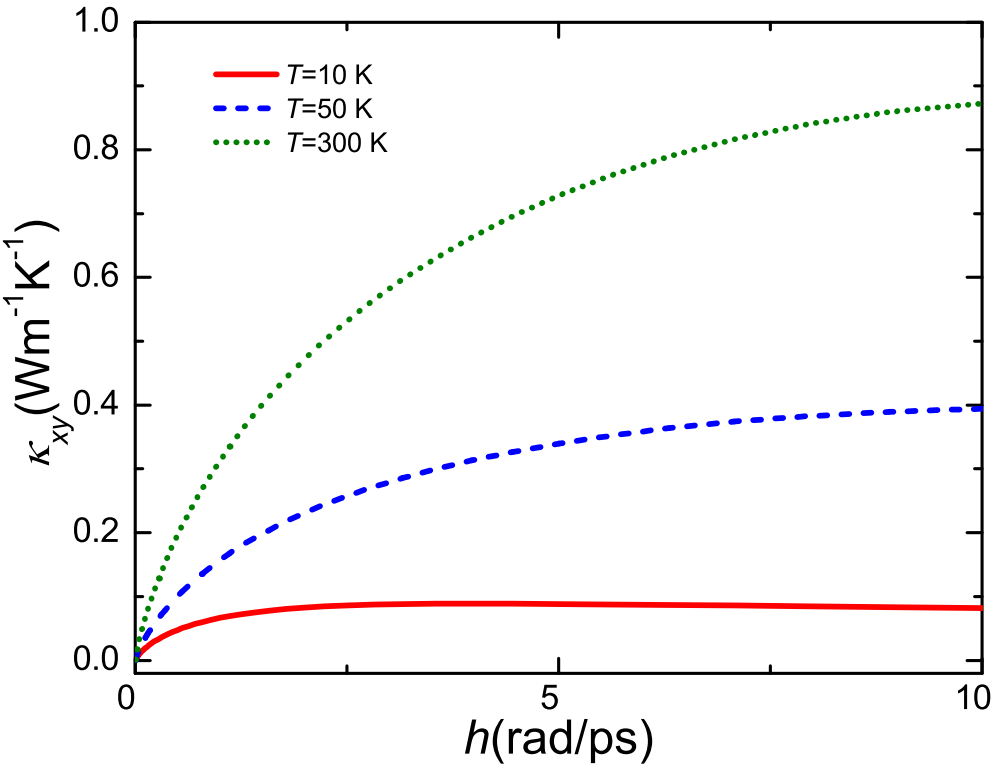

Figure 4.2: Phonon Hall conductivity vs applied magnetic field for a two-dimensional honeycomb lattice. The solid, dashed and dotted lines correspond $T = 10, 50$, and 300 K, respectively.

With increasing the magnetic field, we find that the dependence of κ_{xy} on h becomes nonlinear, which also verify our results in the previous chapter.

At low temperatures, if we increase the magnetic field h, we find that the phonon Hall conductivity κ_{xy} will not be linear with h, after some maximum point, κ_{xy} will decrease, to zero, then to negative, which is shown in Fig. 4.3(a). The phonon Hall conductivity can change sign with increasing magnetic field at low temperatures. As shown in Fig. 4.3(b), with increasing temperature, the magnitude of the negative Hall conductivity decreases; after the temperature $T > T_0 = 30.5552$ K (for the parameters concerned), there is no negative Hall conductivity in the whole range of positive magnetic field. When the temperature is high, more high energy modes are excited, the strong spin-phonon interaction can not easily turn around the phonons, therefore, there is no negative phonon Hall conductivity.

From Fig. 4.3, we find the phonon Hall conductivity is not a monotonic function of temperature, thus we plot the κ_{xy} as a function of a large range of temperature at a fixed magnetic field $h = 1$ rad/ps in Fig. 4.4. At very low temperatures, the phonon Hall conductivity is proportional to $1/T$. $k_{xy}T$ will be constant for different temperatures lower than 1 K, which can be seen in the inset of Fig. 4.4 . This is due to the contribution from $\kappa_{xy}^{(2)}$ of Eq. (4.43): if $T \to 0$, $1 + f \to 1$, then the conductivity linear with $1/T$ tends infinity. While the longitudinal thermal conductivity κ_{xx} is infinite for any temperature [149], thus when $T \to 0$, the transverse Hall conductivity, $\kappa_{xy} \to \infty$, has the ballistic property similar to the longitudinal one. If temperature is very high, all the modes contribute to the thermal transport, and $f \simeq k_B T/(\hbar\omega)$, then the

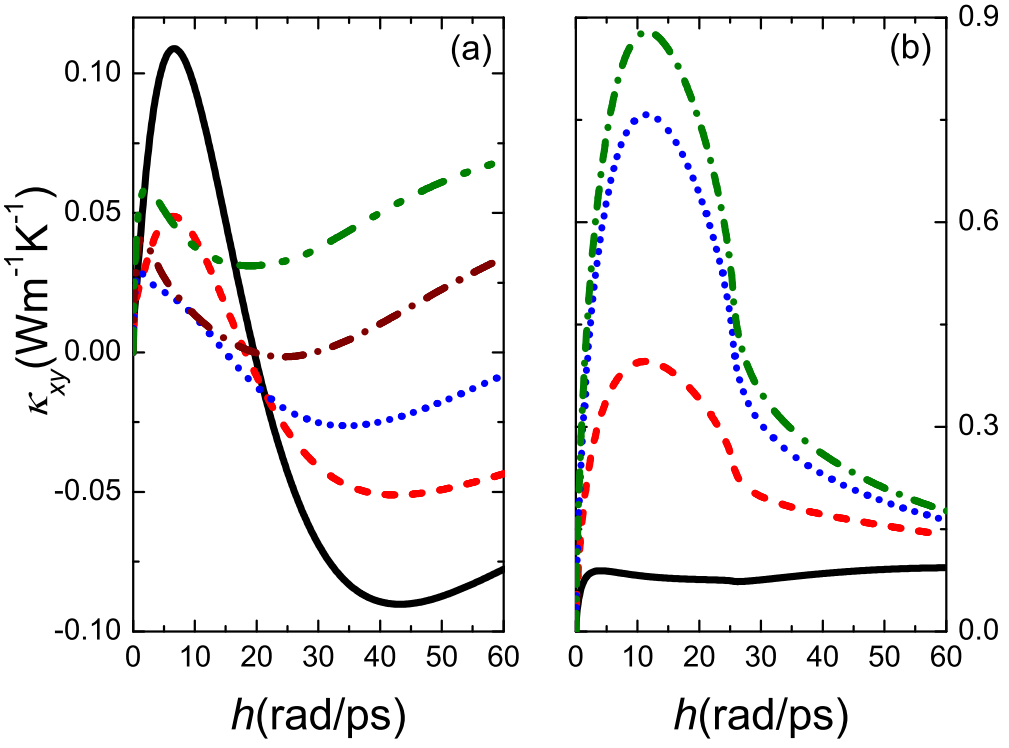

Figure 4.3: Phonon Hall conductivity vs magnetic field for different temperatures. (a) The solid, dash, dot, dash-dot, and dash-dot-dot lines correspond to fixed temperature $T = 5, 10, 20, 30$, and 40 K, respectively. (b) The solid, dash, dot, and dash-dot lines correspond to fixed temperature $T = 50, 100, 200$, and 300 K, respectively.

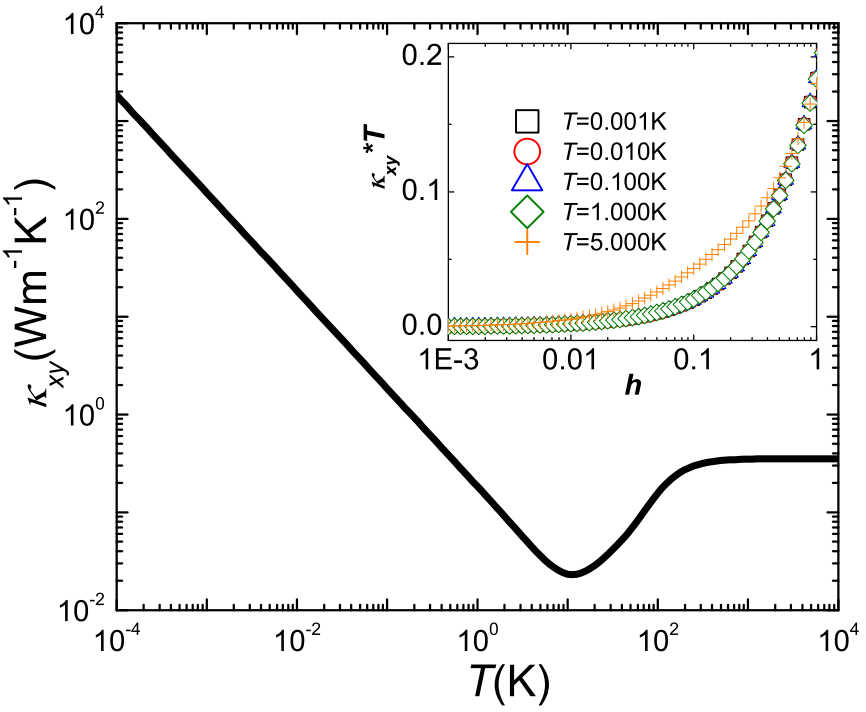

Figure 4.4: Phonon Hall conductivity vs temperature at fixed magnetic field $h = 1$ rad/ps. The inset of (b) shows the product of phonon Hall conductivity and temperature $\kappa_{xy}T$ vs magnetic field h for different temperatures.

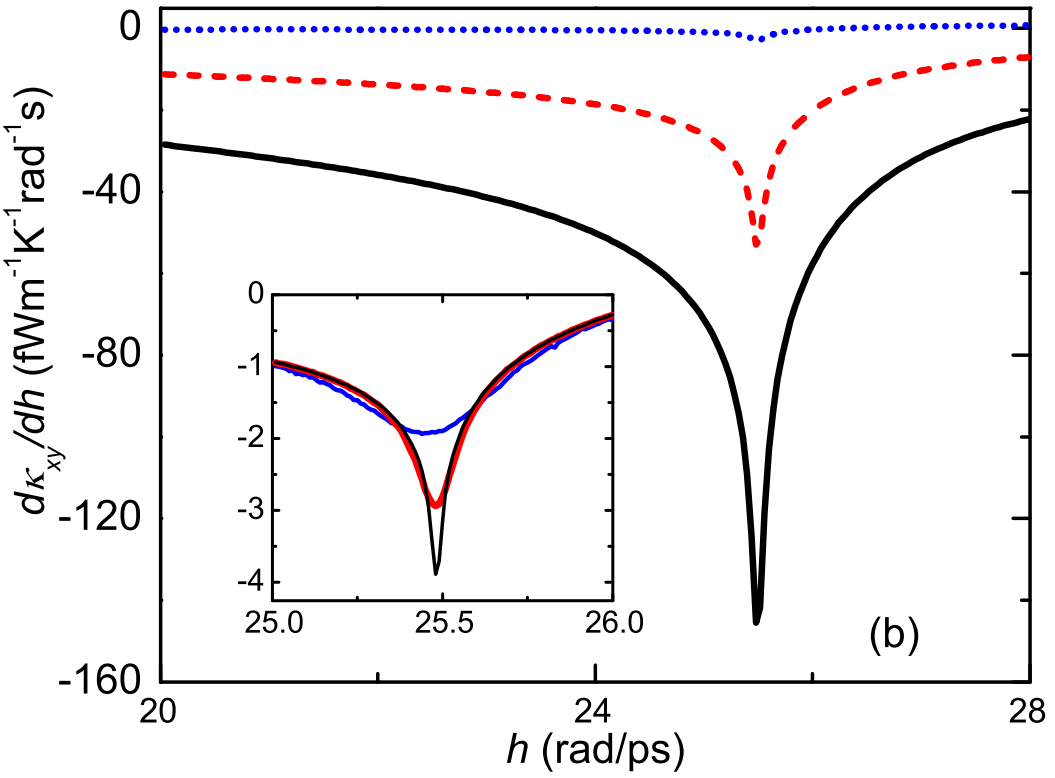

Figure 4.5: $d\kappa_{xy}/dh$ as a function of h at different temperatures: $T = 50$ (dotted line), 100 (dashed line), and 300 K (solid line); here $N_L = 400$. The inset in (b) shows the h-dependence of $d\kappa_{xy}/dh$ for different size N_L at $T = 50$ K, around $h \approx 25.5$ rad/ps; from top to bottom, $N_L = 80, 320$, and 1280, respectively.

phonon Hall conductivity becomes a constant, which can be seen in Fig. 4.4.

At the relative higher temperatures, the phonon Hall conductivity will have a sudden decrease at the same magnetic field. From Fig. 4.3(b), for all the high temperatures, the sudden changes for the hall conductivity all happen at the same magnetic field around $h \simeq 25$ rad/ps, we thus plot the first derivative of κ_{xy} with respect to h at different temperatures in Fig. 4.5. It shows that, at the relatively high temperatures, the first derivative of phonon Hall conductivity has a minimum at the magnetic field $h_c \simeq 25.4778$ rad/ps for

the finite-size sample $N_L = 400$ (the sample has $N = N_L^2$ unit cells). The first derivative $d\kappa_{xy}/dh$ at the point h_c diverges when the system size increases to infinity. The inset in Fig. 4.5 shows the finite-size effect. At the point h_c, the second derivative $d^2\kappa_{xy}/dh^2$ is discontinuous. Therefore, h_c is a critical point for the PHE, across which a phase transition occurs. At low temperatures, the divergence of $d\kappa_{xy}/dh$ is not so evident as that at high temperatures. However, if the sample size becomes larger, the discontinuity of $d^2\kappa_{xy}/dh^2$ is more obvious, as illustrated in Fig. 4.5. For different temperatures, the phase transition occurs at exactly the same critical value h_c, which strongly suggests that the phase transition of the PHE is related to the topology of the phonon band structure.

Chern numbers of the phonon bands

To calculate the integer Chern numbers, large $\mathbf{k}$-sampling points N is needed. However there is always a zero eigenvalue at the Γ point of the dispersion relation, which corresponds to a singularity of the Berry curvature. Therefore, we cannot sum up the Berry curvature very near this point to obtain Chern number of this band, unless we add a negligible on-site potential $\frac{1}{2}u^T V_{\text{onsite}} u$ to the original Hamiltonian. In Fig. 4.6(a), without the on-site potential, the Chern number of the fourth band is not an integer, no matter how large the sample size $N = N_L^2$ is (see Fig. 4.6(b)). If we add the external on-site potential, the Chern number of the fourth band will become an integer. In Fig. 4.6(a), the C_4 changes gradually to -1 with increasing the on-site potential, while other Chern numbers do not change. And from Fig. 4.6(b), we see that with larger on-site potential, the Chern number of the fourth band

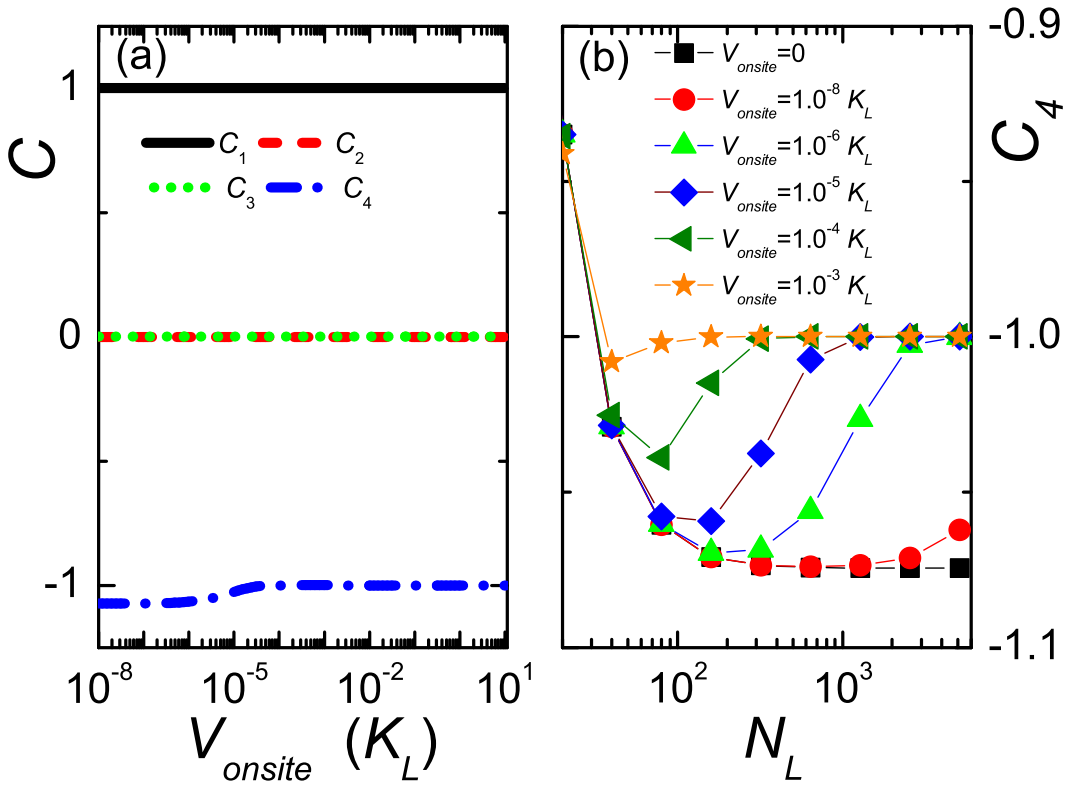

Figure 4.6: (a) The four Chern number vs onsite potential V_{onsite}. The unit for onsite potential is longitudinal spring constant K_L. Here $N = N_L^2 = 160000$; (b) The Chern number of the fourth band changes with N_L for different onsite potentials. For both (a) and (b), $h = 1$ rad/ps.

could be an integer for smaller sample sizes.

Without Raman spin-phonon interaction, that is, $h = 0$, the contribution from different band σ' to the Berry curvature of band σ: $\Omega^{\sigma\sigma'}_{k_x k_y} = 0$, thus Berry curvature is zero everywhere and the phonon Hall conductivity is zero. When we apply nonzero magnetic field, the Berry curvature changes to nonzero, which can be seen from Fig. 4.7, and the phonon Hall conductivity becomes nonzero, phonon Hall effect can be present in the lattice. In Fig. 4.7, we plot the Berry curvatures and Chern numbers for four energy bands with negative eigenvalues ω_σ, the ones for other four bands have the opposite values. Figure 4.7 (a)-(d) show the contour maps of Berry curvature at the magnetic field $h = 1$ rad/ps. Near the Γ points and/or K, K' points, the Berry curvatures have nonzero values. But for different bands, the Berry curvatures are different, and all of which show the symmetry of the reciprocal lattice. If the magnetic field changes, the Berry curvatures change. From Fig. 4.7(a)-(d) to Fig. 4.7(e)-(h), the magnetic field changes from 1 to 2 rad/ps, the Berry curvatures are quite different. However, we find that the corresponding Chern numbers are kept constant integers in a large range of the magnetic field. From Fig. 4.7(i), the Chern numbers of the first band and the fourth band are nonzero integer, and the ones of other two bands are zero. Therefore, the Chern numbers given by Eq. (4.62) are topological invariant integers, which indeed illustrate the topology of the band structure of the ballistic phonon Hall model. For the triangular lattice, the topology of band structure has the similar property: an applied magnetic field induces nonzero Berry curvature, and the corresponding Chern numbers are topological invariant integers. Although the Chern numbers are quantized as integers, because of the phonon Hall con-

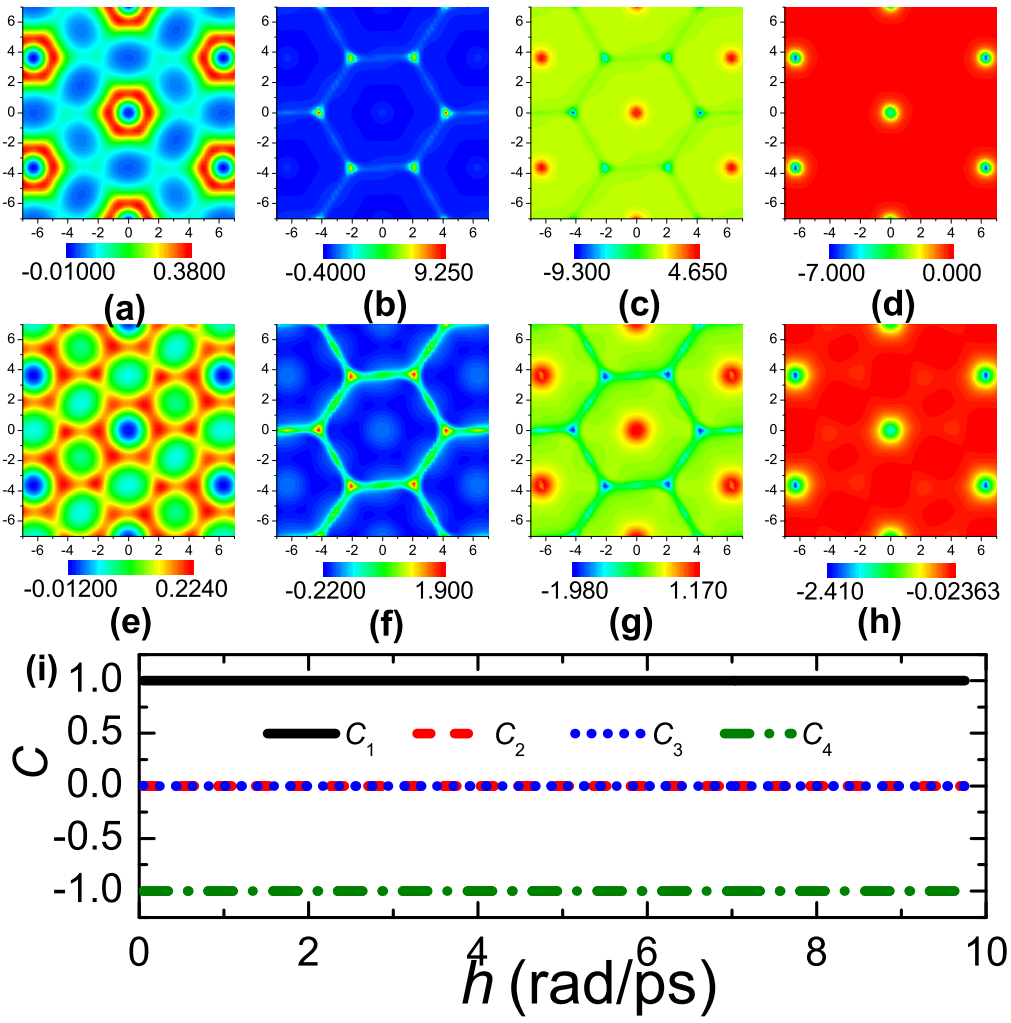

Figure 4.7: (a)-(d) The contour map of Berry curvatures for 1 - 4 energy bands at $h = 1$ rad/ps; (e)-(h) The contour map of Berry curvatures for 1 - 4 energy bands at $h = 2$ rad/ps; (i) The Chern numbers for four energy bands, the solid, dash, dot, and dash-dot lines correspond to energy band 1, 2, 3 and 4, respectively.

ductivity written in the form as Eq. (4.47) which can not be represented as a simple relation with Chern numbers, we can not obtain a quantized phonon Hall conductivity.

Associated phase transition

In the vicinity of the critical magnetic field h_c, we find that the phase transition is indeed related to the abrupt change of the topology of band structures. The Berry curvatures for different bands near the critical magnetic field are illustrated in Fig. 4.8(a-h). We find that with an infinitesimal change of magnetic field around h_c, the Berry curvatures around the Γ ($\mathbf{k} = 0$) point of bands 2 and 3 are quite different, whereas those of band 1 and 4 remain unchanged. To illustrate the change of the Berry curvatures clearly, we plot the cross section of the Berry curvatures along the k_x direction for bands 2 and 3 in Fig. 4.8(i), which shows explicitly that the Berry curvatures change dramatically above and below the critical magnetic field h_c. Below the critical point, the Berry curvature for band 2 in the vicinity of Γ point contributes Berry phase 2π (-2π for band 3), which cancels that from K,and K' points, so that the Chern number is zero for bands 2 and 3, as indicated in Fig. 4.8(j). However, above the critical point, the sum of Berry curvature at Γ point is zero, and only the monopole at K, and K' points contributes to Berry phase (-2π for band 2 and 2π for band 3). Therefore, the Chern numbers jump from 0 to ± 1, as shown in Fig. 4.8(j). This jump indicates that the topology of the two bands suddenly changes at the critical magnetic field, which is responsible for the phase transition.

To further investigate the mechanism of the abrupt change of the phonon

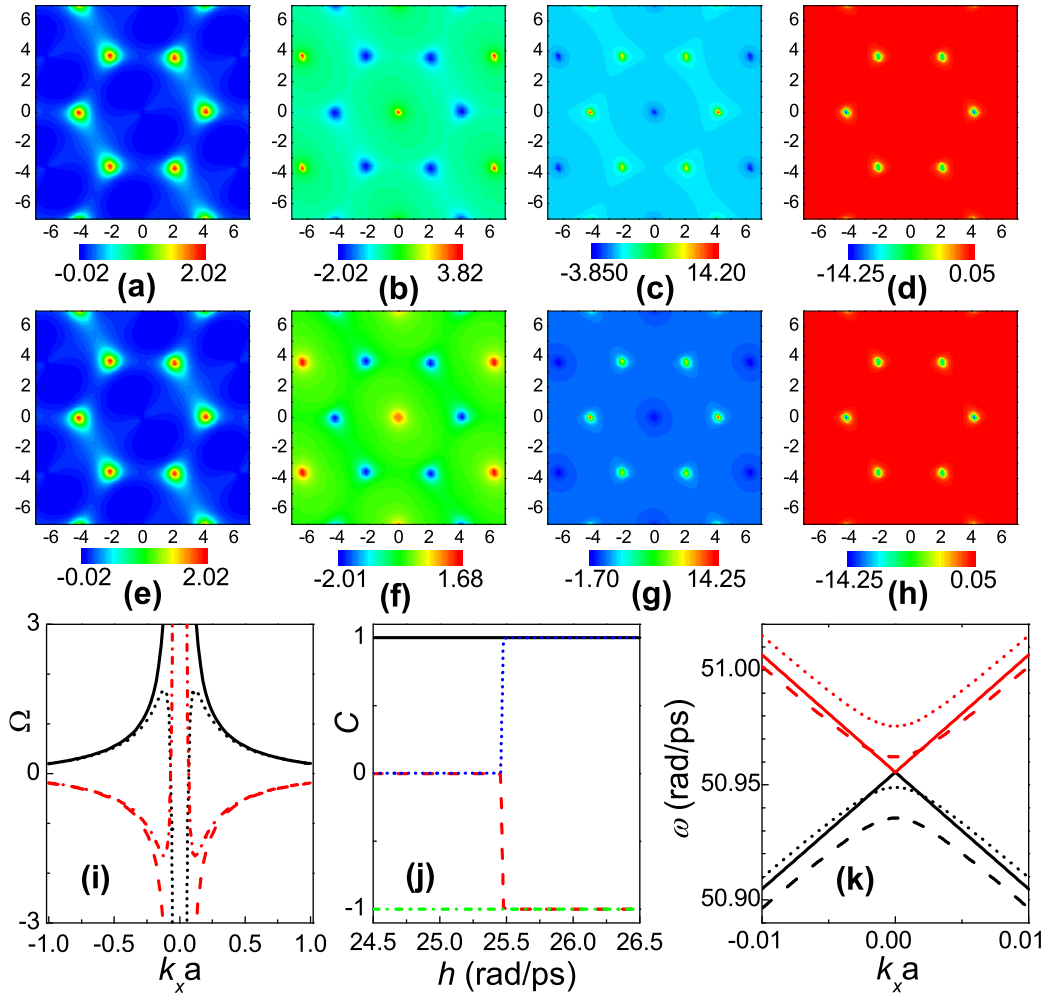

Figure 4.8: (a)-(d) The contour map of Berry curvatures for bands $1-4$ at $h_{c-} = h_c - 10^{-2}$ rad/ps; (e)-(h) The contour map of Berry curvatures for bands $1-4$ at $h_{c+} = h_c + 10^{-2}$ rad/ps. For (a)-(h), the horizontal and vertical axes correspond to wave vector k_x and k_y, respectively. (i) Ω at different magnetic fields. The solid and dashed lines correspond to Ω^2 and Ω^3 at h_{c-} respectively, while dotted and dash-dotted lines correspond to those at h_{c+}. (j) Chern numbers of four bands: C^1 (solid line), C^2 (dashed line), C^3 (dotted line), and C^4 (dash-dotted line). (k) The dispersion relation of band 2 and 3 at different magnetic fields in the vicinity of h_c. The dashed, solid and dotted lines correspond to the bands at h_{c-}, h_c, and h_{c+}, respectively. The lower three and upper three correspond to bands 2 and 3, respectively. $k_y = 0$ in (i) and (k).

band topology, we study the dispersion relation near the critical magnetic field. From Fig. 4.8(k), we can see that band 2 and 3 are going to touch with each other at the Γ point if the magnetic field increases to h_c; at the critical magnetic field, the degeneracy occurs and the two bands possess the cone shape; above the critical point h_c, the two bands split up. Therefore, the difference between the two bands decreases below and increases above the critical point h_c. The property of the dispersion relation in the vicinity of the critical magnetic field directly affects the Berry curvature of the corresponding bands.

4.5.2 Kagome Lattices

Dynamic matrix and dispersion relations

For the two-dimensional kagome lattice, as shown in Fig. 4.9, each unit cell has three atoms, thus $n = 3$. The three kinds of spring-constant matrices between two atoms are $K_{01} = K_x$ (between atoms 1 and 2 in Fig. 4.9), $K_{02} = U(\pi/3)K_xU(-\pi/3)$ (between atoms 2 and 3), $K_{03} = U(-\pi/3)K_xU(\pi/3)$ (between atoms 3 and 1), which are 2×2 matrices. Then we can obtain the on-site spring-constant matrix and the six spring-constant matrices between the unit cell and its nearest neighbors as:

$$K_0 = \begin{pmatrix} 2(K_{01}+K_{02}) & -K_{01} & -K_{02} \\ -K_{01} & 2(K_{01}+K_{03}) & -K_{03} \\ -K_{02} & -K_{03} & 2(K_{02}+K_{03}) \end{pmatrix},$$

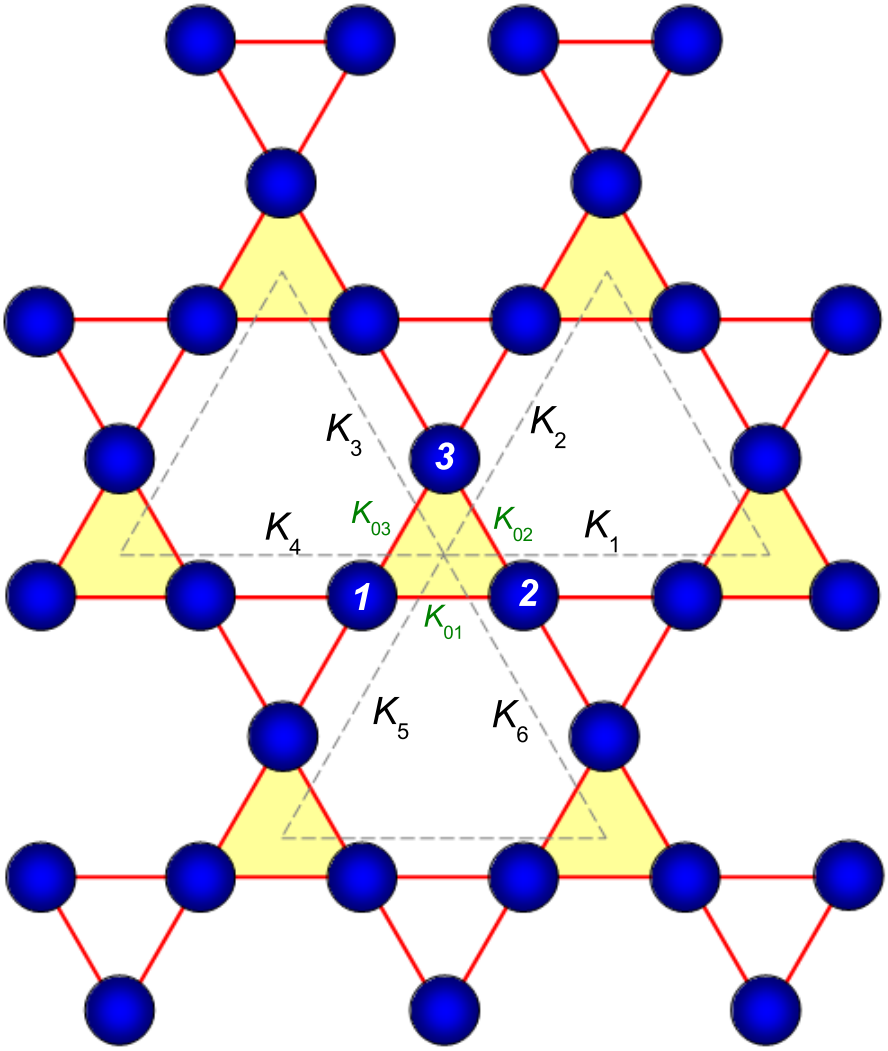

Figure 4.9: The schematic picture of kagome lattice. Each unit cell has three atoms such as the number shown 1,2,3. The coupling between the atoms are K_{01}, K_{02}, K_{03}. Each unit cell has six nearest neighbors; the coupling between the unit cell and the neighbors are $K_1, K_2, ..., K_6$.

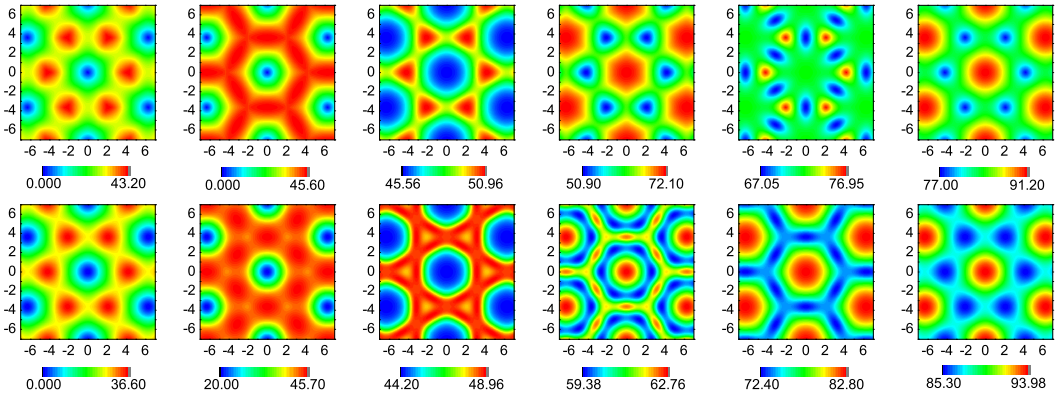

Figure 4.10: The contour map of dispersion relations for the positive frequency bands. For all the insets, the horizontal and vertical axes correspond to wave vector k_x and k_y, respectively. The upper six insets are the dispersion relations for bands 1 to 6 (from left to right) at $h = 0$, respectively. And $h = 10$ rad/ps for the lower ones.

$$K_1 = \begin{pmatrix} 0 & 0 & 0 \\ -K_{01} & 0 & 0 \\ 0 & 0 & 0 \end{pmatrix}, \; K_2 = \begin{pmatrix} 0 & 0 & 0 \\ 0 & 0 & 0 \\ -K_{02} & 0 & 0 \end{pmatrix},$$

$$K_3 = \begin{pmatrix} 0 & 0 & 0 \\ 0 & 0 & 0 \\ 0 & -K_{03} & 0 \end{pmatrix}, \; K_4 = \begin{pmatrix} 0 & -K_{01} & 0 \\ 0 & 0 & 0 \\ 0 & 0 & 0 \end{pmatrix},$$

$$K_5 = \begin{pmatrix} 0 & 0 & -K_{02} \\ 0 & 0 & 0 \\ 0 & 0 & 0 \end{pmatrix}, \; K_6 = \begin{pmatrix} 0 & 0 & 0 \\ 0 & 0 & -K_{03} \\ 0 & 0 & 0 \end{pmatrix},$$

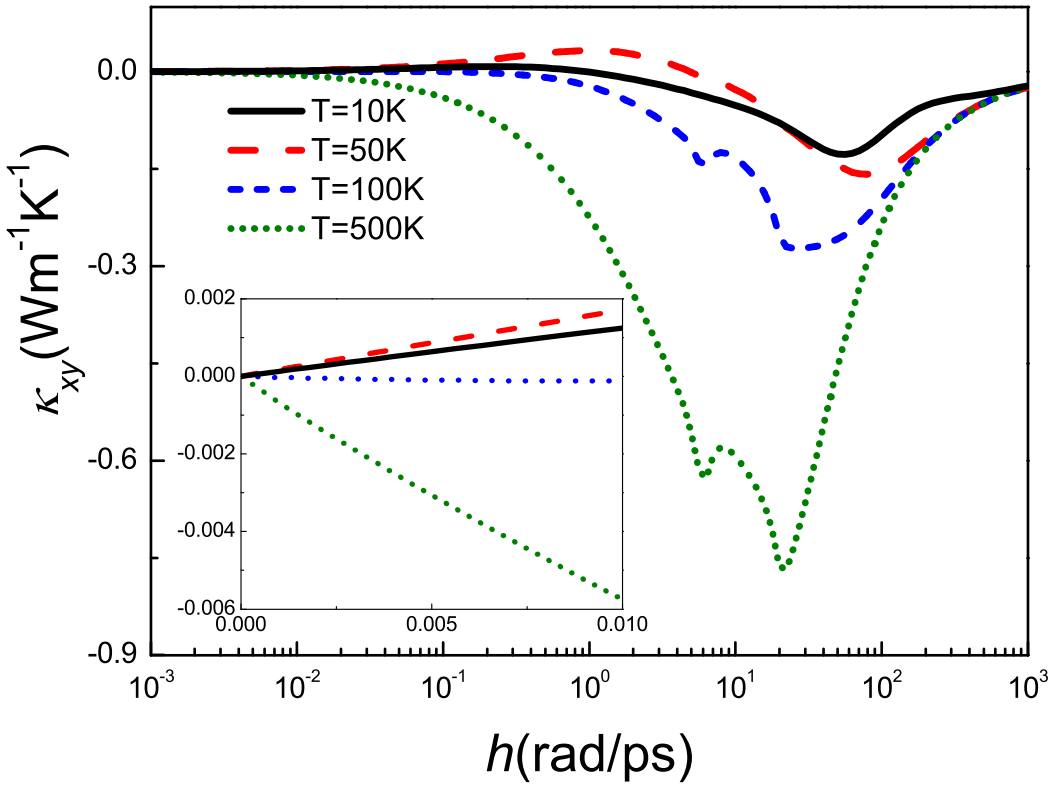

Figure 4.11: The phonon Hall conductivity vs magnetic field at different temperatures. The inset is the zoom-in curve of the phonon Hall conductivity at weak magnetic field. Here the sample size N_L=400.

which are 6×6 matrices. Finally we can obtain the 6×6 dynamic matrix $D(\mathbf{k})$ as

$$\begin{aligned} D(\mathbf{k}) &= -A^2 + K_0 + K_1 e^{ik_x} + K_2 e^{i(\frac{k_x}{2}+\frac{\sqrt{3}k_y}{2})} \\ &\quad + K_3 e^{i(-\frac{k_x}{2}+\frac{\sqrt{3}k_y}{2})} + K_4 e^{-ik_x} \\ &\quad + K_5 e^{i(-\frac{k_x}{2}-\frac{\sqrt{3}k_y}{2})} + K_6 e^{i(\frac{k_x}{2}-\frac{\sqrt{3}k_y}{2})}, \end{aligned} \tag{4.98}$$

where, $A^2 = -h^2 \cdot I_6$, here I_6 is the 6×6 identity matrix.

Inserting the dynamic matrix Eq. (4.98) to the effective Hamiltonian Eq. (4.18), we can calculate eigenvalues and eigenvectors of the system, and also get the dispersion relation of the system.

For a kagome lattice, because each unit cell has three atoms, and we only consider the two-dimensional motion, we can get six phonon branches with positive frequencies. The branches with negative frequencies have similar behavior because of $\omega_{-\sigma}(-\mathbf{k}) = -\omega_{\sigma}(\mathbf{k})$. We show the contour map of the dispersion relation in Fig. 4.10. We can see that the dispersion relations have a 6-fold symmetry. For different bands, they are different. With a changing magnetic field, the dispersion relations vary. The point $\mathbf{\Gamma}$ ($\mathbf{k} = (0, 0)$) is the 6-fold symmetric center; the point $\mathbf{K}$ ($\mathbf{k} = (\frac{4\pi}{3}, 0)$) is 3-fold symmetric center; and the middle point of the line between two 6-fold symmetric centers, $\mathbf{X}$ ($\mathbf{k} = (\pi, \frac{\sqrt{3}\pi}{3})$) is a 2-fold symmetric center.

The PHE and the associated phase transition

Using the formula Eq. (4.47), we calculate the phonon Hall conductivity of the kagome lattice systems in Fig. 4.11. Similar to the honeycomb case, we find a nontrivial behavior of the phonon Hall conductivity as a function of the magnetic field. When h is small, κ_{xy} is proportional to h, which is shown in the inset of Fig.4.11; while the dependence becomes nonlinear when h is large. As h is further increased, the magnitude of κ_{xy} increases before it reaches a maximum magnitude at certain value of h. Then the magnitude of κ_{xy} decreases and goes to zero at very large h. The on-site term $\tilde{A}^2$ in the Hamiltonian (4.6) increases with h quadratically so as to blockade the phonon transport, which competes with the spin-phonon interaction. Because of the coefficient of $f(\omega_{\sigma})$ in the summation of the formula Eq. (4.47), the sign of the Hall conductivity will change with temperatures.

For kagome lattices , we plot the curves of the Chern numbers of bands 2

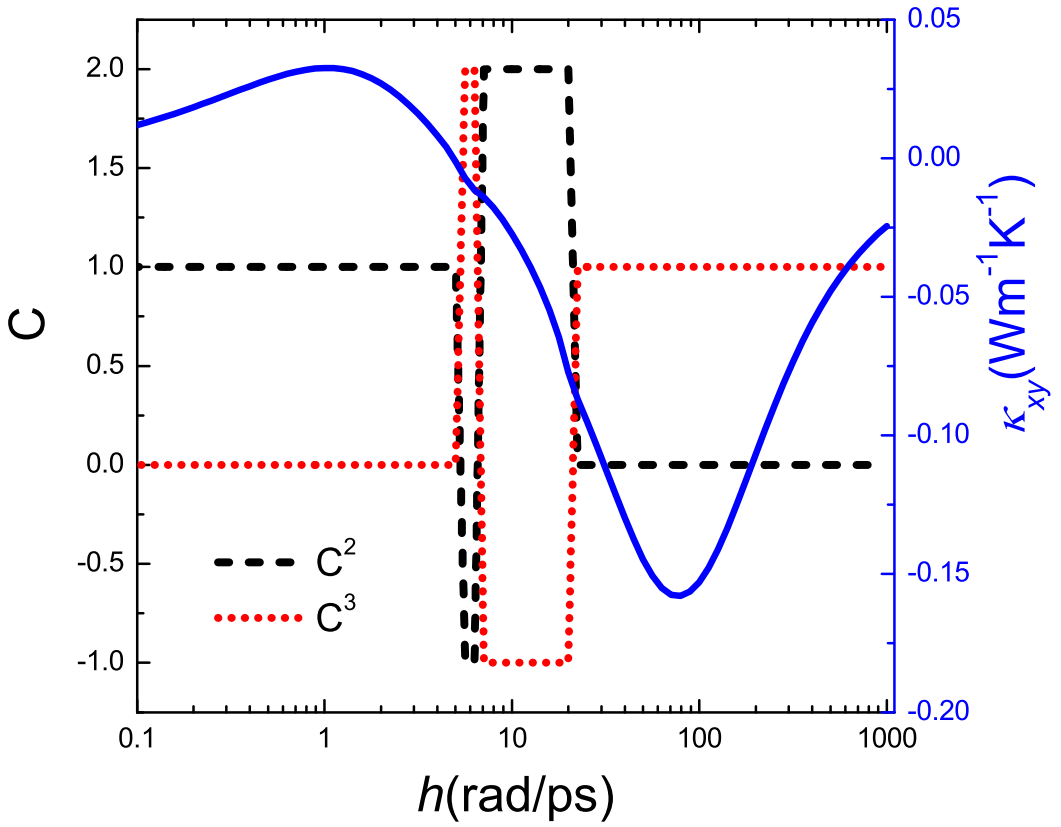

Figure 4.12: (color online) The Chern numbers and the phonon Hall conductivity vs magnetic field. The dashed line and the dotted line correspond to the Chern numbers of phonon bands 2 and 3 (left scale). The solid line correspond to the phonon Hall conductivity (right scale) at $T = 50$ K.

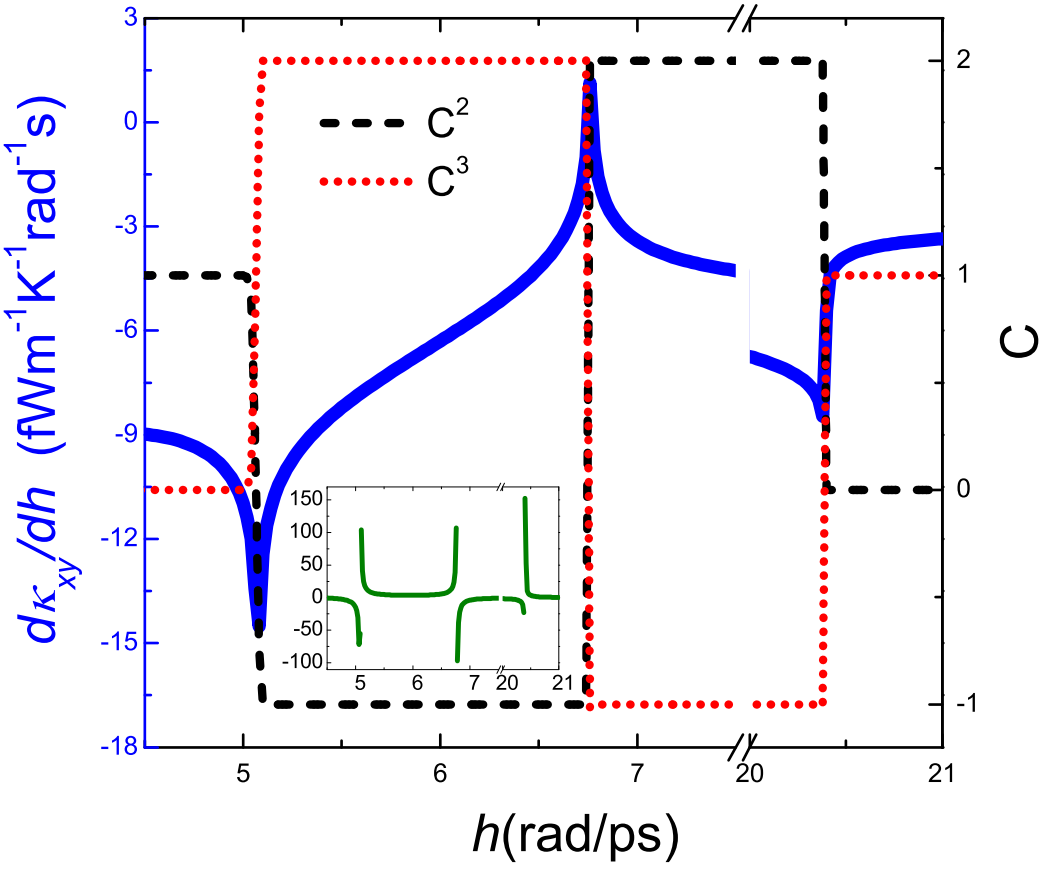

Figure 4.13: The first derivative of the phonon Hall conductivity dk_{xy}/dh at $T = 50K$ and the Chern numbers of bands 2 and 3 in the vicinity of the magnetic fields. The solid line correspond to the dk_{xy}/dh at $T = 50$K (left scale); the dashed and dotted lines correspond to the Chern numbers of bands 2 and 3, respectively (right scale). The inset shows the second derivative with respective to the magnetic field dk_{xy}^2/dh^2 (vertical axis) vs magnetic field h (horizontal axis) at $T = 50$ K.

and 3 as a function of the magnetic field in Fig. 4.12. In Fig. 4.12, we set the $V_{\text{onsite}} = 10^{-3}K_L$ similar as the honeycomb-lattice case. The Chern numbers of bands 2 and 3 have three jumps with the increasing of the magnetic field, although the phonon Hall conductivity is continuous. For other bands, the Chern numbers keep constant: $C^1 = C^4 = -1$, $C^5 = 0$, and $C^6 = 1$. For the electronic Hall effect, we know it is quantized because the Hall conductivity is proportional to the quantized Chern numbers. Here we also find the quantized effect of the Chern numbers from Fig. 4.12, while there is no quantization for the phonon Hall conductivity. Such difference of the PHE from the electronic Hall effect comes from the different nature of phonons respective to electrons. In Eq. (4.47), in the summation, an extra term $(\omega_\sigma + \omega_{\sigma'})^2$ relating to the phonon energy which is an analog of the electrical charge term e^2 in the electron Hall effect, can not be moved out from the summation. Combining with the Bose distribution, the term $f(\omega_\sigma)(\omega_\sigma+\omega_{\sigma'})^2$ make the phonon Hall conductivity smooth, no discontinuity comes out although the Chern numbers have some sudden jumps. From the above discussion on honeycomb lattices the discontinuity of the Chern numbers correspond to the phase transitions and would relate to the divergency of derivative of the phonon Hall conductivity.

Figure 4.13 shows the curves of the derivative of the phonon Hall conductivity and the Chern numbers at the critical magnetic fields. The first derivative of phonon Hall conductivity has a minimum or maximum at the magnetic fields $h_{c1} = 5.07, h_{c2} = 6.75, \text{and} h_{c3} = 20.39$ rad/ps for the finite-size sample (the sample has $N = N_L^2$ unit cells). The first derivative $d\kappa_{xy}/dh$ at the the points h_{c1}, h_{c2}, h_{c3} diverges when the system size increases to infinity [152]. At the three critical points the second derivative $d^2\kappa_{xy}/dh^2$ is discontinuous,

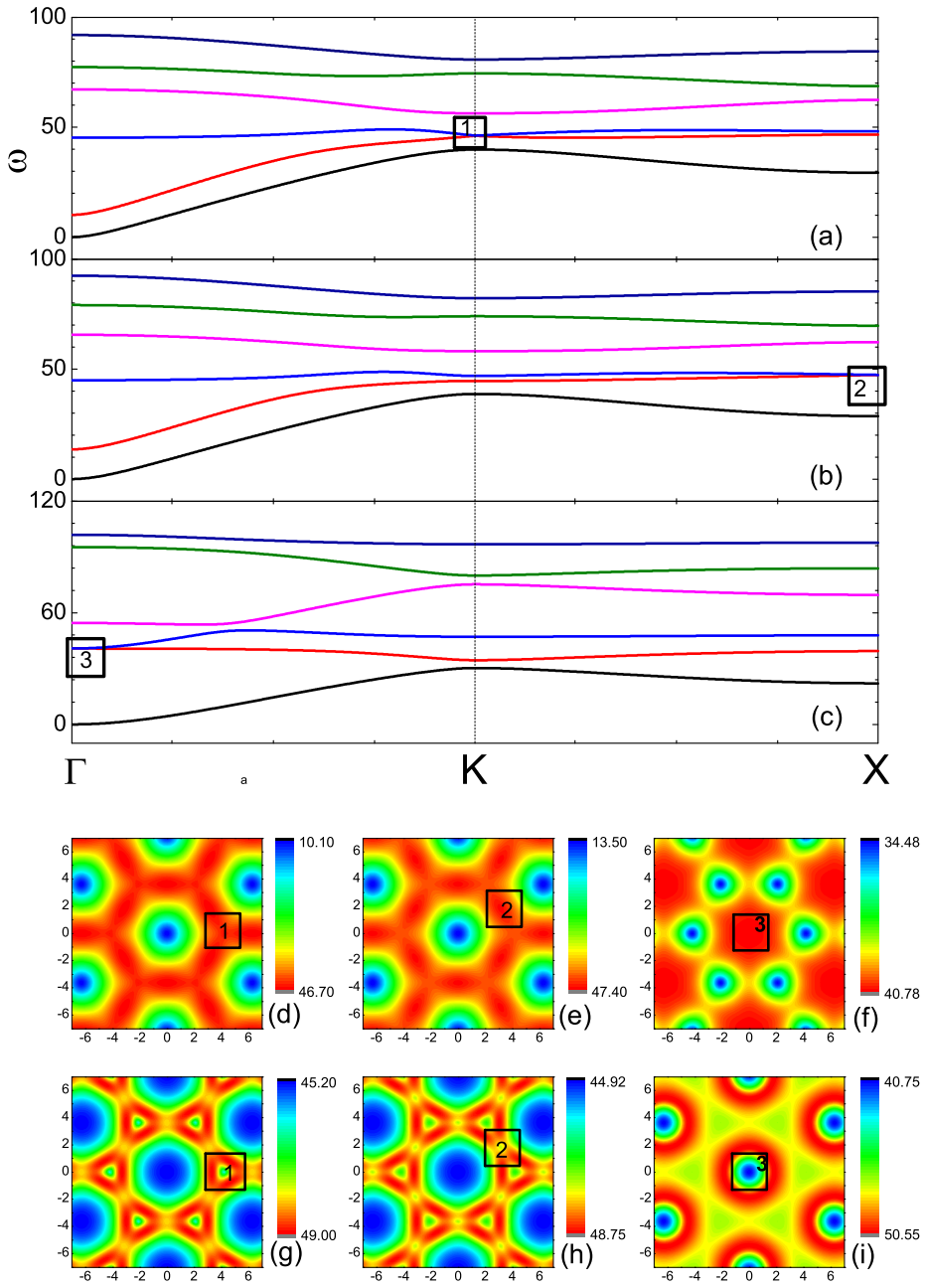

Figure 4.14: The dispersion relations around the critical magnetic fields. (a), (b), and (c) show the dispersion relations along the direction from $\mathbf{\Gamma}$ ($\mathbf{k}$=(0,0)) to $\mathbf{K}$ ($\mathbf{k} = (\frac{4\pi}{3}, 0)$) and to $\mathbf{X}$ ($\mathbf{k} = (\pi, \frac{\sqrt{3}\pi}{3})$) at the critical magnetic fields $h_{c1} = 5.07$rad/ps, $h_{c2} = 6.75$rad/ps, and $h_{c3} = 20.39$rad/ps, respectively. (d)-(f) show the contour maps of the dispersion relation of band 2 at the three critical magnetic fields. (g)-(i) show the contour maps of the dispersion relation of band 3 at the three critical magnetic fields. The squares with number 1, 2, and 3 are marked for the touching points. In (d), (g) and (e), (h), we only mark one of the six symmetric points by squares of number 1 and 2 for simplicity.

which is shown in the inset of Fig. 4.13, across which phase transitions occur. For different temperatures, the phase transitions occur at exactly the same critical values. Thus the temperature-independent phase transition does not come from the thermodynamic effect, but is induced by the topology of the phonon band structure, which corresponds to the sudden change of the Chern numbers. While there is one discontinuity of the Chern numbers for the honeycomb lattice system, for the kagome lattice system, there are three discontinuities corresponding to the divergency of the derivative of the phonon conductivity, which can be seen in Fig. 4.13.

The touching and splitting of the phonon bands near the critical magnetic field induces the abrupt change of Chern numbers of the phonon band [152]. In the above discussion on honeycomb lattices, we know that band 2 and 3 are going to touch with each other at the $\mathbf{\Gamma}$ point if the magnetic field increases to h_c; at the critical magnetic field, the degeneracy occurs and the two bands possess the cone shape; above the critical point h_c, the two bands split up. Therefore, the difference between the two bands decreases below and increases above the critical magnetic field, and is zero at the critical point. The eigenfrequency difference is in the denominator of the Berry curvature; thus the variation of the difference around the critical magnetic field dramatically affects the Berry curvature of the corresponding bands. In the kagome lattice systems, we find that the touching and splitting of the phonon bands not only occurs at the $\mathbf{\Gamma}$ point, but also occurs at other points, which is shown in Fig. 4.14. At the first critical points h_{c1}, the bands 2 and 3 touch at the point $\mathbf{K}$ (marked by a square with number 1); at h_{c2} the two bands touch at $\mathbf{X}$ (marked by a square with number 2); while only for the third critical one

h_{c3}, band 2 and 3 degenerate at the point $\mathbf{\Gamma}$ (marked by a square with number 3). From the contour maps of bands 2 and 3, we clearly see that the critical magnetic fields h_{c1}, h_{c2}, and h_{c3}, there are local maximum for the band 2 and the local minimum for the band 3. Therefore, for all the critical magnetic fields where the Chern numbers have abrupt changes, in the wave-vector space we can always find the phonon bands touching and splitting at some symmetric center points.

4.5.3 Discussion on Other Lattices

For a square lattice with nearest-neighbor interaction, we find that $\Omega^{\sigma\sigma'}_{k_x k_y} = 0$, thus $\kappa_{xy} = 0$, which verify our symmetry criterion we proposed earlier. Therefore, if the system exhibits symmetry satisfying $SDS^{-1} = D$, $SAS^{-1} = -A$ (e.g., mirror reflection symmetry), the phonon Hall conductivity is zero.

For a triangular lattice, we also find that, in the absence of applied magnetic field, the Berry curvature is zero everywhere, and the phonon Hall conductivity is also zero. If a magnetic field is applied, the Berry curvature will be nonzero, which can be seen from Fig. 4.15 (we use the same spring constant of the honeycomb lattice for calculation triangular lattices). In Fig. 4.15(a), (b) are the Berry curvatures for first and second bands at $h = 5$ rad/ps, and (c), (d) are the ones at $h = 20$ rad/ps. For different applied magnetic field, the Berry curvature are different; however, the Chern numbers are always zero. The Berry curvatures at Γ and K (or K') points cancel each other, the sum is zero. Although all the Chern numbers are zero, the Berry curvatures are not zero, and the phonon Hall conductivity is nonzero for the triangular lattice

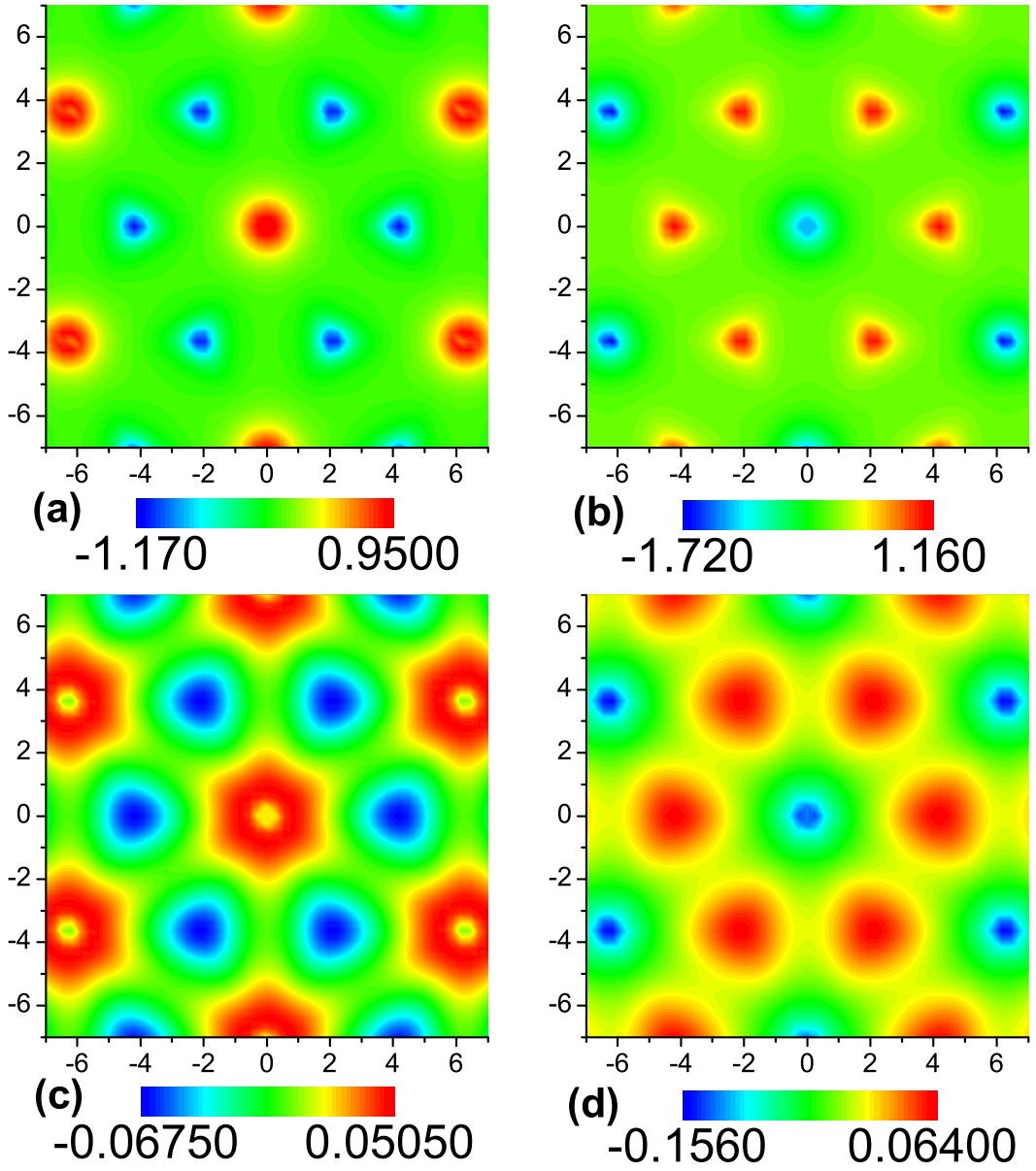

Figure 4.15: The Berry curvature for triangle lattice. (a), (b) The Berry curvatures for first and second bands at $h = 5$ rad/ps; (c), (d) The Berry curvatures for first and second bands at $h = 20$ rad/ps.

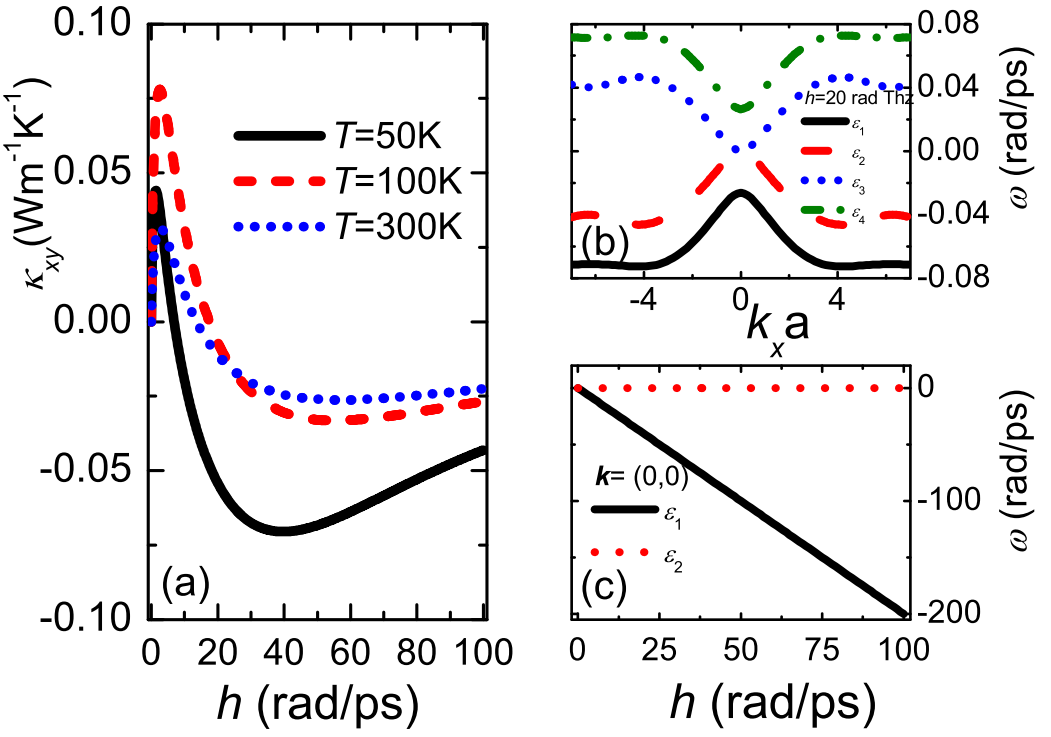

Figure 4.16: (a) The phonon Hall conductivity vs magnetic field for different temperature. The solid, dash and dot lines correspond to $T = 50, 100$ and 300 K; (b) The dispersion relation of the triangle lattice, the olid, dash, dot and dash dot lines correspond to band 1, 2, 3, and 4; $h = 20$ rad/ps. (c) The frequencies of band 1 and 2 at Γ point vs the applied magnetic field, the olid and dash lines correspond to band 1 and 2.

system, which can be seen from Fig. 4.16(a). The phonon Hall conductivity can change sign with an applied magnetic field. However, there is no phase transition in this system. Without the magnetic field, there are only acoustic modes in the system, with increasing magnetic field, the two acoustic modes will split, see Fig. 4.16(b) (the phonon band 1 and 4 are opposite numbers, band 2 and band 3 are also opposite ones). Figure 4.16(c) shows that the frequency difference of this two levels are linear with magnetic field, they never touch again, therefore the topology of Brillouin torus will not change, the Chern numbers keep zero, and no phase transition for the phonon Hall effect in the triangular lattice.

4.6 Summary

In summary, we have studied the PHE from a topological point of view. We have proposed two different theoretical derivations for the PHE in two-dimensional periodic lattice systems. In the first derivation, from the Green-Kubo formula and considering the contributions from all the phonon bands, we obtain the general formula for the phonon Hall conductivity; then by looking at the phases of the polarization vectors of both the displacements and conjugate momenta as a function of the wave vector, a Berry curvature can be defined uniquely for each band. Combining the above two steps, at last the phonon Hall conductivity can be written in terms of Berry curvatures. Such derivation gives us the clear picture of the contribution to the phonon Hall current from all the phonon branches, and the relation between the phonon Hall conductivity with the geometrical phase of the polarization vectors, thus

helps us to understand the topological picture of the PHE. In the second theoretical derivation, by the modified second quantization for the Hamiltonian, we obtain the formula for the heat current density, which considering all the phonon bands including both positive and negative frequencies. The heat current density can be divided into two parts, one is the diagonal, another is off-diagonal. The diagonal part corresponds to the normal velocity; and the off-diagonal part corresponds to the anomalous velocity which is induced by the Berry vector potential. Such anomalous velocity induces the PHE in the crystal lattice. Using the Green-Kubo formula, we derive the formula of the phonon Hall conductivity. The second theoretical derivation of the PHE provides a clear picture of the Berry phase effect inducing the anomalous velocity which contributes to the extra term of the heat current. Thus the Berry phase effect is straightforward to take the responsibility of the PHE.

We also find the same symmetry criterion for the PHE as described in last chapter - if under a symmetry operation the magnetic field reverses while the system dynamic matrix keeps constant, there is no PHE in this system, such as square lattices with nearest neighbor interaction. For a general lattice, the PHE presents with an applied magnetic field.

Both of the theories give us exactly the same formula of phonon Hall conductivity in terms of Berry curvatures, which are defined uniquely for each band. We find a nonmonotonic behavior of phonon Hall conductivity as a function of the magnetic field. Our formulism predicts that the direction of phonon Hall conductivity can be reversed by tuning magnetic fields or temperatures, which we hope can be verified by experiments in the future. Because

of the nature of phonons, the phonon Hall conductivity, which is not directly proportional to the Chern number, is not quantized. However, the quantization effect, in the sense of discontinuous jumps in Chern numbers, manifests itself in the phonon Hall conductivity as a singularity of the first derivative with respect to the magnetic field. For honeycomb lattices, with increasing the magnetic field, we find the discontinuous in the second order derivative of the phonon Hall conductivity with respect to the magnetic field, which a phase transition occurs. Such phase transition corresponds to a jump of the Chern numbers of two phonon bands at the critical point. The mechanism for the change of topology of band structures comes from the energy bands touching and splitting. And in the kagome lattices there are three singularities of d^2k_{xy}/dh^2 induced by the abrupt change of the phonon band topology, which correspond to the touching and splitting at three different symmetric center points in the wave-vector space.

Chapter 5

Conclusion

This dissertation presented theoretical studies of phonon Hall effect in finite lattice systems and infinite periodic lattices. To investigate the existence of ballistic PHE and its various properties, the nonequilibrium Green's function method was applied to the finite-junction systems and the Green-Kubo formula was applied to the infinite periodic lattices.

To examine whether the ballistic PHE can exist, a theory of the PHE in finite paramagnetic dielectrics was proposed. By using the NEGF approach, we derived the Green's functions for the four-terminal junctions with a spin-phonon interaction. Using the derived Green's functions, this thesis developed a formula of the relative Hall temperature difference to denote the PHE in four-terminal junctions. The results calculated from our theory are consistent with the essential experimental features of PHE, such as the magnitude of the PHE and linear dependence of the observed transverse temperature difference on magnetic fields. The dependence on large range of magnetic fields and temperatures was also studied. With increasing magnetic field, the PHE changes from a linear dependance to a sublinear one, and then decreases and changes

sign from positive to negative after a certain magnetic field. The size effect of the PHE was also discussed; it was found that the Hall temperature difference changes sign as the system size increases, which could be verified by experiments in nanostructures. Our theory of the PHE in four-terminal junctions provides an efficient way to study the PHE in finite systems, which is generally applicable for different crystal systems.

By applying our theory of PHE in the multi-terminal junctions to the ballistic thermal rectification, two necessary conditions for thermal rectification were found: one is phonon incoherence, another is asymmetry. This result is significant because this two conditions are more fundamental for understanding the thermal rectification than the current prevalent view which takes the nonlinearity and structural asymmetry as necessary conditions. Furthermore, it was found that the thermal rectification can change sign in a certain parameter range, which is a universal phenomenon for the thermal transport.

To investigate the PHE in infinite periodic systems, by using Green-Kubo formula we proposed a topological theory of the PHE from two different theoretical derivations. In the first derivation, firstly the phonon Hall conductivity and Berry curvatures were separately derived. Then combining these two formulae, the phonon Hall conductivity in terms of Berry curvatures was developed. Such derivation gives us a clear picture of the contribution to the phonon Hall current from all the phonon branches, which include both positive and negative frequencies. The connection between the phonon Hall conductivity and the Berry curvatures is helpful to understand the topological picture of the PHE. To investigate how the Berry phase effect affect the heat current and thus

take responsibility of the PHE, we proposed a second theoretical derivation. By proposing a proper second quantization for the non-Hermite Hamiltonian in the polarization-vector space, we obtained a new heat current density operator with two separate contributions: the normal velocity responsible for the longitudinal phonon transport, and the anomalous velocity manifesting itself as the Hall effect of transverse phonon transport. By inserting the new heat current to the Green-Kubo formula, a phonon Hall conductivity in terms of Berry curvature was derived in the same form as that in the first derivation. This derivation is systematic and straightforward to inspect the Berry phase effect of the PHE.

The proposed topological theory of the PHE offers us a useful way to study the phonon Hall conductivity in the infinite periodic system and a new understanding of the topological nature of the PHE. Similar to the relative Hall temperature difference in a four terminal junction, a nonmonotonic behavior of phonon Hall conductivity as a function of the magnetic field was found. It was also found that the direction of phonon Hall conductivity can be reversed by tuning magnetic field or temperature, which we hope can be verified by experiments in the future.

Because of the nature of phonons, the phonon Hall conductivity, which is not directly proportional to the Chern number, is not quantized. Therefore different from the quantum Hall effect of electrons, there is no quantum phonon Hall effect. However, it was found that the quantization effect, in the sense of discontinuous jumps in Chern numbers, manifests itself in the phonon Hall conductivity as discontinuities of the second derivative with respect to the

magnetic field. For honeycomb lattices, there exists a phase transition which occurs at the critical magnetic field corresponding to the discontinuity. The mechanism for the change of topology of band structures comes from the energy bands touching and splitting. And in the kagome lattices there are three singularities of d^2k_{xy}/dh^2 induced by the abrupt change of the phonon band topology, which correspond to the touching and splitting at three different symmetric center points in the Brillouin zone.

Both the theories of PHE in four-terminal junctions and in infinite crystal systems predicted a symmetry criterion for the PHE, that is, there is no PHE if the lattice satisfies a certain symmetry which makes the dynamic matrix unchanged and the magnetic field reversed. The symmetry broken of the dynamic matrix is the necessary condition for the existence of PHE. For instance, there is no PHE in square lattices with nearest neighbor interaction. For a general lattice with an applied magnetic field, the PHE can exist. This finding is of crucial importance in terms of theoretical applications and experimental measurement on the PHE because it is the necessary condition for PHE and provides guidance for searching the PHE in different structures.

Overall, one key contribution of our study is the confirmation of the ballistic PHE from the proposed PHE theories in both finite and infinite systems, that is, nonlinearity is not a necessary condition for the PHE. Our proposed PHE theories are general and can be applied to the thermal Hall effect in phonon and magnon systems for different materials in low temperatures in which the thermal transport is ballistic. Combing with the numerical finding of the various properties this study can give sufficient guidance for the

experimental study on the PHE. The proposed topological interpretation of the PHE is very important not only for deep understanding of PHE but also for the discipline of phononics especially for the studies aimed at uncovering intriguing Berry phase effects and topological properties in phonon transport. The new finding of the associated phase transition in the PHE, which is explained from topological description and dispersion relations, suggests a novel understanding on various phase transitions.

In this study, we did not consider the nonlinearity in the phonon transport. Although the nonlinearity is not necessary for the PHE, it may give more ample properties in the diffuse PHE. To address the issue of nonlinear interaction, future studies should attempt to consider it in the phonon transport. This study did not explore much on the spin-phonon interaction, a first principle investigation on this interaction in the future will give the PHE deeper understanding.

Bibliography

[1] B. Li, L. Wang, and G. Casati, Phys. Rev. Lett. **93**, 184301 (2004).

[2] B. Li, L. Wang, and G. Casati, Appl. Phys. Lett. **88**, 143501 (2006).

[3] L. Wang and B. Li, Phys. Rev. Lett. **99**, 177208 (2007).

[4] L. Wang and B. Li, Phys. Rev. Lett. **101**, 267203 (2008).

[5] D. Segal and A. Nitzan, Phys. Rev. E 73, 026109 (2006).

[6] R. Marathe, A. M. Jayannavar, and A. Dhar, Phys. Rev. E **75**,030103 (R) (2007).

[7] L. Wang and B. Li, Physics World **21**, No.**3**, 27 (2008).

[8] H. Castella, X. Zotos, and P. Prelovsek, Phys. Rev. Lett. **74**, 972 (1995).

[9] K. Saito, S. Takesue, and S. Miyashita, Phys. Rev. E **54**, 2404 (1996).

[10] X. Zotos, F. Naef, and P. Prelovsek, Phys. Rev. B **55**, 11029 (1997).

[11] F. Naef and X. Zotos, J. Phys.: Condens. Matter **10**, L183 (1998).

[12] C. Strohm, G. L. J. A. Rikken, and P. Wyder, Phys. Rev. Lett. **95**, 155901 (2005).

[13] L. Sheng, D. N. Sheng, and C. S. Ting, Phys. Rev. Lett. **96**, 155901 (2006).

[14] Y. Kagan and L. A. Maksimov, Phys. Rev. Lett. **100**,145902 (2008).

[15] M. Terraneo, M. Peyrard, and G. Casati, Phys. Rev. Lett. **88**, 094302 (2002).

[16] C. W Chang, D. Okawa, A. Majumdar, and A. Zettl, Science **314**, 1121 (2006).

[17] R. Scheibner, M. König, D. Reuter, A. D. Wieck, C. Gould, H. Buhmann, L. W. Molenkamp, New J. Phys. **10**, 083016 (2008).

[18] D. Segal, A. Nitzan, Phys. Rev. Lett. **94**, 034301 (2005).

[19] D. Segal, Phys. Rev. B **73**, 205415 (2006)

[20] J.-P. Eckmann and C. Mejía-Monasterio, Phys. Rev. Lett. **97**, 094301 (2006).

[21] B. Hu, L. Yang, and Y. Zhang, Phys. Rev. Lett. **97**, 124302 (2006)

[22] G. Casati, C. Mejia-Monasterio, T. Prosen, Phys. Rev. Lett. **98**, 104302 (2007).

[23] J. Lan and B. Li, Phys. Rev. B **75**, 214302 (2007).

[24] N. Yang, N. Li, L. Wang, and B. Li, Phys. Rev. B **76**, 020301 (2007).

[25] G. Wu and B. Li, Phys. Rev. B **76**, 085424 (2007).

[26] D. Segal, Phys. Rev. Lett. **100**, 105901 (2008).

[27] N. Zeng and J.-S. Wang, Phys. Rev. B **78**, 024305 (2008).

[28] N. Yang, G. Zhang, B. Li, Appl. Phys. Lett. **93**, 243111, (2008)

[29] Y. Yan, C.-Q. Wu, and B. Li, Phys. Rev. B **79**, 014207 (2009).

[30] L.-A. Wu and D. Segal, Phys. Rev. Lett. **102**, 095503 (2009).

[31] L. Zhang, Y. Yan, C.-Q. Wu, J.-S. Wang, and B. Li, Phys. Rev. B **80**, 172301 (2009).

[32] P. E. Hopkins and J. R. Serrano, Phys. Rev. B **80**, 201408 (2009).

[33] L. Zhang, J.-S. Wang, and B. Li, Phys. Rev. B **81**, 100301 (2010)

[34] C. R. Otey, W. T. Lau, and S. Fan, Phys. Rev. Lett. **104**, 154301 (2010)

[35] D. M.-T. Kuo and Y.-C. Chang, Phys. Rev. B **81**, 205321 (2010).

[36] C. Yu; L. Shi, Z. Yao, D. Li, A. Majumdar, Nano Lett. **5**, 1842 (2005).

[37] M. Fujii,X. Zhang, H. Xie, H. Ago, K. Takahashi, T. Ikuta, H. Abe, T. Shimizu, Phys. Rev. Lett. **95**, 065502 (2005).

[38] E. Pop, D. Mann, Q. Wang, K. Goodson, and H. Dai, Nano Lett. **6**, 96 (2006).

[39] J. Wang and J.-S. Wang, Appl. Phys. Lett. **88** 111909 (2006).

[40] C. W. Chang, D. Okawa, H. Garcia, A. Majumdar, and A. Zettl, Phys. Rev. Lett. **99**, 045901 (2007).

[41] I. Savić, N. Mingo, and D. A. Stewart, Phys. Rev. Lett. **101**, 165502 (2008).

[42] W. Choi, S. Hong, J. T. Abrahamson, J.-H. Han, C. Song, N. Nair, S. Baik, and M. S. Strano, Nat. Mater. **9**, 423 (2010).

[43] R. S. Prasher, X. J. Hu, Y. Chalopin, N. Mingo, K. Lofgreen, S. Volz, F. Cleri, and P. Keblinski, Phys. Rev. Lett. **102**, 105901 (2009).

[44] A. N. Volkov and L. V. Zhigilei, Phys. Rev. Lett. **104**, 215902 (2010).

[45] A. A. Balandin, S. Ghosh, W. Bao, I. Calizo, D. Teweldebrhan, F. Miao, C. N. Lau, Nano Lett. **8**, 902 (2008).

[46] J. Hu, X. Ruan and Y. P. Chen, Nano Lett. **9**, 2730 (2009).

[47] J. H. Seol, I. Jo, A. L. Moore, L. Lindsay, Z. H. Aitken, M. T. Pettes, X. Li, Z. Yao, R. Huang, D. Broido, N. Mingo, R. S. Ruoff, and Li Shi, Science **328**,213 (2010).

[48] D. Li, Y. Wu, P. Kim, L. Shi, P. Yang, and A. Majumdar, Appl. Phys. Lett. bf 83, 2934 (2003).

[49] A. I. Hochbaum, R. Chen, R. D. Del gado, W. Liang, E. C. Garnett, M. Najarian, A. Majumdar, and P. Yang, Nature **451**, 163 (2008).

[50] A. I. Boukai, Y. Bunimovich, J. Tahir-Kheli, J.-K. Yu, W. A. Goddard III, and J. R. Heath, Nature **451**, 168 (2008).

[51] B. Li, J. Lan, and L. Wang, Phys. Rev. Lett. **95**, 104302 (2005).

[52] Z. Ge, D. G. Cahill, and P. V. Braun, Phys. Rev. Lett. **96**, 186101 (2006).

[53] M. Hu, P. Keblinski, B. Li, Appl. Phys. Lett. **92**, 211908 (2008).

[54] P. Martin, Z. Aksamija, E. Pop, and U. Ravaioli, Phys. Rev. Lett. **102**, 125503 (2009).

[55] C. Chiritescu, D. G. Cahill, N. Nguyen, D. Johnson, A. Bodapati, P. Keblinski and P. Zschack, Science **315**, 351 (2007).

[56] N. Yang, G. Zhang, and B. Li, Nano Lett. **8**, 276 (2008).

[57] A. V. Sologubenko, K. Berggold, T. Lorenz, A. Rosch, E. Shimshoni3, M. D. Phillips, and M. M. Turnbull, Phys. Rev. Lett. **98**, 107201 (2007).

[58] A. V. Sologubenko, T. Lorenz, J. A. Mydosh, A. Rosch, K. C. Shortsleeves, and M. M. Turnbull, Phys. Rev. Lett. **100**, 137202 (2008).

[59] M. A. Tanatar, J.-P. Reid, H. Shakeripour, X. G. Luo, N. Doiron-Leyraud, N. Ni, S. L. Budko, P. C. Canfield, R. Prozorov, and L. Taillefer, Phys. Rev. Lett. **104**, 067002 (2010).

[60] E. H. Hall, Am. J. Math. **2**, 287 (1879).

[61] K. v. Kilitzing, G. Dorda, and M. Pepper, Phys. Rev. Lett. **45**, 494 (1980).

[62] D. C. Tsui, H. L. Stormer, and A. G. Gossard, Phys. Rev. Lett. 48, 1559 (1982).

[63] R. B. Laughlin, Phys. Rev. Lett. **50**, 1395 (1983).

[64] K. v. Klitzing, Rev. Mod. Phys. **58**, 519 (1986).

[65] D. R. Yennie, Rev. Mod. Phys. **59**, 781 (1987).

[66] B. Huckestein, Rev. Mod. Phys. **67**, 357 (1995).

[67] H. L. Stormer, D. C. Tsui, and A. C. Gossard, Rev. Mod. Phys. **71**, S298 (1999).

[68] G. Murthy and R. Shankar, Rev. Mod. Phys. **75**, 1101 (2003)

[69] N. Nagaosa, J. Sinova, S. Onoda, A. H. MacDonald, and N. P. Ong, Rev. Mod. Phys. **82**, 1539 (2010)

[70] J. E. Hirsch, Phys. Rev. Lett. **83**, 1834 (1999).

[71] S. Murakami, N. Nagaosa, and S. -C. Zhang, Science **301**, 1348 (2003).

[72] J. Sinova, D. Culcer, Q. Niu, N.A. Sinitsyn, T. Jungwirth, and A.H. MacDonald, Phys. Rev. Lett. **92**, 126603 (2004).

[73] C. L. Kane and E. J. Mele. Phys. Rev. Lett. **95**, 226801 (2005).

[74] B. A. Bernevig and S. C. Zhang. Phys. Rev. Lett. **96**, 106802 (2006).

[75] M. Z. Hasan, C. L. Kane, Rev. Mod. Phys. **82**, 3045 (2010).

[76] X.-L. Qi, S.-C. Zhang, arXiv:1008.2026.

[77] R. de L. Kronig, Physica (Amsterdam) **6**, 33 (1939).

[78] J. H. Van Vleck, Phys. Rev. **57**, 426 (1940).

[79] R. Orbach, Proc. R. Soc. A **264**, 458 (1961).

[80] *Spin-Lattice Relaxation in Ionic Solids*, edited by A. A. Manenkov and R. Orbach (Harper & Row, New York, 1966).

[81] H. Capellmann and K. U. Neumann, Z. Phys. B **67**, 53 (1987).

[82] H. Capellmann, S. Lipinski, and K. U. Neumann, Z. Phys. B **75**, 323 (1989).

[83] H. Capellmann and S. Lipinski, Z. Phys. B **83**, 199 (1991).

[84] A. S. Ioselevich and H. Capellmann, Phys. Rev. B **51**,11 446 (1995).

[85] A. Holz, Il Nuovo Cimento B 9, 83 (1972).

[86] A. V. Inyushkin and A. N. Taldenkov, JETP Lett. **86**, 379 (2007).

[87] M. V. Berry, Proc. R. Soc. Lond. A **392**, 45 (1984).

[88] D. Xiao, M.-C. Chang, and Q. Niu, Rev. Mod. Phys. **82**, 1959 (2010).

[89] B. Simon, Phys. Rev. Lett. **51**, 2167 (1983).

[90] T. Kato, J. Phys. Soc. Jpn. **5**, 435 (1950).

[91] A. Messiah, *Quantum Mechanics, volume II* (North Holland, Amsterdam, 1962).

[92] D. J. Thouless, M. Kohmoto, M. P. Nightingale, and M. den Nijs, Phys. Rev. Lett. **49**, 405 (1982).

[93] M. Kohmoto, Ann. Phys. **160**, 343 (1985).

[94] Z. Fang, N. Nagaosa, K. S. Takahashi, A. Asamitsu, R. Mathieu, T. Ogasawara, H. Yamada, M. Kawasaki, Y. Tokura, and K. Terakura, Science **302**, 92 (2003).

[95] D. Xiao, Y. Yao, Z. Fang, and Q. Niu, Phys. Rev. Lett. **97**, 026603 (2006).

[96] D. N. Sheng, Z. Y. Weng, L. Sheng, and F. D. M. Haldane Phys. Rev. Lett. **97**, 036808 (2006).

[97] M. Koenig, et al. J. Phys. Soc. Jpn. **77**, 031007 (2008).

[98] E. Prodan and C. Prodan, Phys. Rev. Lett. **103**, 248101 (2009).

[99] J. Ren, P. Hänggi, and B. Li, Phys. Rev. Lett. **104**, 170601 (2010).

[100] J.-T. Lü, M. Brandbyge, and P. Hedegård, Nano Lett. **10**, 1657 (2010).

[101] J. Schwinger, PNAS **37**, 452 (1951); J. Schwinger, PNAS **37**, 455 (1951).

[102] J. Schwinger, J. Math. Phys. (New York) **2**, 407 (1961).

[103] L..P. Kadanoff, G. Baym, *Quantum Statistical Mechanics* (Benjamin/Cummings, 1962).

[104] L.V. Keldysh, Soviet Phys. JETP **20**, 1018 (1965).

[105] M. Wagner, Phys. Rev. B **44**, 6104 (1991).

[106] Y. Meir, N.S. Wingreen, Phys. Rev. Lett. **68**, 2512 (1992).

[107] A.P. Jauho, N.S. Wingreen, Y. Meir, Phys. Rev. B **50**, 5528 (1994).

[108] S. Datta, *Electronic Transport in Mesoscopic Systems* (Cambridge Univ. Press, 1995)

[109] H. Haug, A.P. Jauho, *Quantum Kinetics in Transport and Optics of Semiconductors* (Springer, 1996)

[110] A. Ozpineci, S. Ciraci, Phys. Rev. B **63**, 125415 (2001).

[111] S. Ciraci, A. Buldum, I.P. Batra, J. Phys.:Condens. Matter **13**, R537 (2001).

[112] T. Yamamoto, K. Watanabe, Phys. Rev. Lett. **96**, 255503 (2006).

[113] A. Dhar, Adv. Phys. **57**, 457 (2008).

[114] J.-S. Wang, J. Wang, N. Zeng, Phys. Rev. B **74**, 033408 (2006).

[115] J.-S. Wang, N. Zeng, J. Wang, C.K. Gan, Phys. Rev. E **75**, 061128 (2007).

[116] N. Mingo, Phys. Rev. B **74**, 125402 (2006).

[117] H.-P. Liu, L. Yi, Chin. Phys. Lett. **23**, 3194 (2006).

[118] M. Galperin, A. Nitzan, M.A. Ratner, Phys. Rev. B **75**, 155312 (2007).

[119] J.-S. Wang, J. Wang, and J. T. Lü, Eur. Phys. J. B **62**, 381 (2008).

[120] S. Doniach, E.H. Sondheimer, *Green's Functions for Solid State Physicists* (W. A. Benjamin, 1974)

[121] G.D. Mahan, *Many-Particle Physics*, 3rd edn. (Kluwer Academic, 2000).

[122] D.C. Langreth, in *Linear and Nonlinear Electron Transport in Solids*, edited by J.T. Devreese, E. van Doren (Plenum, 1976).

[123] N. Zeng, Ph.D. thesis, National Univ. Singapore (2007).

[124] C. Niu, D.L. Lin, T.H. Lin, J. Phys.:Condens. Matter **11**, 1511 (1999).

[125] M. S. Green, J. Chem. Phys. **22**, 398, (1954).

[126] R. Kubo, M. Yokota, and S. Nakajima, J. Phys. Soc. Jpn. **12**, 1203, (1957).

[127] M. S. Green, Phys. Rev. **119**, 829 (1960).

[128] R. Kubo, M. Toda, and N. Hashitsume, *Statistical Physics II*(Springer-Verlag, Berlin, 1985).

[129] H. Mori, Phys. Rev. **112**, 1829 (1958) .

[130] Kadanoff and Martin, Annals of Physics **24**, 419 (1963).

[131] J. M. Luttinger, Phys. Rev. **135**, A1505, (1964) .

[132] W. M. Visscher, Phys. Rev. A. **10**, 2461 (1974).

[133] D. Forster, *Hydrodynamic Fluctuations, Broken Symmetry, and Correlation Functions* (Benjamin, Reading, 1975).

[134] G. D. Mahan, Many-Particle Physics (Plenum, New York, 1990).

[135] A. Dhar, Adv. Phys. **57**, 457 (2008).

[136] S. Liu and B. Li, arXiv: 1103.2835 (2011).

[137] H. Zhao, Phys. Rev. Lett. **96**, 140602 (2006).

[138] K. R. Allen and J. Ford, Phys. Rev. **176**, 1046 (1968).

[139] D. S. Fisher and P. A. Lee, Phys. Rev. B **23**, 6851 (1981).

[140] J. -S. Wang and B. Li, Phys. Rev. Lett. **92**, 074302 (2004).

[141] G. Gallavotti, Phys. Rev. Lett. **77**, 4334 (1996).

[142] G. Gallavotti, J. Stat. Phys. **84**, 899 (1996).

[143] J.L. Lebowitz and H. Spohn, J. Stat. Phys. **95**, 333 (1999).

[144] D. Andrieux and P. Gaspard, J. Stat. Mech. P02006, (2007).

[145] K. Saito and A. Dhar, Phys. Rev. Lett. **99**, 180601 (2007).

[146] C.-W Chang et al, Phys. Rev. Lett. **101**, 075903 (2008).

[147] S. Datta, *Electronic Transport in Mesoscopic Systems* (Cambridge Univ. Press, 1995).

[148] M. Büttiker, Phys. Rev. Lett. **57**, 1761 (1986); M. Büttiker, IBM J. Res. Developm. **32**, 317 (1988).

[149] J.-S. Wang and L. Zhang, Phys. Rev. B **80**, 012301 (2009).

[150] L. Zhang, J.-S. Wang, and B. Li, New J. Phys. **11**, 113038 (2009).

[151] R. J. Hardy, Phys. Rev. **132**, 168 (1963).

[152] L. Zhang, J. Ren, J.-S. Wang, and B. Li, Phys. Rev. Lett. **105**, 225901 (2010).

[153] L. Zhang, J. Ren, J.-S. Wang, and B. Li, J. Phys.: Cond. Matt. **23**, 305402 (2011).

[154] B. K. Agarwalla, L. Zhang, J.-S. Wang, B. Li, Eur. Phys. J. B **81**, 197 (2011).

List of Publications

[1] L. Zhang, J. Ren, J.-S. Wang, and B. Li, "The phonon Hall effect: theory and application", J. Phys.: Cond. Matt. **23**, 305402 (2011).

[2] B. K. Agarwalla, L. Zhang, J.-S. Wang, and B. Li, "Phonon Hall effect in ionic crystals in the presence of static magnetic field", Eur. Phys. J. B, **81**, 197 (2011).

[3] L. Zhang, P. Keblinski, J.-S. Wang, and B. Li, "Interfacial thermal transport in atomic junctions," Phys. Rev. B, **83**, 064303 (2011)

[4] L. Zhang, J. Ren, J.-S. Wang, and B. Li, "Topological nature of phonon Hall effect,", Phys. Rev. Lett., **105**, 225901 (2010).

[5] L. Hu, L. Zhang, M. Hu, J.-S. Wang, B. Li, and P. Keblinski, "Phonon interference at self-assembled monolayer interfaces: Molecular dynamics simulations," Phys. Rev. B **81**, 235427 (2010).

[6] L. Zhang, J.-S. Wang, and B. Li, "Ballistic thermal rectification in nanoscale three-terminal junctions," Phys. Rev. B **81**, 100301(R) (2010).

[7] L. Zhang, J.-S. Wang, and B. Li, "Phonon Hall effect in four-terminal junctions," New J. Phys. **11**, 113038 (2009).

[8] L. Zhang, Y. Yan, C.-Q. Wu, J.-S. Wang, B. Li, "Reversal of thermal rectification in quantum systems," Phys. Rev. B **80**, 172301(2009).

[9] J.-S. Wang and L. Zhang, "Phonon Hall thermal conductivity from Green-Kubo formula," Phys. Rev. B **80**, 012301 (2009).

[10] L. Zhang, J.-S. Wang, and B. Li, "Ballistic magneto-thermal transport in a Heisenberg spin chain at low temperatures," Phys. Rev. B **78**, 144416 (2008).